

# The Planning of Three Dimensional Fully Extended Arm Pointing Movements

By  
Jason Friedman



Under the Supervision of  
Prof. Tamar Flash  
Faculty of Mathematics and Computer Science  
The Weizmann Institute of Science

Thesis for the M.Sc. degree submitted to the Feinberg  
Graduate School of the Weizmann Institute of Science

Submitted February 10, 2002

Revised version submitted May 23, 2002

# Contents

<b>1</b>	<b>General introduction</b>	<b>1</b>
1.1	Trajectory formation . . . . .	1
1.2	Internal models . . . . .	3
1.3	Thesis Outline . . . . .	4
<b>2</b>	<b>Representations of rotations</b>	<b>6</b>
2.1	Rotation vectors . . . . .	9
2.2	Coordinate velocity vectors . . . . .	11
2.3	Angular velocity vectors . . . . .	11
<b>3</b>	<b>Background on kinematic redundancy</b>	<b>14</b>
3.1	Introduction . . . . .	14
3.2	Results from studies of eye saccades . . . . .	16
3.3	Results from eye and head studies . . . . .	17
3.4	Results from studies of hand movements . . . . .	19
3.5	Double step paradigm . . . . .	21
<b>4</b>	<b>Kinematic redundancy strategies</b>	<b>22</b>
4.1	Introduction . . . . .	22
4.2	Methods . . . . .	22
4.2.1	Experimental setup . . . . .	22
4.2.2	Experimental protocol . . . . .	25
4.2.3	Instructions to subject . . . . .	27
4.2.4	Techniques of analysis . . . . .	28

4.3	Results . . . . .	31
4.3.1	Variation at movement endpoints . . . . .	31
4.3.2	Effect of considering orientation relative to starting point	38
4.3.3	Distribution of rotation vectors throughout the workspace	39
4.3.4	Constraints on rotation vectors . . . . .	43
4.4	Discussion . . . . .	57
<b>5</b>	<b>Background on models of motor control</b>	<b>60</b>
5.1	Double step movements and the superposition strategy . . . . .	61
5.2	Abort-replan model . . . . .	62
5.3	Models for 2D movements in a plane . . . . .	62
5.4	Models for saccade generation in the eye . . . . .	64
5.5	Incorporation of Listing’s law . . . . .	67
5.6	Trajectory modification with rotation vector models . . . . .	68
5.7	Incorporation of Donders’ law for non-flat surfaces . . . . .	74
5.8	Models in Fick coordinates . . . . .	77
5.9	Three-dimensional “Velocity box” model . . . . .	79
5.10	Conclusions . . . . .	82
<b>6</b>	<b>Models of motion planning for extended arm pointing move-</b>	
	<b>ments</b>	<b>85</b>
6.1	Introduction . . . . .	85
6.2	Methods . . . . .	85
6.2.1	Techniques of analysis . . . . .	86
6.3	Results . . . . .	92
6.3.1	Analysis of control movements . . . . .	92
6.3.2	Analysis of double step movements . . . . .	104
6.4	Discussion . . . . .	115
<b>7</b>	<b>Summary</b>	<b>119</b>
	<b>Bibliography</b>	<b>122</b>

Appendix A	Quaternions	129
Appendix B	Velocity rules with “Velocity box” model	131
Appendix C	Spread of rotation vectors at end points	136
Appendix D	Paths of control movements (position)	141
Appendix E	Orientations of forearm control movements	144
Appendix F	Orientations of upper arm control movements	147
Appendix G	Velocity of control (single step) movements	150
Appendix H	Forearm angular velocity of single step movements	153
Appendix I	Upper arm angular velocity of single step movements	156
Appendix J	Comparison of planning schemes for double step movements in two-dimensional Fick coordinates	159
Appendix K	Summary of errors during 2D superposition	168
Appendix L	Comparison of planning schemes for double step movements in rotation vector space	171
Appendix M	Summary of errors after superposition in rotation vector space	180

# Chapter 1

## General introduction

This work deals with strategies for the generation of three dimensional, fully extended arm pointing movements. These are movements where the out-stretched arm moves from pointing at one target to another. Such a movement is performed by humans with little thought, but despite the apparent simplicity of these movements, there is much that is still unclear about the mechanisms that generate these movements.

### 1.1 Trajectory formation

Early studies of arm movements with the hand constrained to a plane (and hence two dimensional movements) showed that the hand path during such movements is consistent, both for a single subject and between subjects (Georgopoulos et al., 1981; Soechting & Lacquaniti, 1981). Such movements have an invariant, single peaked velocity profile. Movements in the horizontal plane have also been observed to follow a straight line (Morasso, 1981). These findings suggest that such movements are planned in Cartesian coordinates at the hand level (Hollerbach, 1982), that is, in extrinsic coordinates. This implies that the central nervous system (CNS) later transforms the plan from extrinsic coordinates into a pattern of joint covariation (the plan in terms of joint coordinates). This transformation is non-linear and non-trivial be-

cause additional functional constraints are required due to joint redundancy. (Desmurget et al., 1998).

The other option would be to plan the movements in joint coordinates - the Cartesian coordinates at the start and the end of the movement would be converted to joint coordinates, and then the movement would be planned in joint space, in intrinsic coordinates. Due to the non-linear relationship between Cartesian and joint coordinates, invariant paths in joint coordinates do not in general represent invariant paths in Cartesian coordinates. In contrast to the above results, some experiments suggest that invariance is not seen in Cartesian coordinates. For example, in Atkeson & Hollerbach (1985) it was found that the curvature of unrestrained point to point movements in the vertical plane was dependent on the location in the workspace. In a cylinder grasping experiment, Desmurget & Prablanc (1997) found stable joint covariation patterns, while the spatial paths were consistently curved and varied with respect to the orientation of the object to be grasped.

An explanation of the conflicting results mentioned previously was suggested by Desmurget et al. (1997). From their experimental results and those from other studies, they concluded that compliant and unconstrained movements are planned differently - compliant movements (motion that is constrained by an external contact) are planned in task space and hence show straight line trajectories, while unconstrained movements are not planned in task space. Desmurget et al. (1998) presented several possible explanations for the different planning strategies. They suggested that in constrained movements, the general strategies used by the CNS are not relevant because of the constraints of the task. Planning planar compliant movements, which entails constraints on the direction of the acceleration in extrinsic coordinates, is easier in task space, while unconstrained movements do not need to consider these constraints.

Alternatively, it has been suggested that the differences in curvature between horizontal and vertical movements may be due to difficulties in dealing with gravity (Atkeson & Hollerbach, 1985), or due to distortions in the per-

ception of a straight line (Wolpert et al., 1995).

## 1.2 Internal models

Internal models are a way of modeling the processes in the brain from the desired motor event to the issuing of motor commands (Kawato, 1999), and can be used for modeling the generation of extended arm trajectories. Arm movements are too fast for the brain to solely use biological feedback to control the movement (Kawato, 1999). Internal models, which contain an acquired inverse dynamics model of the arm, can be executed to achieve the movement.

The kinematics of the arm refer to the geometrical and time-based properties of the motion - the displacements, velocities and accelerations. Kinematic models look at the motion without considering the forces necessary to achieve such movements. The minimum jerk model (Flash & Hogan, 1985) is an example of a kinematic model - it predicts straight line paths for movements in a horizontal plane. After planning at a kinematic level, the forces necessary to generate the movement must be computed. In the case of the minimum jerk model, the necessary joint torques for these movements could be calculated using the equilibrium point hypothesis (Flash, 1987).

The subject of dynamics deals with the forces and torques that produce motion. The forces and torques are related to the kinematics through coupled nonlinear differential equations. An example of a dynamic model is the minimum torque-change model (Uno et al., 1989). This model predicts hand path by minimizing the sum of square of the rate of change of torque integrated over the entire movement.

Soechting & Flanders (1998) concluded that neither a kinematic nor a dynamic model could successfully account for all features of arm movements, but that movements are constrained by optimality criteria that take into account both kinematic and dynamic considerations.

## 1.3 Thesis Outline

This work considers the following questions:

1. What strategies, if any, are used in extended arm movements to deal with kinematic redundancy, that is, which orientations from the infinite number of possibilities are selected? Can a rule valid for extended arm movements in the entire workspace be determined? Is adherence to the rule different during the movement and when stationary, or different for point to point or perturbed trajectories?
2. What models can be used to describe the generation of trajectories for extended arm movements? Do the models describe both simple point to point movements and double step movements where the target jumps after the movement has begun? Is a superposition strategy used, or some other strategy? How is the torsion of the upper arm and forearm constrained throughout the movement?

**Chapter 2** presents different representations of rotations adopted in this research. Methods for the generation of, and conversion between rotation matrices, Fick coordinates and rotation vectors are presented, as well as techniques for calculating the coordinate and angular velocity.

**Chapter 3** introduces the concepts involved with kinematic redundancy. It explains a solution to the degrees of freedom problem known as Donders' law, and describes studies of the eye, eye/head system and the arm that show the applicability of this law.

**Chapter 4** presents the methods and results of an experiment designed to test the validity of Donders' law under a range of situations. The variation seen in the different components of the rotation vectors are compared, and surfaces, which can act as constraints on the rotations, are fitted to the rotation vectors that describe the movements. These surfaces are compared

for movements in several different situations. The study aims to determine which strategies could realistically be used for constraining the orientations of the arm.

**Chapter 5** describes in more detail models for trajectory generation for eye saccades and arm movements, and suggests some novel models. The use of superposition to describe double step movements is explained and the implications for the various models are considered. The theoretical feasibility of these models is considered, and predictions are generated for the appropriate schemes.

**Chapter 6** presents an experiment to test the predictive powers of the appropriate models presented in Chapter 5. In relation to these models, the features of the trajectories are considered. The aim of this chapter is to find and experimentally confirm a model that describes the full three dimensional behaviour of the arm during extended arm pointing movements.

# Chapter 2

## Representations of rotations

There are many ways of parameterizing 3D rotations, and the selection of an appropriate parameterization can aid in analysis. The representations adopted in this research will be presented in this chapter. Unlike position, the combination of rotations is not commutative, and with some parameterizations, even the seemingly simple task of composing two rotations becomes very difficult.

The coordinate system adopted in this research was defined such that the  $x$  axis is straight ahead, the  $y$  axis points horizontally to the left, and the  $z$  axis points vertically up. The origin is fixed in space. This is shown graphically in Figure 2.1.

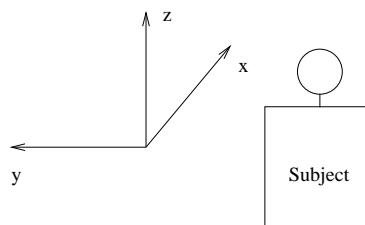


Figure 2.1: Coordinate system (back view).

A popular way of describing the rotation of a vector is a rotation matrix. A rotation matrix  $\mathbb{R}$  is a 3 by 3 matrix such that a vector in the direction of

$\vec{a}$  will be rotated to a vector  $\vec{b}$  by the rotation matrix  $\mathbb{R}$ :

$$\vec{b} = \mathbb{R} \cdot \vec{a} \quad (2.1)$$

where  $\cdot$  denotes matrix multiplication.

A rotation about the space-fixed  $z$  axis by  $\theta$  is given by (Haslwanter, 1995):

$$\mathbb{R}_z(\theta) = \begin{bmatrix} \cos \theta & -\sin \theta & 0 \\ \sin \theta & \cos \theta & 0 \\ 0 & 0 & 1 \end{bmatrix} \quad (2.2)$$

Similarly for rotations of  $\phi$  about the space-fixed  $y$  axis and  $\psi$  about the space-fixed  $x$  axis:

$$\mathbb{R}_y(\phi) = \begin{bmatrix} \cos \phi & 0 & \sin \phi \\ 0 & 1 & 0 \\ -\sin \phi & 0 & \cos \phi \end{bmatrix}, \quad \mathbb{R}_x(\psi) = \begin{bmatrix} 1 & 0 & 0 \\ 0 & \cos \psi & -\sin \psi \\ 0 & \sin \psi & \cos \psi \end{bmatrix} \quad (2.3)$$

Rotation matrices can be combined by matrix multiplication - this is equivalent to performing one rotation followed by another. For example, the rotation of the vector  $\vec{a}$  by  $\theta$  about the space-fixed  $z$  axis, followed by a rotation of  $\phi$  about the space-fixed  $y$  axis is given by

$$\vec{c} = \mathbb{R}_y(\phi) \cdot \mathbb{R}_z(\theta) \cdot \vec{a} \quad (2.4)$$

Equation (2.4) can also be reinterpreted as rotations about limb-fixed axes, that rotate with the limb. It is equivalent to performing a rotation about the limb-fixed  $y$  axis by  $\phi$ , then about the rotated  $z$  axis by  $\theta$ . A more complete description of this phenomenon is given in Haslwanter (1995).

A three dimensional rotation can be expressed as the composition of three one-dimensional rotations. In robotics, a commonly used system is that of Euler angles Craig (1986). A different system used in the oculomotor community (which is one of many possible representations) is the Fick system (Van Opstal, 1993). A rotation is first made about the vertical axis ( $\theta_F$ ), then

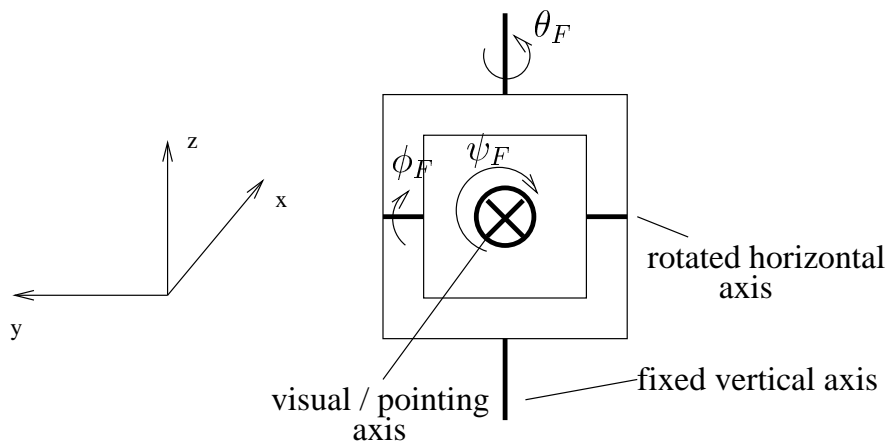


Figure 2.2: A Fick system of rotations (back view). A rotation is first made about the fixed vertical axis with angle  $\theta_F$ , followed by a rotation about the rotated horizontal axis, with angle  $\phi_F$ , and lastly a rotation about the visual / pointing axis of  $\psi_F$ .

about the rotated horizontal axis ( $\phi_F$ ), and finally about the new visual / pointing axis ( $\psi_F$ ), as shown in Figure 2.2. This sequence of rotations can be written using rotation matrices:

$$\mathbb{R}_F = \mathbb{R}_z(\theta_F) \cdot \mathbb{R}_y(\phi_F) \cdot \mathbb{R}_x(\psi_F) \quad (2.5)$$

This sequence of rotations is arbitrary, and could be replaced by a different sequence. Another commonly used system is the Helmholtz system (Van Opstal, 1993), which consists of a rotation about the horizontal axis by  $\phi_H$ , followed by a rotation about the rotated horizontal axis by  $\theta_H$ , followed by a rotation about the new visual / point axis by  $\psi_H$ :

$$\mathbb{R}_H = \mathbb{R}_y(\phi_H) \cdot \mathbb{R}_z(\theta_H) \cdot \mathbb{R}_x(\psi_H) \quad (2.6)$$

A more efficient method can be used to describe rotations, that also avoids the need to describe a rotation as a composition of three rotations. A non-redundant representation will be used here - the so called 'rotation vector' (Haslwanter, 1995).

## 2.1 Rotation vectors

The *rotation vector* (which strictly speaking is not actually a vector) describes a rotation about an axis  $\vec{n}$  (which is a unit vector) by the angle  $\theta$ , is defined by

$$\vec{r} = \vec{n} \tan\left(\frac{\theta}{2}\right) \quad (2.7)$$

The inverse of a rotation vector  $\vec{r}$  is defined by  $\vec{r}^{-1} = -\vec{r}$ . A rotation vector has 3 coefficients. The direction of the vector indicates the axis of rotation, while its magnitude is a measure of the angle. The use of the length to represent the angle can be problematic, because with angles close to  $180^\circ$ , the length of the vector will approach infinity. The pointing range used for this experiment will not come close to  $180^\circ$  hence this will not be a problem.

The composition of two rotation vectors, that is  $\vec{r}_a$  followed by  $\vec{r}_b$  is given by

$$\vec{r}_b \circ \vec{r}_a = \frac{\vec{r}_b + \vec{r}_a + (\vec{r}_b \times \vec{r}_a)}{1 - \vec{r}_b \cdot \vec{r}_a} \quad (2.8)$$

where  $\times$  is the vector (cross) product, and  $\cdot$  is the dot (inner) product. We can find the rotation necessary to go from a rotation  $\vec{r}_c$  (relative to some fixed orientation) to  $\vec{r}_d$  (relative to the same fixed orientation) which we will call  $\vec{r}_{dc}$  by letting  $\vec{r}_a = \vec{r}_c^{-1}$  and  $\vec{r}_b = \vec{r}_d$  in (2.8) to give

$$\vec{r}_{dc} = \frac{\vec{r}_d - \vec{r}_c + (\vec{r}_c \times \vec{r}_d)}{1 + \vec{r}_c \cdot \vec{r}_d} \quad (2.9)$$

The rotation of a vector  $\vec{s}_0 = [x_0 \ y_0 \ z_0]'$  by the rotation represented by a rotation vector  $\vec{r} = [r_x \ r_y \ r_z]'$  can be found using equations (A.2),(A.3)

and (A.4):

$$s = \begin{bmatrix} x \\ y \\ z \end{bmatrix} = \frac{1}{1 + r_x^2 + r_y^2 + r_z^2} * \begin{bmatrix} (1 + r_x^2 - r_y^2 - r_z^2)x_0 + 2(r_x r_y y_0 - r_z y_0 + r_y z_0 + r_x r_z z_0) \\ 2r_x r_y x_0 + 2r_z x_0 + y_0 - r_x^2 y_0 + r_y^2 y_0 - r_z^2 y_0 - 2r_x z_0 + 2r_y r_z z_0 \\ -2r_y x_0 + 2r_x r_z x_0 + 2r_x y_0 + 2r_y r_z y_0 + z_0 - r_x^2 z_0 - r_y^2 z_0 + r_z^2 z_0 \end{bmatrix} \quad (2.10)$$

In the special case that this rotation is from the reference orientation that is pointing straight ahead ( $\vec{s}_0 = [1 \ 0 \ 0]^t$ ), the above equation simplifies to

$$s = \begin{bmatrix} x \\ y \\ z \end{bmatrix} = \frac{1}{1 + r_x^2 + r_y^2 + r_z^2} \begin{bmatrix} 1 + r_x^2 - r_y^2 - r_z^2 \\ 2(r_x r_y + r_z) \\ 2(-r_y + r_x r_z) \end{bmatrix} \quad (2.11)$$

A rotation vector can be derived from a rotation matrix (Haslwanter, 1995):

$$\vec{r} = \frac{1}{1 + R_{1,1} + R_{2,2} + R_{3,3}} \begin{bmatrix} R_{3,2} - R_{2,3} \\ R_{1,3} - R_{3,1} \\ R_{2,1} - R_{1,2} \end{bmatrix} \quad (2.12)$$

where  $R_{x,y}$  is the element in row  $x$  and column  $y$  in the rotation matrix.

The rotation vector corresponding to an orientation in the Fick system  $(\theta_F, \phi_F, \psi_F)$  can be found using Equations (2.5) and (2.12):

$$\vec{r}_{(\theta_F, \phi_F, \psi_F)} = \frac{1}{1 + \cos \psi \cos \theta + \cos \phi (\cos \psi + \cos \theta) + \sin \phi \sin \psi \sin \theta} * \begin{bmatrix} \cos \phi \sin \psi + \cos \theta \sin \psi - \cos \psi \sin \phi \sin \theta \\ \sin \phi + \cos \psi \cos \theta \sin \phi + \sin \psi \sin \theta \\ -\cos \theta \sin \phi \sin \psi + (\cos \phi + \cos \psi) \sin \theta \end{bmatrix} \quad (2.13)$$

## 2.2 Coordinate velocity vectors

There are two measures of velocity when considering rotations - coordinate velocity and angular velocity. Coordinate velocity,  $\dot{\vec{r}}$ , is calculated as the derivative of the rotation vector with respect to time (Van Opstal, 1993):

$$\dot{\vec{r}} = \frac{d\vec{r}}{dt} \quad (2.14)$$

As this gives the relative displacement per time unit, it is independent of the current position.

Velocities in Fick coordinate space can be converted to coordinate velocity space by taking the time derivative of (2.13):

$$\dot{\vec{r}}_{(\dot{\theta}_F, \dot{\phi}_F, \dot{\psi}_F, \theta_F, \phi_F, \psi_F)} = \frac{1}{4 \left( \cos \frac{\phi}{2} \cos \frac{\psi}{2} \cos \frac{\theta}{2} + \sin \frac{\phi}{2} \sin \frac{\psi}{2} \sin \frac{\theta}{2} \right)^2} * \begin{bmatrix} (1 + \cos \phi \cos \theta) \dot{\psi} - \dot{\theta} \sin \phi - \dot{\phi} \sin \theta \\ (\cos \psi + \cos \theta) \dot{\phi} + \cos \phi (\dot{\theta} \sin \psi + \dot{\psi} \sin \theta) \\ (1 + \cos \phi \cos \psi) \dot{\theta} - \dot{\psi} \sin \phi - \dot{\phi} \sin \psi \end{bmatrix} \quad (2.15)$$

Note that the coordinate velocity is dependent not only on the velocity in Fick angles ( $\dot{\theta}_F, \dot{\phi}_F, \dot{\psi}_F$ ) but also on the Fick angles themselves ( $\theta_F, \phi_F, \psi_F$ ).

## 2.3 Angular velocity vectors

The angular velocity vector describes an instantaneous rotation from one position to the next. The direction of the angular velocity vector indicates the axis of rotation, while the length describes the speed of rotation. The derivation of angular velocity is clearer using quaternions (which can then be converted into rotation vectors). Appendix A contains the definition of a quaternion.

The rotation of a vector  $\vec{s}_0$  can be expressed as

$$\vec{s}(t) = q(t) \vec{s}_0 q^{-1}(t) \quad (2.16)$$

Taking the derivative of this with respect to time gives:

$$\dot{\vec{s}}(t) = \dot{q}(t)\vec{s}_0q^{-1}(t) + q(t)\vec{s}_0\dot{q}^{-1}(t) \quad (2.17)$$

The definition of unity for quaternions says that  $qq^{-1} = 1$ . The time derivative of this is:

$$\dot{q}q^{-1} + q\dot{q}^{-1} = 0 \quad (2.18)$$

$$\Rightarrow \dot{q}^{-1} = -q^{-1}\dot{q}q^{-1} \quad (2.19)$$

$$\Rightarrow \dot{q} = -q\dot{q}^{-1}q \quad (2.20)$$

Using these identities, and (2.16), (2.17) can be rewritten as

$$\begin{aligned} \dot{\vec{s}}(t) &= \dot{q}q^{-1}q\vec{s}_0q^{-1} - q\vec{s}_0q^{-1}\dot{q}q^{-1} \\ &= \dot{q}q^{-1}\vec{s}(t) - \vec{s}(t)\dot{q}q^{-1} \end{aligned} \quad (2.21)$$

Now using the identity for quaternions (Van Opstal, 2001) (which can be easily obtained from (A.2)):

$$pq - qp = 2p \times q \quad (2.22)$$

(2.21) can be simplified to

$$\dot{\vec{s}}(t) = (\dot{q}q^{-1}) \times \vec{s}(t) \quad (2.23)$$

The angular velocity is related to the rotation by the kinematic relationship (Kreyszig, 1993)

$$\dot{\vec{s}}(t) = \vec{\omega}(t) \times \vec{s}(t) \quad (2.24)$$

Hence we have the expression for angular velocity (as a quaternion, although the scalar part is zero):

$$w(t) = 2\dot{q}q^{-1} \quad (2.25)$$

To convert this into rotation vector notation, first expand using quaternion multiplication.

$$\begin{aligned} \omega(t) &= 2(\dot{q}_0q_0^{-1} - \dot{\vec{q}} \cdot \vec{q}^{-1} + q_0\dot{\vec{q}} - \dot{q}_0\vec{q} + \vec{q} \times \dot{\vec{q}}) \\ \omega(t) &= 2(q_0\dot{\vec{q}} - \dot{q}_0\vec{q} + \vec{q} \times \dot{\vec{q}}) \end{aligned} \quad (2.26)$$

Note that the scalar component is zero, this is because

$$\begin{aligned}
\frac{d(|q|^2)}{dt} &= \frac{d}{dt} (q_0^2 + \vec{q} \cdot \vec{q}) \\
&= 2\dot{q}_0 q_0 + 2\dot{\vec{q}} \cdot \vec{q} \\
&= 0
\end{aligned} \tag{2.27}$$

and  $\dot{q}_0 q_0^{-1} = \dot{q}_0 q_0$  and  $-\dot{\vec{q}} \cdot \vec{q}^{-1} = \dot{\vec{q}} \cdot \vec{q}$ . Equation (2.27) equals zero because  $|q|$  is always 1. Converting into rotation vectors using (A.4) gives:

$$\begin{aligned}
\vec{\omega}(t) &= 2(q_0 \dot{\vec{q}} - \dot{q}_0 \vec{q} + \vec{q} \times \dot{\vec{q}}) \\
&= 2(q_0 \dot{q}_0 \vec{r} + q_0 q_0 \dot{\vec{r}} - \dot{q}_0 q_0 \vec{r} + q_0 \vec{r} \times (\dot{q}_0 \vec{r} + q_0 \dot{\vec{r}})) \\
&= 2(q_0^2 \dot{\vec{r}} + q_0 \dot{q}_0 (\vec{r} \times \vec{r}) + q_0^2 (\vec{r} \times \dot{\vec{r}})) \\
&= 2q_0^2 (\dot{\vec{r}} + \vec{r} \times \dot{\vec{r}}) \\
&= \frac{2(\dot{\vec{r}} + \vec{r} \times \dot{\vec{r}})}{1 + \vec{r} \cdot \vec{r}}
\end{aligned} \tag{2.28}$$

The last step was obtained by noting that for unit quaternions,

$$\begin{aligned}
\sqrt{q_0^2 + \vec{q} \cdot \vec{q}} &= 1 \\
\Rightarrow q_0^2 + \vec{q} \cdot \vec{q} &= 1 \\
\Rightarrow q_0^2 &= 1 - \vec{q} \cdot \vec{q} \\
\Rightarrow q_0^2 &= 1 - q_0^2 (\vec{r} \cdot \vec{r}) \\
\Rightarrow q_0^2 (1 + \vec{r} \cdot \vec{r}) &= 1 \\
\Rightarrow q_0^2 &= \frac{1}{1 + \vec{r} \cdot \vec{r}}
\end{aligned} \tag{2.29}$$

# Chapter 3

## Background on kinematic redundancy

### 3.1 Introduction

This chapter focuses on the kinematic redundancy of human limbs. Human limbs are made up of joints, which may have more than one degree of freedom - for example the shoulder has three rotational degrees of freedom. Due to the redundant degrees of freedom in the limbs, a certain posture of the end effector, whether it be the eye, head or hand, can be reached by numerous joint configurations.

In the tasks being considered here, the extended arm has four rotational degrees of freedom. A model of the arm being considered is shown in Figure 3.1. It should be noted that the joints have limited ranges due to physiological constraints - the approximate ranges of the joints are given in Table 3.1.

The workspace for this experiment, movements in front of the body, can be defined by half a sphere. To specify a point on this surface, only two degrees of freedom are needed. This means that any position on the surface of this half sphere can be achieved by an infinite number of joint configurations. When the arm is pointing in some direction, it is easy to see that just by

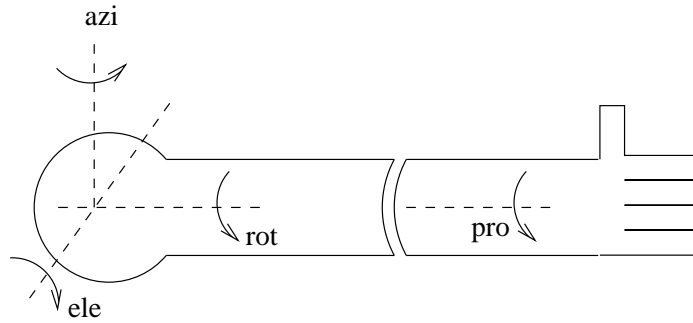


Figure 3.1: The model of the arm used in this research. The shoulder is approximated by a spherical joint, which can be modeled as rotations about three intersecting axes. The rotation about these axes gives the azimuth (azi), elevation (ele) and rotation (rot) of the upper arm. The rotation of the forearm relative to the upper arm is known as the pronation (pro). Flexion of the elbow was not allowed in this model. Additionally, rotation was not allowed at the wrist (due to the brace) and so the forearm and hand were considered as one link.

rotating the arm about its own axis, alternate configurations can be found that still maintain the same pointing direction.

The orientation of an object after rotations along two noncolinear axes is dependent on the order of the rotations (Gielen et al., 1997). This means that the orientation of a three degrees of freedom joint such as the shoulder or eye depends on previous rotations. If attention is not paid to the torsion, then physiologically impossible positions may result as an accumulation of torsion. A system is required to prevent such situations from occurring.

Studying solutions to the problem of kinematic redundancy in the eye may shed light on possible solutions for pointing with the arm. While dynamically the properties of the upper arm and the eye are very different, both have three degrees of freedom while only two are required for the task being considered (pointing with the arm, or gaze fixation with the eye).

From measurements of visual after-images at various positions, Donders discovered in 1848 that for the upright and stable head, each gaze direction

Joint angle	range (degrees)
elevation (ele)	180
azimuth (azi)	180
rotation (rot)	90
pronation (pro)	90

Table 3.1: Approximate range of motion of the joints in terms of the joint angles. The data is based on average values from Luttgens & Hamilton (1997).

has a unique 3-D eye orientation (Crawford, 1998). This is despite the fact that the eye is physically capable of rotating about the line of sight and generating many orientations that have the same gaze direction. The uniqueness of eye orientation for any gaze direction that was found became known as Donders' law. It does not, however, specify which orientation is to be used.

Listing later quantified this idea by stating that the axes of rotation from a particular reference position to any eye position will lie in a plane (Henn, 1997). This plane is now known as Listing's plane. Hence the orientation at any eye position is specified. These results were published and indirectly confirmed by Helmholtz in 1867 (Crawford, 1998).

## 3.2 Results from studies of eye saccades

Listing's plane can be parameterized using rotation vectors:

$$r_x = a + br_y + cr_z \quad (3.1)$$

where  $r_x, r_y$  and  $r_z$  are components of rotation vectors. If the coordinate system is appropriately translated and rotated (see section 4.2.4), so that the rotations are as if they came from a certain reference position, then (3.1) simplifies to be the Y-Z plane, that is

$$r_x = 0 \quad (3.2)$$

Such a system has the benefit that torsion is not accumulated, and is uniform everywhere. This has been experimentally confirmed for head-fixed, eye saccades fixating on distant targets (Tweed et al., 1990).

However it should be noted that for other situations, Listing’s law is modified or violated in a systematic fashion, such as when the eyeballs rotate inwards to see a close object or during head-free gaze shifts. A more detailed review can be found in Crawford (1998).

### 3.3 Results from eye and head studies

From an experiment examining gaze shifts under different situations, Glenn & Vilis (1992) found that the orientation of the head also obeys Donders’ law. However, the orientations were not confined to a flat Listing surface, but rather to a twisted surface. A second-order surface can be parameterized by the equation (Glenn & Vilis, 1992):

$$r_x = d + er_y + fr_z + gr_y^2 + hr_yr_z + jr_z^2 \quad (3.3)$$

The coefficient  $h$  is often called the twist score, as it is a quantitative measure of the degree of any twist in the surface.

The surfaces for head orientations found by Glenn and Vilis were discovered to be similar to the surface produced by a Fick gimbal system, with the torsional Fick angle ( $\psi_F$ ) set to zero. A gimbal is a system where the axes are nested within each other. A Fick gimbal, shown in Figure 2.2, is where the horizontal axis is nested in the vertical.

The Fick strategy (Hore et al., 1992) is where rotations are made where the torsional component in Fick coordinates,  $\psi_F$ , is set to zero. Expanding

(2.5) (while setting  $\psi_F = 0$ ) gives:

$$\begin{aligned} \mathbb{R}_F(\psi_f = 0) &= \begin{bmatrix} \cos \theta_F & -\sin \theta_F & 0 \\ \sin \theta_F & \cos \theta_F & 0 \\ 0 & 0 & 1 \end{bmatrix} \begin{bmatrix} \cos \phi_F & 0 & \sin \phi_F \\ 0 & 1 & 0 \\ -\sin \phi_F & 0 & \cos \phi_F \end{bmatrix} \begin{bmatrix} 1 & 0 & 0 \\ 0 & 1 & 0 \\ 0 & 0 & 1 \end{bmatrix} \\ &= \begin{bmatrix} \cos \theta_F \cos \phi_F & -\sin \theta_F & \cos \theta_F \sin \phi_F \\ \sin \theta_F \cos \phi_F & \cos \theta_F & -\sin \theta_F \sin \phi_F \\ -\sin \phi_F & 0 & \cos \phi_F \end{bmatrix} \end{aligned} \quad (3.4)$$

This can then be converted into a rotation vector using (2.12):

$$\vec{r} = \frac{1}{1 + \cos \theta_F \cos \phi_F + \cos \theta_F + \cos \phi_F} \begin{bmatrix} -\sin \theta_F \sin \phi_F \\ \cos \theta_F \sin \phi_F + \sin \phi_F \\ \sin \theta_F \cos \phi_F + \sin \theta_F \end{bmatrix} \quad (3.5)$$

Then the product of  $r_y r_z$  will be

$$\begin{aligned} r_y r_z &= \frac{\sin \theta_F \sin \phi_F \cos \theta_F \cos \phi_F + \sin \theta_F \sin \phi_F \cos \theta_F + \sin \theta_F \sin \phi_F \cos \phi_F + \sin \theta_F \sin \phi_F}{(1 + \cos \theta_F \cos \phi_F + \cos \theta_F + \cos \phi_F)^2} \\ &= \frac{\sin \theta_F \sin \phi_F (1 + \cos \theta_F \cos \phi_F + \cos \theta_F + \cos \phi_F)}{(1 + \cos \theta_F \cos \phi_F + \cos \theta_F + \cos \phi_F)^2} \\ &= \frac{\sin \theta_F \sin \phi_F}{1 + \cos \theta_F \cos \phi_F + \cos \theta_F + \cos \phi_F} \end{aligned} \quad (3.6)$$

It can be seen from equations (3.5) and (3.6) that  $r_x$  can be expressed in terms of this product:

$$r_x = s(r_y r_z), \text{ where } s = -1 \quad (3.7)$$

By repeating the above process in Helmholtz coordinates (2.6), then equation (3.7) will be the same, but with  $s = +1$ . Thus this formula provides a simple way of converting from coordinates in Fick and Helmholtz coordinates in the special case that the torsional component (in Fick or Helmholtz coordinates) is zero.  $s$  is known as the gimbal score (Glenn & Vilis, 1992). A score of

$-1$  refers to a Fick gimbal, and  $+1$  to a Helmholtz gimbal. A score of  $0$  is equivalent to a Listing's plane (3.2). An advantage of both types of gimbals with torsional angles of zero is that the orientation of the horizontal axis of the limb with respect to the horizon, and with respect to the pointing arm, remains constant.

A common example given of a Fick gimbal system is that of an earth-fixed telescope, which can rotate about a fixed vertical axis, and a moving horizontal axis. Although this is a multiple joint system, the Fick system can also be used with a single joint system like the extended arm. Whereas with the earth fixed telescope the rotation about each axis involves a separate joint, with the arm both rotations are applied to the same joint in order. The orientations reachable using such a sequence of rotations produce the surface which can act as a constraint on the permissible rotation vectors.

While the head showed a twisted Fick-like surface for regular gaze shifts, Ceylan et al. (2000) found that if pinhole goggles were worn, making the gaze shifts for the head similar to those of an eye, the twisted surface become flat like that for the eye. They concluded that this was because the motor system selects appropriate rules for motor optimization based on the constraints of the limb and the task.

The orientation of the eye in space (during head-free eye movements) was also found to have a Fick-like surface (Glenn & Vilis, 1992). A suggested reason for this was that the use of a Fick gimbal system means that horizontal gaze shifts are predominantly performed by the head, whereas vertical gaze shifts are predominantly performed by the eyes. This may serve to conserve energy - vertical gaze shifts using the eye use much less energy than rotating the head to achieve the same gaze shift.

### **3.4 Results from studies of hand movements**

Straumann et al. (1991) found that the orientations of the upper arm (while the elbow angle was fixed) during movements over a small range ( $\pm 25^\circ$  rela-

tive to the forward position) were a good fit to a flat plane, suggesting that arm rotations may also be planned on the basis of a Listing's plane.

Over a larger range ( $\pm 45^\circ$ ), Hore et al. (1992) observed that during straight-arm pointing, the arm assumed a similar orientation at a particular target irrespective of where it came from. The orientations were restricted to a surface similar to that produced by a Fick gimbal with zero torsional component. The twist was always in the same direction, and always less than that for a Fick gimbal (ie the gimbal score was between 0 and -1).

During pointing movements of the arm, Miller et al. (1992) and Theeuwes et al. (1993) also found a unique orientation of the arm for each pointing position, with a curved rather than flat plane.

Liebermann (1998) claimed that Listing's law was applicable for the orientation of the hand, as the deviations from a flat Listing's plane were small (1-2% of the available range). These deviations, he suggested, could be due to noise inherent in the system and need to be considered taking into account the desired accuracy of the task. These results are in contradiction to the conclusions reached by Soechting et al. (1995), that Donders' law does not hold in general for arm movements. They suggest that the posture of the arm at the end point is dependent on the starting point, and that kinematic factors alone could not predict the final posture of the arm. Instead they propose that a minimal work strategy could be used to predict the final orientation.

Postural invariance of the arm when reaching towards a cylinder has been found in several studies (Desmurget & Prablanc, 1997; Soechting & Flanders, 1993; Paulignan et al., 1997), and also for a small sphere (Grea et al., 2000). Posture is defined as a vector made up of the joint angles of the arm. Desmurget et al. (1998) noted that the posture of the end point is varied systematically as a function of the movement starting point. It is important to note that the findings provide evidence that the final posture is planned in advance, and not that there is a unique correspondence between an object location and posture (Grea et al., 2000).

Recently, in Admiraal et al. (2002), it was found that the fit of rotation vectors to a surface is different when the arm is stationary and when the arm is moving, in that the scatter, or thickness, of the surface was found to be less when the arm is stationary compared to when it is moving.

### 3.5 Double step paradigm

The double step target displacement paradigm (Georgopoulos et al., 1981; Soechting & Lacquaniti, 1983; Flash & Henis, 1991) is where a target is initially set for the subject to move towards, then a certain time after presentation of the first target, known as the inter-stimulus interval (ISI), the target jumps instantly to another location.

In an analysis of eye saccades using the double-step paradigm, Minken et al. (1993) found that the double-step paradigm sometimes produced strongly curved saccades. Listing's law was obeyed equally well in these cases even though they are not single axis rotations (as are point to point saccades).

Flash & Henis (1991) used the double-step paradigm to test a model of trajectory generation for compliant arm movements in a horizontal plane. They found that the resultant trajectory plan could be modeled as the superposition of the original trajectory plan in extrinsic coordinates (before the perturbation) added to a second trajectory plan for a movement from the first to the second target location. This issue will be examined in more detail in Chapter 5.

# Chapter 4

## Kinematic redundancy strategies

### 4.1 Introduction

The aim of this experiment was to test Donders' law for the extended arm during a pointing task, and to test the goodness of fit of various surfaces to the orientation of the arm under different conditions.

### 4.2 Methods

#### 4.2.1 Experimental setup

The subjects were required to point towards virtual balls, back projected on a screen (using a Barco Ltd projector). The virtual balls, generated by an OpenGL program running on a Silicon Graphics Octane workstation, were produced by means of different images presented to the left and right eyes (at 60Hz to each eye) using Crystal Eyes LCD stereo glasses which caused the subject to perceive the balls to be in front of the screen. The experimental setup is shown in Figure 4.1.

Throughout the experiments, data were collected by the placement of

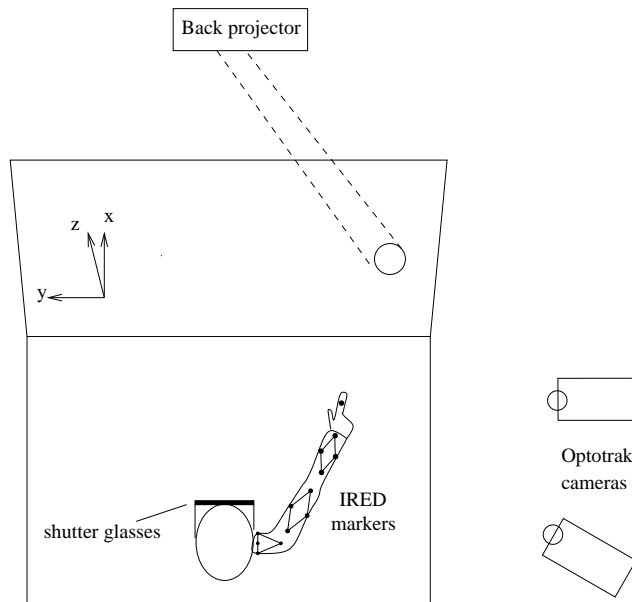


Figure 4.1: Experimental setup

14 infrared emitting diodes (IREDs), using the Northern Digital Optotrak system, to determine the location and orientation of the arm. The wrist and the forearm were considered as a single joint; this was forced on the subjects by use of a wrist brace to prevent movements at the wrist. Exo-skeleton frames were used to measure the rotations and position of the joints, as used in Liebermann (1998):

- The shoulder was defined as the centroid of a flat isosceles triangle, with its base fixed above the acromion, and positioned so that the base is orthogonal to the screen.
- The frame attached to the upper arm was rhomboidal, with its lower corner placed on the axis of rotation of the elbow joint.
- The forearm frame was also rhomboidal, but smaller, and attached to the wrist, measuring the rotations of the combined wrist/hand joint, and the position of the wrist.

- Two markers were attached to the index finger to provide the position of the end of the arm.

Redundant markers were used in order to have usable data when some markers were not recorded by the Optotrak. Markers not recorded were sometimes recovered using interpolation.

The data were collected in the coordinate system of the Optotrak, then transformed into a coordinate system relative to the screen. The data were collected at 100Hz, and smoothed by a 6th order Butterwoth filter. A point in the middle of the left edge of the screen was defined as the origin. The subjects stood so that their parasaggital plane was perpendicular to the screen, and the coordinate axes were defined so that the  $x$  axis points staight ahead (into the screen), the  $y$  axis points horizontally to the left, and the  $z$  axis points vertically upward (see Figure 2.1). A structure with markers was placed at the origin of this coordinate system, so that there was a marker at the origin, and one at 15cm along each of the  $x$ ,  $y$  and  $z$  axes. By recording the location of these markers in Optotrak coordinates for a period of ten seconds, a homogeneous transformation (Craig, 1986), represented as a 4 by 4 matrix, between the two coordinate systems was determined using linear regression.

As extended arm movements were considered, the objects were positioned to appear just beyond the finger tip (so that the subject's arm would not interfere with the perception of the target). The locations of the targets are shown in Figure 4.2.

It is possible from the markers to determine 5 joint parameters that fully define the orientation and rotation of the arm, while here, as only extended arm movements are being considered, only 4 parameters are being considered (see Figure 4.3). In addition, it is possible to calculate the location of the end effector in 3D space, and to generate rotation vectors for the arm (see section 4.2.4).

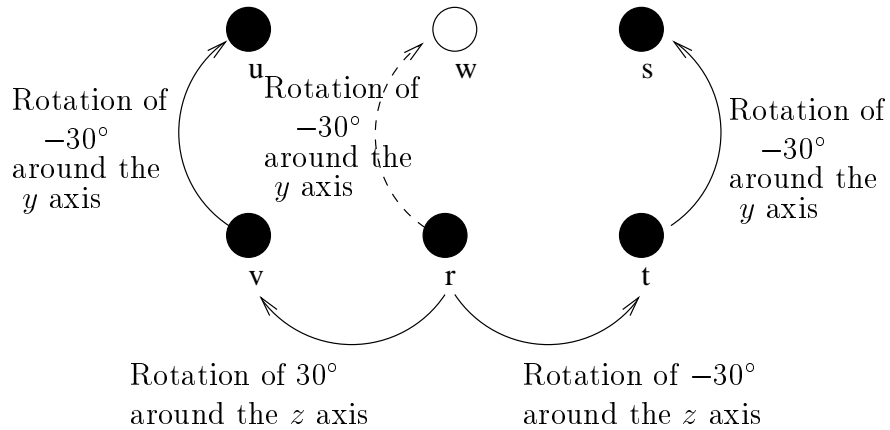


Figure 4.2: Locations of the targets. The central target  $r$  was positioned to be straight ahead just beyond the finger tip, at shoulder height. The location of the other targets relative to this are shown in the diagram. Target  $w$  was only used for subjects 1 and 2. The rotations are about a body fixed coordinate system with its origin at the shoulder.

## 4.2.2 Experimental protocol

Initially, the subjects were presented with a random display of balls to point at, to give them time to become familiar with operating in the environment. No measurements were taken during this time.

The subjects were asked to point with the arm straight ahead at shoulder level. This was recorded by the Optotrak for 10 seconds, and used for the initial reference position for generating rotation vectors.

Two types of movements were presented. The first were point to point, where the subject began with the arm pointing at some point (A), then at the start of the event the ball moved to a new location (B) to which the subject then needed to point at. The second type of movements were double step movements. They began like the point to point movements, however after the target in the new location has been presented (B), at some later time, the target jumped to a third location (C), to which the subject needed to point at instead of the first target. The experiment was divided into four

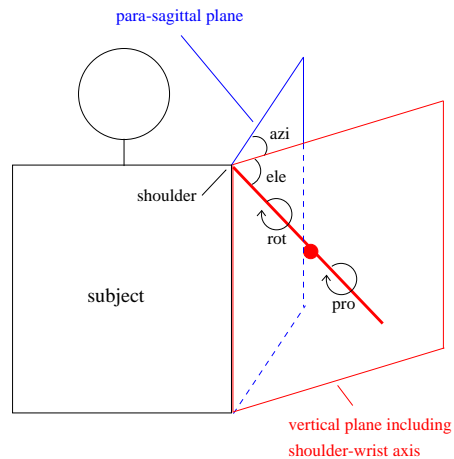


Figure 4.3: Extended arm joint parameters - three are required to define the orientation, treating the hand and forearm as one joint: azimuth( $azi$ ), elevation( $ele$ ), rotation ( $rot$ ) of the upper arm, and pronation( $pro$ ) of the forearm (based on notation from Grea et al. (2000)). These joint angles correspond to those shown in the model of the arm in Figure 3.1.

sets. Each set used two Inter Stimulus Intervals (ISI), defined as the time between the time the second (B) and third (C) targets were presented in the double step case. The ISI times used were 50ms & 300ms, 100ms & 400ms, 150ms & 550ms and 200ms & 700ms. This broad range of ISI times, including times shorter and longer than reaction time, were selected to investigate the different strategies depending on the time of switching.

Within each of these four sets, the movements were divided into 4 blocks, with the movements in each block beginning at the same point. The movements considered are shown in Table 4.1.

The single step (control) movements were selected so that for each double step movement, there would be a control movement corresponding to an unperturbed movement from the starting position to the first target, and another control movement from the first target to the second target. For example, the double step movement  $r \rightarrow s \rightarrow v$  had the corresponding control movements  $r \rightarrow s$  and  $s \rightarrow v$ .

	Starting at $r$	Starting at $s$	Starting at $t$	Starting at $u$
Double step movements	$r \rightarrow s \rightarrow v$ $r \rightarrow s \rightarrow t$ $(r \rightarrow t \rightarrow u)$ $(r \rightarrow t \rightarrow w)$	$s \rightarrow t \rightarrow u$	$t \rightarrow u \rightarrow s$	$u \rightarrow s \rightarrow v$
Control (point to point movements)	$r \rightarrow s$ $(r \rightarrow t)$	$s \rightarrow t$ $s \rightarrow v$	$t \rightarrow u$ $(t \rightarrow w)$	$u \rightarrow s$

Table 4.1: The movements performed in each trial, from the targets shown in Figure 4.2. Those in brackets were only performed for subjects 1 and 2

Each block consisted of 100 movements - each control movement was repeated 10 times and each double step movement was repeated 5 times, for each ISI. Between movements, there was a break of one second. A short rest was given between each block, and a longer rest was given between sets. The order of presentation of movements with the same starting location was randomized so the subject would not be able to predict the next movement.

### 4.2.3 Instructions to subject

*The following instructions were read to the subject at the beginning of the experiment:*

- You are free to drop out of the experiment at any time without any further explanation.
- For all the experiments, please stand straight, and try not to rotate your torso.
- Each movement will begin with a white ball. When you see the white ball, point towards the ball with your index finger. As with all the pointing, the ball will be just beyond your fingertip.

- For each block of movements, the ball will begin at the same location, although this may be different between blocks.
- When the ball turns red, this means that the ball is about to move.
- The ball will then turn green. You need to move your arm so that your index finger points to the current location of the ball.
- In some cases, the ball will then jump to a new location. If this occurs, you need to point to the ball at the new location.
- You may rest your hand on the stand when the ball disappears.
- There will be time to rest between blocks.

#### 4.2.4 Techniques of analysis

The rotation vectors need to be extracted from the 3D position data of the markers. The rotation vectors considered here are those of the rotation of the upper arm, and the forearm segments. The rotations were initially calculated relative to the reference position defined at the beginning of each trial, when the subject pointed straight ahead at shoulder height for 10 seconds.

A set of axes was defined based on the markers, shown in Figure 4.4, at the reference position, and at each time step. The rotation matrix  $\mathbb{R}$  (a 3 by 3 matrix) that defined the rotation from the reference axes ( $A$ ) to the axes at each time step ( $B$ ) can be stated as:

$$\mathbb{R}A = B \tag{4.1}$$

and hence can be found by

$$\mathbb{R} = BA^{-1} \tag{4.2}$$

More general methods, using singular value decomposition (Söderkvist & Wedin, 1993; Arun et al., 1987), were found to give the same results.

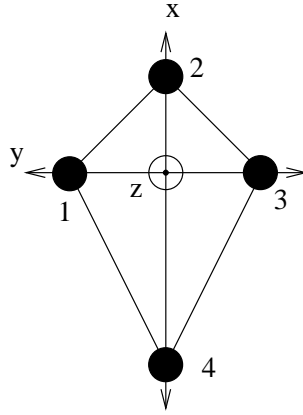


Figure 4.4: A set of axes was defined based on the forearm markers. The x-axis is defined as the unit vector in the direction from marker 4 to marker 2. The y-axis is the unit vector in the direction from marker 3 to 1. The z-axis (coming out of the page) was calculated by the cross product of the x and y-axes. A similar definition was used for the upper arm. The origin is located at the intersection of the three axes.

The rotation matrix  $\mathbb{R}$  was then converted to a rotation vector using equation (2.12).

In order to fit the data to the various surfaces that have been suggested (i.e., those in Equations (3.1),(3.3),(3.7)), it is necessary first to ensure that the rotation vectors are in the appropriate frame of reference.

In the eye, there is a reference position, known as the primary position, which is the unique position such that from this position, any other position can be reached by a rotation where the axis of rotation lies within Listing's plane. If this is the same as the reference position used for calculating rotation vectors, then in the eye, the torsion is always zero (i.e.  $r_x = 0$ ). It is possible to recalculate the rotation vectors so they will be as if they came from the actual primary position, which will not necessarily be the same as the reference position used in the experiments. The primary position will be orthogonal to the plane of rotation vectors.

However, for second order surfaces there is no vector that is orthogonal

to the plane (Gielen et al., 1997). If the second order terms are small, then fitting a flat plane will give similar coefficients to that for a second order surface. So the same transformation was applied for all the surfaces.

These calculations were performed based on the description in Tweed et al. (1990). First, the plane needs to be shifted so that the reference position will lie in the plane. If the parameter  $a$  in equation (3.1) is not zero, then the reference position does not lie in the plane. However, the rotation vector  $e = \begin{bmatrix} a & 0 & 0 \end{bmatrix}'$  is in the same direction as the reference position  $\begin{bmatrix} 1 & 0 & 0 \end{bmatrix}'$ , but will lie in the plane. So by rotating from this position rather than the reference position, the plane will pass through the origin. This can be achieved by composing the inverse of this vector with the rotation vectors, i.e. the rotation vector  $r$  becomes  $r \circ e^{-1}$  ( $e^{-1}$  is easily calculated as  $e^{-1} = -e = \begin{bmatrix} -a & 0 & 0 \end{bmatrix}'$ ).

Next, the plane should be rotated so that it will have the property that the torsion is zero in the plane, i.e.  $r_x = 0$ . This will enable Listing's law to be easily seen. The normal vector to the recalculated plane will be given by

$$\vec{V}_e = \frac{\begin{bmatrix} 1 \\ -b \\ -c \end{bmatrix}}{\sqrt{1 + b^2 + c^2}} \quad (4.3)$$

The rotation vector that then represents a rotation to the current representation from one where the normal vector of the plane will point down the  $x$  axis (ie so the rotation vectors in the plane will have zero torsion) can be obtained by performing the Clifford product (Tweed et al., 1990):

$$p = \frac{-\vec{V}_e \times \vec{i}}{\vec{V}_e \cdot \vec{i}} \quad (4.4)$$

where  $\vec{i}$  is a vector point in the direction of the  $x$  axis. So composing a rotation vector  $r$  with the inverse of the vector  $p$  will give the rotation  $p^{-1} \circ r$ . The plane will now be equivalent to the Y-Z plane.

By fitting a surface after these rotations it should be possible to see if it is better modeled by a flat plane, or a twisted surface. In terms of equation

(3.3),  $h$  can be considered as the twist score if it is not a flat plane. The rotation vectors were fit, after rotation, in a least squares sense to the 3 surfaces - a flat plane (3.1), a second order surface (3.3) and gimbal-like surface (3.7).

For the sake of comparison, the surfaces were fit to stationary points and non-stationary points. Additionally, to test if Donders' law applies differently during single step and double step movements, the fit of the surface was compared for both cases.

The “thickness” of the surfaces will be calculated to give a sense of how good a fit the surface is. This is defined here as the standard deviation of the distance from the plane in the torsional ( $r_x$ ) direction (Tweed & Vilis, 1990a).

Additionally, the variation of torsion ( $r_x$ ) was compared to the variation in the other components of the rotation vectors ( $r_y$  and  $r_z$ ).

## 4.3 Results

In the range of rotations being considered in this study, there is an approximately linear relationship between the rotation vector and the angle (because  $\tan(\theta) \approx \theta$  for small angles), so for ease of understanding, the axes will be marked in degrees.

### 4.3.1 Variation at movement endpoints

The variation of the rotation vectors at the movement endpoints were compared. Figures 4.5 and 4.6 show the range of rotation vectors of the forearm and the upper arm for subject 1. For both the forearm and the upper arm, the left column shows a ball around the target location - the spread of values in the  $r_y$  and  $r_z$  components is approximately equal - these are probably errors in locating and pointing to the target.

However, in the other two columns, an elliptical shape can be seen, with the major axis of the ellipse roughly parallel with the  $r_x$  axis. This shows

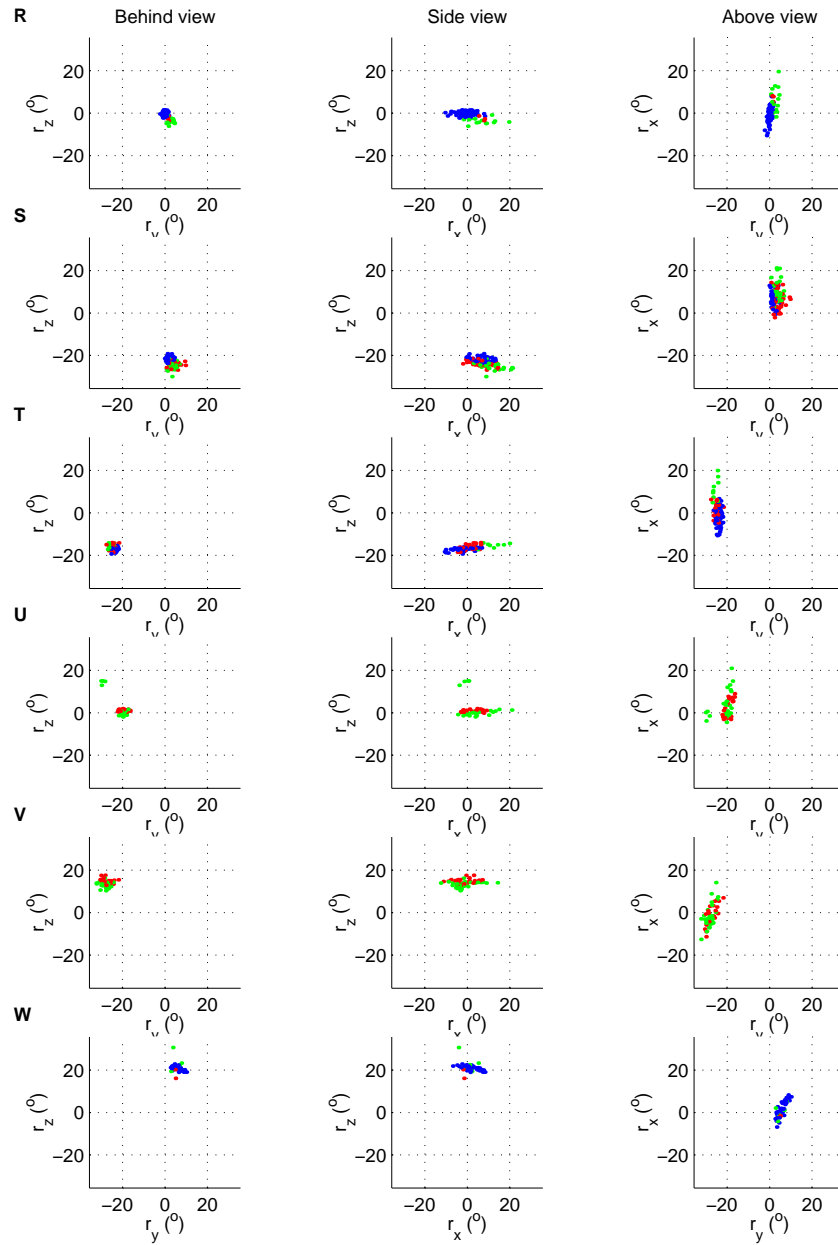


Figure 4.5: End point spread of forearm rotation vectors for Subject 1. Blue denotes movements starting at a particular point. Green denotes double step movements and red denotes control movements that end at a particular point.

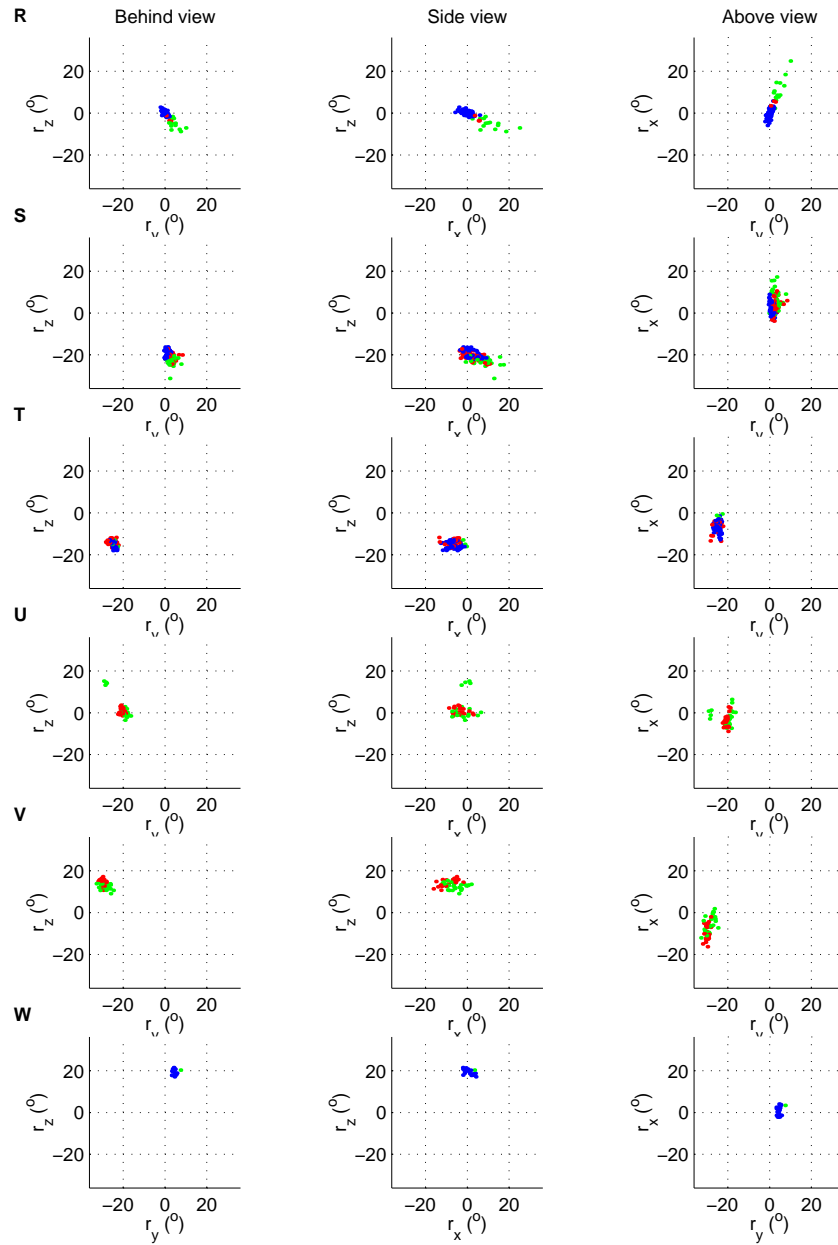


Figure 4.6: End point spread of upper arm rotation vectors for subject 1. Blue denotes movements starting at a particular point. Green denotes double step movements and red denotes control movements that end at a particular point.

that there is much greater variation in the  $r_x$  component than the other two components. The variation in the torsion at the start of the movements (shown in blue) is less than the variation at the end of the movements.

The reason why the major axis of the ellipse is not parallel to the torsional axis is because of the definition of the coordinate axes. The  $r_x$  component is the rotation relative to a space-fixed axis, and not to a limb fixed axis. This is known as the problem of “false torsion” (Haslwanter, 1995).

The major axis of the ellipse covering the points is shorter for upper arm movements, indicating less variation in the torsion. For some subjects, for example for subject 3, the difference in variation between the components is negligible for rotation vectors of the upper arm. The distribution of rotation vectors at a point for this subject is approximately circular. This can be seen in Figure 4.7.

Graphs for the other subjects can be found in Appendix C.

To summarize the results of the variation at the end points, the standard deviation in the  $r_x$ ,  $r_y$  and  $r_z$  components was calculated for movements ending at each end point. The results for the forearm and upper arm are presented in Figures 4.8 and 4.9 respectively.

If the torsional component ( $r_x$ ) is planned to a similar degree of accuracy, it would be expected that the variations in  $r_x$  at the endpoints would be the same as those found in  $r_y$  and  $r_z$ .

For the forearm, the variation in the torsional component ( $r_x$ ) can be seen to be significantly larger than the other components (this was confirmed by a t-test at the 0.2 level compared to one of the other components in 73% of the cases.) A similar result was found for the upper arm, although for some sets, such as the one shown in Figure 4.7 the variation between the components is very similar.

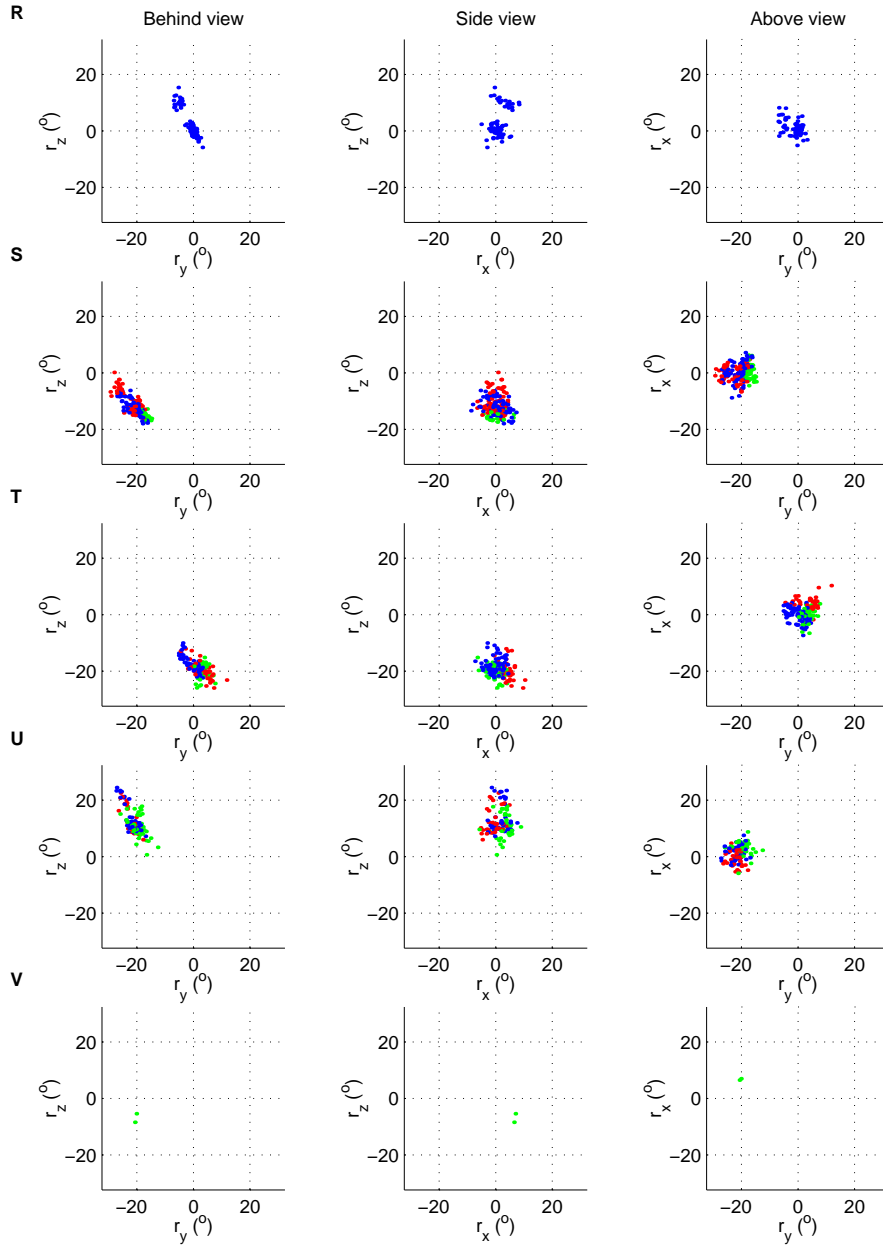


Figure 4.7: End point spread of upper arm rotation vectors for subject 3. Blue denotes movements starting at a particular point. Green denotes double step movements and red denotes control movements that end at a particular point.

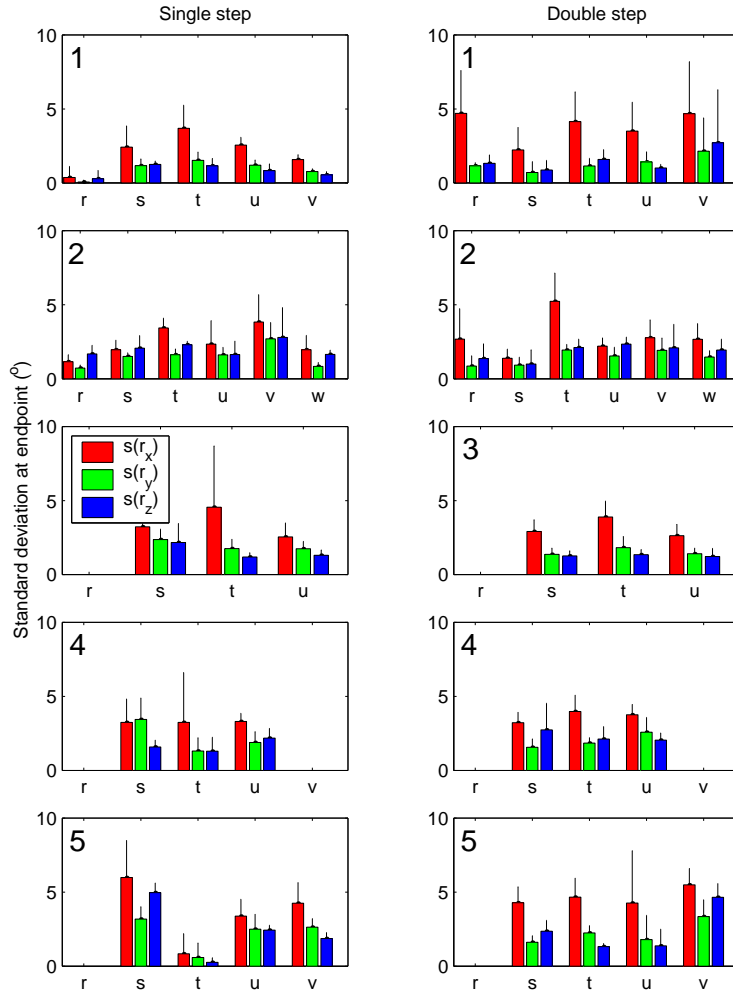


Figure 4.8: End point variation of rotation vectors of the forearm in components for the subjects 1-5. The letters ( $r, s, \text{etc}$ ) indicate the target position (see Figure 4.2). The bars show the mean of the standard deviation of each component of the rotation vector at each endpoint, while the error bars show it's standard deviation. The left column is for single step movements, the right column for double step movements. It is clearly seen that the variation in  $r_x$  (in red) is greater than that in  $r_y$  and  $r_z$ .

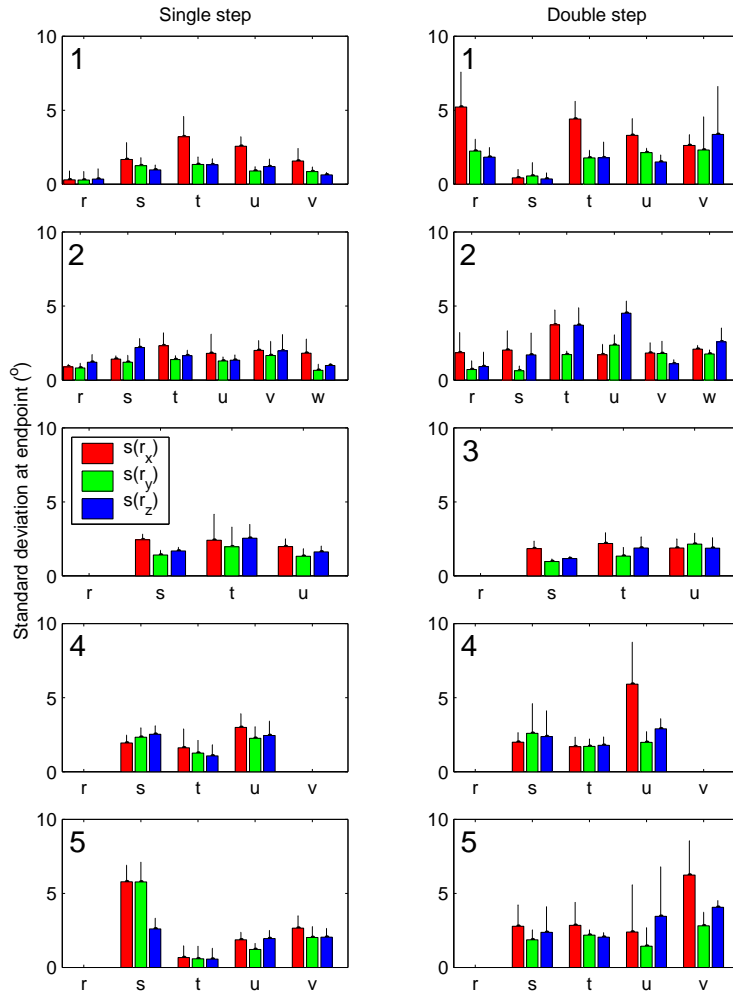


Figure 4.9: End point variation of rotation vectors of the upper arm in components for the subjects 1-5. The letters ( $r,s,etc$ ) indicate the target position (see Figure 4.2). The bars show the mean of the standard deviation of each component of the rotation vector at each endpoint, while the error bars show it's standard deviation. The left column is for single step movements, the right column for double step movements. Unlike the forearm rotations, the variation is not very different between the components.

### 4.3.2 Effect of considering orientation relative to starting point

In Hore et al. (1992), it was mentioned that the constraints on orientation were not dependent on the starting orientation of the hand. With a Fick gimbal rule, the orientation of the hand with respect to the horizon remains constant. They observed that when subjects were told to begin with different starting orientations, this orientation (with respect to the horizon) was fixed.

As no explicit instructions were given to the subjects about starting orientations, different starting orientations could be seen for the same starting point. In order to remove this effect each movement was considered as a rotation from its starting point. To allow movements starting from different starting points to be compared together, the rotation vectors for movements from a particular starting point were composed with the average starting orientation at that starting point.

To test whether this improved the fit to the surfaces, the thickness of a second order surface was compared, for movements considered relative to their starting points, and those unchanged. The results of this can be seen in Table 4.2.

From the table, for most movements, a slight improvement can be seen in using the modified method, although for some movements method 1 is equally as good or better. The values of thickness of the fitted surfaces for the forearm for all subjects were significantly better (t-test at 0.15 significance level) using Method 1, although this was not seen for the upper arm (this may be due to the larger values of thickness observed for the forearm).

Hence, this operation will be performed for the rest of the results, in order to remove the effect of the starting configuration. While the effect of this operation is small when fitting a surface to the rotation vectors from many movements, when considering the behaviour of individual trajectories (as is performed in Chapter 6), this operation can have a significant effect on the results.

Subject	Forearm					Upper arm				
	1	2	3	4	5	1	2	3	4	5
<b>Set 1:</b>										
Method 1	3.53°	3.43°	5.70°	3.86°	8.91°	3.31°	1.85°	3.15°	1.69°	6.28°
Method 2	3.40°	3.46°	3.90°	2.97°	7.99°	3.60°	1.84°	2.46°	1.66°	5.47°
<b>Set 2:</b>										
Method 1	3.32°	3.66°	3.39°	4.04°	6.80°	2.46°	2.17°	2.11°	2.50°	5.45°
Method 2	3.12°	3.71°	3.36°	4.14°	5.53°	2.70°	2.23°	2.14°	2.48°	4.54°
<b>Set 3:</b>										
Method 1	5.64°	4.22°	3.78°	4.58°	4.72°	3.36°	2.69°	2.22°	2.70°	4.29°
Method 2	4.30°	4.01°	3.51°	3.70°	4.82°	3.12°	2.61°	2.27°	2.14°	4.33°
<b>Set 4:</b>										
Method 1	2.84°	3.84°	3.51°	5.50°	5.92°	2.63°	2.76°	2.30°	2.35°	4.88°
Method 2	2.83°	3.80°	3.32°	4.82°	4.75°	2.61°	2.77°	2.24°	2.20°	4.88°

Table 4.2: Thickness of second order surfaces for subjects 1-5, Sets 1-4 for forearm and upper arm movements. Method 1 fits the rotation vectors relative to the reference position. Method 2 first finds the rotation vectors relative to the start of the movement, then this is composed with the average starting position for rotation vectors from this point.

### 4.3.3 Distribution of rotation vectors throughout the workspace

The rotation vectors of the forearm and upper arm, for two representative cases are shown. Figure 4.10 is a case with a (relatively) small range of  $r_x$  values, while Figure 4.11 has a large range of  $r_x$  values.

The workspace was also divided to see whether a better fit to the surfaces would apply for smaller regions. The workspace was trisected in both the  $r_y$  and  $r_z$  components, to give nine subspaces. This is shown visually for the side and top view for forearm and upper arm rotations in Figure 4.12 and 4.13. Figure 4.12 shows that the variation in  $r_x$  is greater than that of the other components, while in Figure 4.13, for the upper arm, the variation in the components is more similar. The variation in torsion is less when divided up in this way. This will be quantified in the following section.

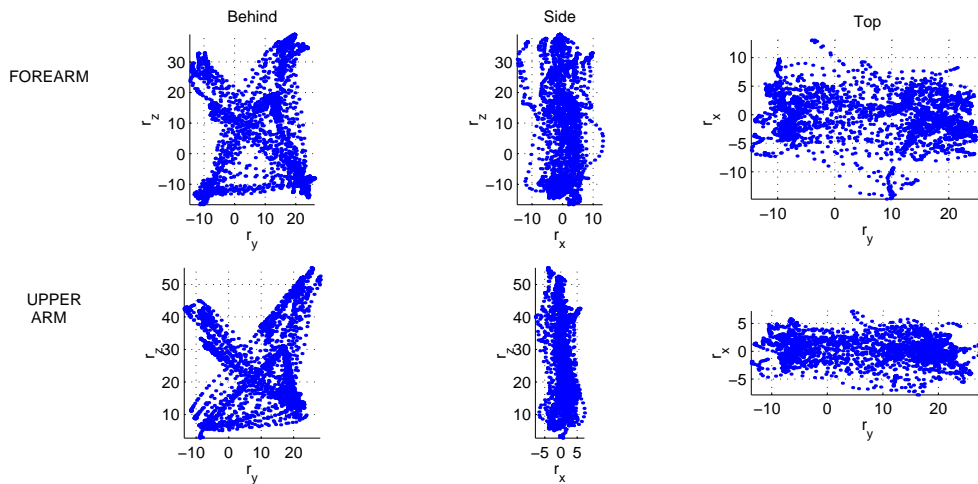


Figure 4.10: Rotation vectors for the forearm and upper arm during 100 3D single step and double step movements at each time step for Subject 2, Set 1. The range of  $r_x$  values is relatively small.

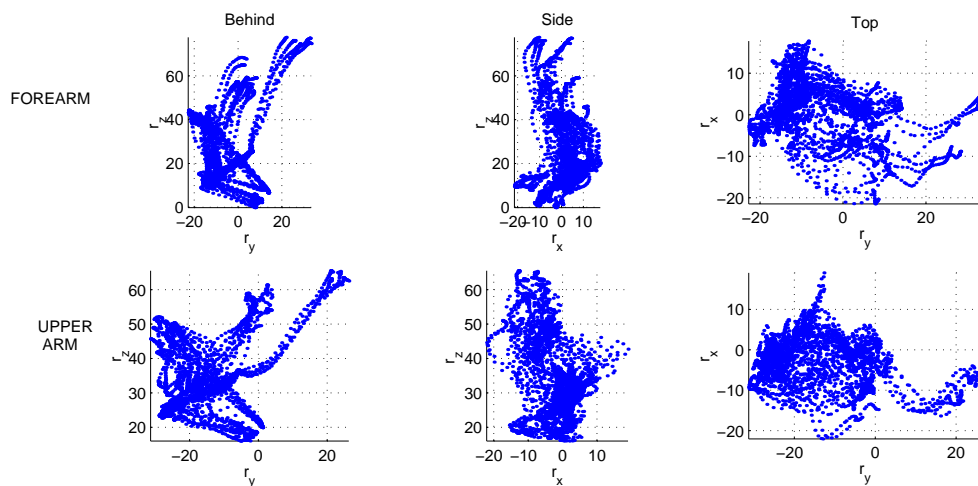


Figure 4.11: Rotation vectors for the forearm and upper arm during 100 3D single step and double step movements at each time step for Subject 5, Set 2. A large range of  $r_x$  values can be seen.

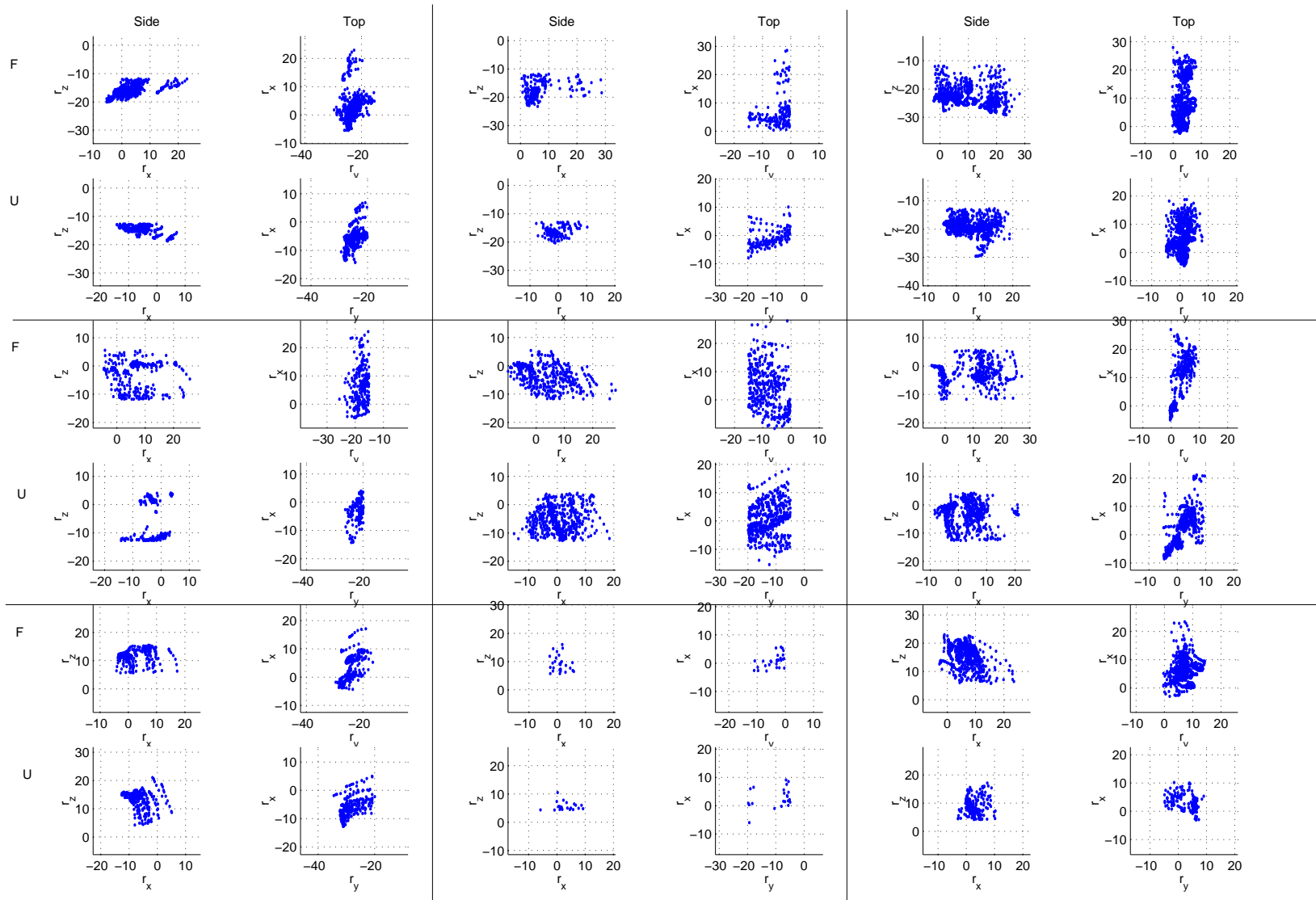


Figure 4.12: Rotation vectors for the forearm and upper arm divided into 9 smaller workspaces, for subject 1, set 3.

$F$  indicates forearm rotations, and  $U$  upper arm rotations.

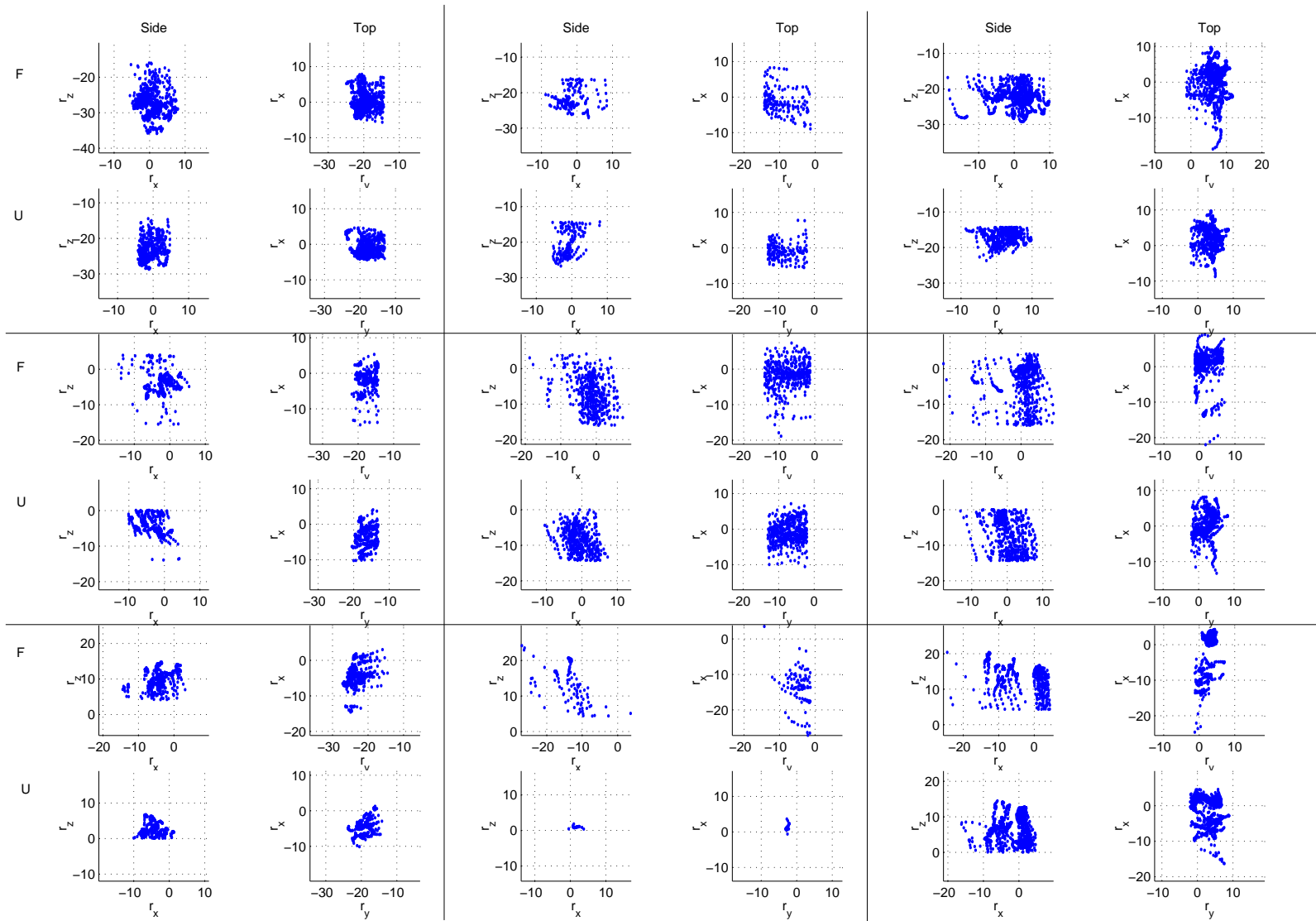


Figure 4.13: Rotation vectors for the forearm and upper arm divided into 9 smaller workspaces, for subject2, set 4.

$F$  indicates forearm rotations, and  $U$  upper arm rotations.

#### 4.3.4 Constraints on rotation vectors

Three different constraints have been suggested for constraining orientations in rotation vector space. These constraints are expressed in the form of a surface of permissible rotation vectors. The three surfaces are the flat Listing's plane, a second order surface, and a gimbal-like surface.

To test which of these surfaces provides the best description of the constraint on the rotation vectors during these movements, the best fit of these surfaces was found for the data in a least-squares sense. To examine how good these surfaces are as a description of the constraints, the goodness of the fit (measured by the thickness of the surface), and the consistency of the parameters will be examined.

Typical examples of these fits can be seen graphically in Figures 4.14 and 4.15. The rotation vectors are plotted together with the surfaces.

Due to the operations involved in making the orientations relative to the reference position, the representation of the orientations in rotation vector space are evenly distributed about the flat surface. In this sense, the flat plane provides a good average description of the rotations vectors found.

The second order surfaces seen are curved, with a small amount of twist. The fact that a curved surface was the best fit second order surface (rather than a flat plane, which would be produced if the last 3 coefficients were zero in equation (3.3)) means that a curved surface is a better fit than a flat plane.

The gimbal-like surface appears very similar to a flat plane - very little twist is seen. This means that the best gimbal-like surface that could be fit is very similar to a flat plane.

The parameters of the second order surfaces and the gimbal score for each subject and set that were calculated are displayed in Tables 4.3 and 4.4. The parameters for the flat plane are not displayed because the rotation vectors were rotated in order that equation (3.2) would hold.

For the forearm, while the twist score ( $h$ ) is mostly negative, there are several examples of where large positive values are found, indicating a twist

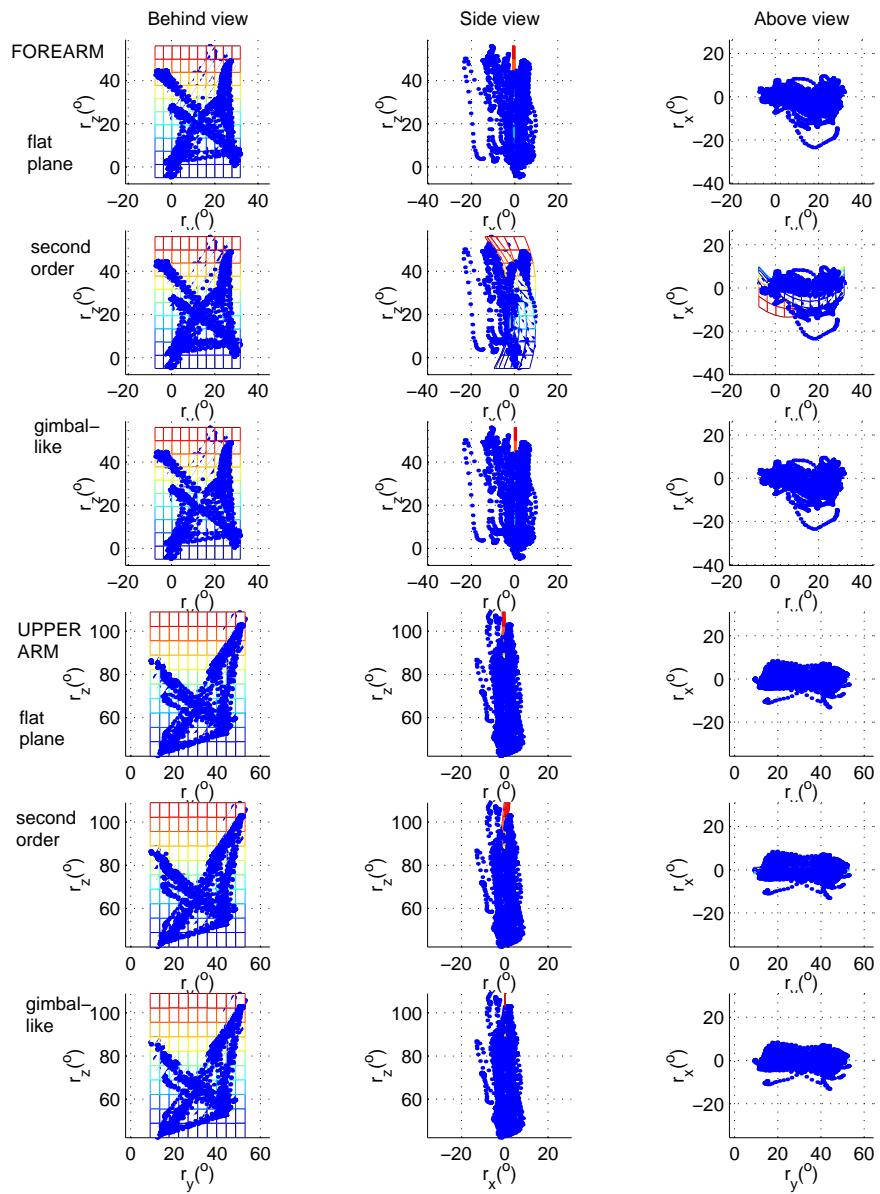


Figure 4.14: Rotation vectors for Subject 2, set 4 for the forearm and the upper arm. Also shown are the best fit plane, second order surface, and gimbal-like surface.

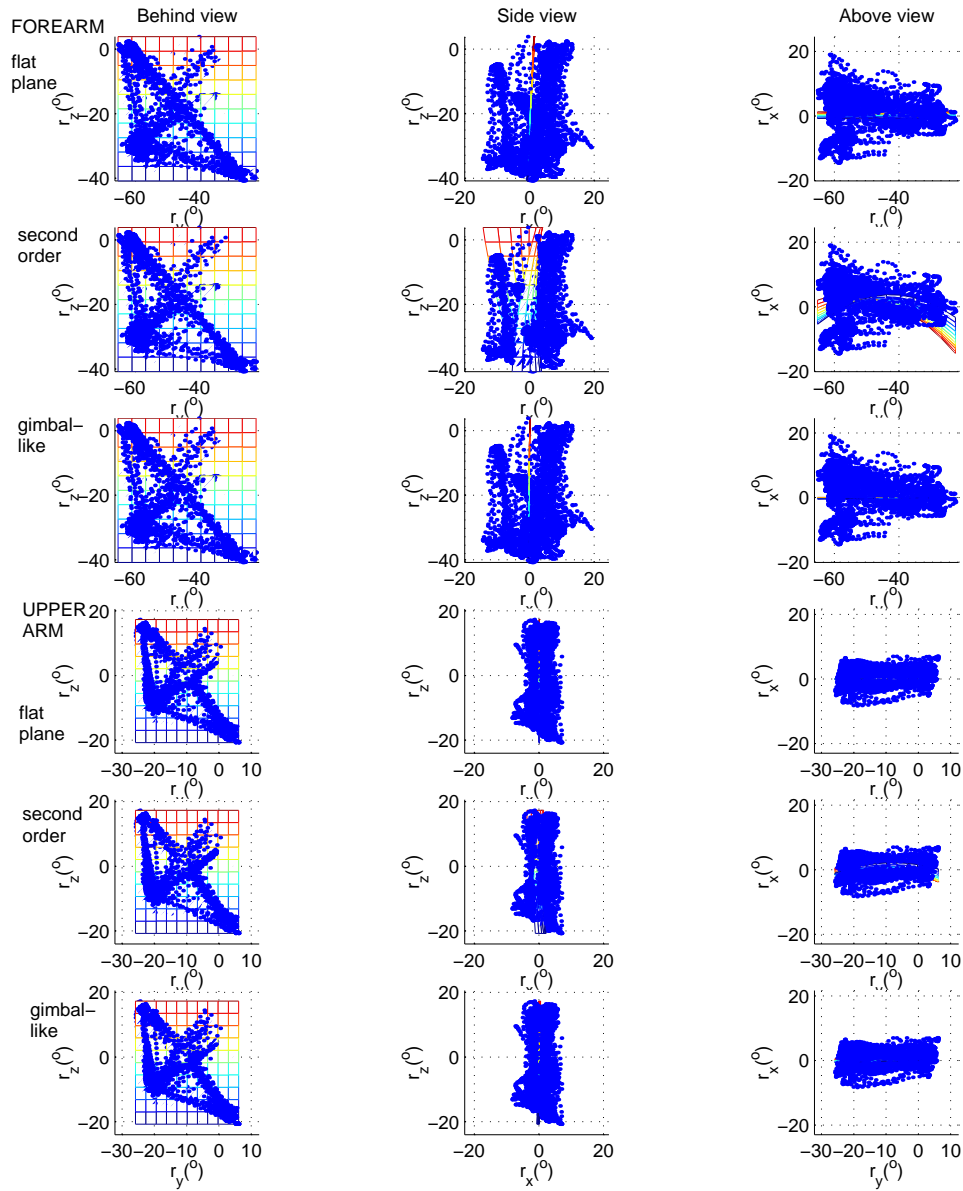


Figure 4.15: Rotation vectors for Subject 3, set 3 for the forearm and the upper arm. Also shown are the best fit plane, second order surface, and gimbal-like surface.

Set	d	e	f	g	h	j	s
<b>Subject 1</b>							
1	-0.008447	-0.009289	-0.052489	0.338877	-0.381586	0.415326	-0.145370
2	-0.017528	0.056516	0.096816	0.418025	-0.289868	-0.159763	-0.035380
3	-0.038689	0.173062	0.182283	2.780967	-0.470340	-0.633707	-0.062614
4	-0.004798	-0.059253	-0.053044	0.579002	0.169736	0.084269	0.064056
<b>Subject 2</b>							
1	0.003649	0.026955	0.030033	-0.096081	-0.242675	-0.144035	-0.192675
2	0.001115	-0.025864	0.037140	0.482575	-0.011960	-0.339512	-0.150335
3	-0.000611	-0.134718	-0.053014	1.489031	0.205208	-0.675133	-0.156943
4	-0.010089	-0.120091	0.051304	2.957662	0.908857	-1.124890	0.069704
<b>Subject 3</b>							
1	-0.385066	-0.289486	-1.470391	0.638212	-1.307160	-1.199910	0.002512
2	-0.086934	-0.837847	0.040417	-1.592400	-1.309902	1.051888	-0.079295
3	-0.026528	-0.700597	0.218490	-2.472881	-0.232724	1.225703	-0.003394
4	0.010540	-0.284482	0.489194	-1.407343	0.417429	1.689425	-0.009640
<b>Subject 4</b>							
1	0.008858	0.097937	0.043550	0.325320	-0.315618	-0.486323	-0.241563
2	0.001949	0.055227	0.012567	0.305771	-0.377662	-0.190073	-0.405073
3	-0.072070	-0.230205	0.384982	-0.380306	-0.254365	-0.660939	-0.156080
4	0.075517	0.390192	0.072054	0.574984	-0.434181	-1.365278	-0.254946
<b>Subject 5</b>							
1	0.029966	0.369797	-0.130575	1.515359	-0.098192	-1.132542	0.063204
2	0.017395	0.205631	0.130691	1.890623	1.165214	-1.352499	0.568675
3	0.041681	0.562959	-0.074129	1.746618	0.461363	-0.819242	0.096126
4	0.016782	0.313448	-0.089161	1.072558	-0.041693	-0.376280	0.091691

Table 4.3: Parameters of second order (d-j) and gimbal (s) surface fit to data for the forearm.

Set	d	e	f	g	h	j	s
<b>Subject 1</b>							
1	0.009701	0.134921	-0.150501	0.058824	-0.488272	0.337278	-0.061026
2	-0.034733	0.106341	0.196376	0.158002	-0.218414	-0.265220	-0.005103
3	0.001801	0.137074	0.001273	0.451447	-0.094167	-0.023114	0.008089
4	0.008347	-0.009145	-0.066692	-0.018922	0.071518	0.129513	0.032944
<b>Subject 2</b>							
1	-0.006850	0.087362	0.033371	0.139463	-0.481659	0.015245	-0.055954
2	-0.008661	0.063494	0.113327	-0.033919	-0.268843	-0.244151	-0.058434
3	-0.002492	0.044825	0.018801	0.039020	-0.408998	0.049321	-0.078882
4	-0.006242	-0.032182	0.048630	0.752270	-0.050517	-0.224167	-0.016369
<b>Subject 3</b>							
1	0.032123	0.354690	-0.184329	0.885276	-0.631129	0.235993	-0.030295
2	0.005716	0.076273	-0.006604	0.194386	-0.029035	0.017630	-0.005076
3	-0.002324	-0.129976	-0.038205	-0.797609	-0.426739	0.161868	-0.116377
4	-0.010221	-0.158729	-0.283794	-0.251591	-1.571283	-1.364667	-0.079147
<b>Subject 4</b>							
1	-0.030892	0.131467	0.294263	0.035608	-0.315464	-0.528033	-0.003059
2	0.001702	0.118376	0.106802	-0.089193	-0.536752	-0.401124	-0.001296
3	-0.035879	-0.410186	-0.129715	-0.926266	-0.725549	-0.237182	0.005402
4	0.000849	0.065549	0.079768	0.201168	0.364677	0.113212	0.000723
<b>Subject 5</b>							
1	0.017581	0.370465	0.350302	0.725894	-1.411697	-2.162019	-0.392372
2	-0.018909	0.204400	0.486142	-0.283048	-0.699817	-1.745229	-0.114350
3	0.011930	-0.070443	-0.101643	-0.689038	-0.992718	-1.076557	-0.553070
4	0.007838	0.023538	-0.286287	-1.236442	-0.316863	-1.523820	-0.351649

Table 4.4: Parameters of second order (d-j) and gimbal (s) surface fit to data for the upper arm.

in the opposite direction (for example, Subject 2, Set 4 and Subject 5, Set 2). The magnitude of the values is considerably smaller than those found by Hore et al. (1992), who found values of the twist score ranging from -0.61 to -1.10. The twist scores are not very consistent across subjects and even between sets.

The first three parameters ( $d, e$  and  $f$ ) are generally close to zero - this is because these parameters will be fit to a flat plane (which in this case will be  $r_x = 0$ ) if the other parameters are small. The parameters  $g$  and  $j$  refer to the curvature of the surface. Although there are a wide range of values for these parameters, for many of the subjects they are similar to the extent that they are of the same sign and order of magnitude.

A similar phenomenon is seen with the gimbal score for the forearm - while most of the values are negative, indicating that the gimbal is twisted in the direction of a Fick gimbal (see Figure 4.18), albeit by a small amount, there are several positive values. The gimbal scores for Subject 5 are all positive. This suggests that for the forearm, a different strategy is used by this subject compared to the other subjects.

The upper arm shows more consistency in the results, with the twist score for most of the sets negative. The gimbal score is also generally negative, although its magnitude is very close to zero (apart from subject 5). The small values for the Gimbal score suggest that, at least for the range being considered here, a gimbal-like surface does not provide a better model for specifying the orientation of the upper arm or forearm than a flat plane (which has a gimbal score of zero).

To show graphically the second order and gimbal-like surfaces, the side views were plotted for each subject and set, without the rotation vectors (for clarity). This is shown for the forearm (Figure 4.16) and the upper arm (Figure 4.17).

The goodness of the fit to the planes are compared by considering the “thickness” - the standard deviation of the distance from the plane. These results are summarized for forearm and upper arm movements in Tables 4.5

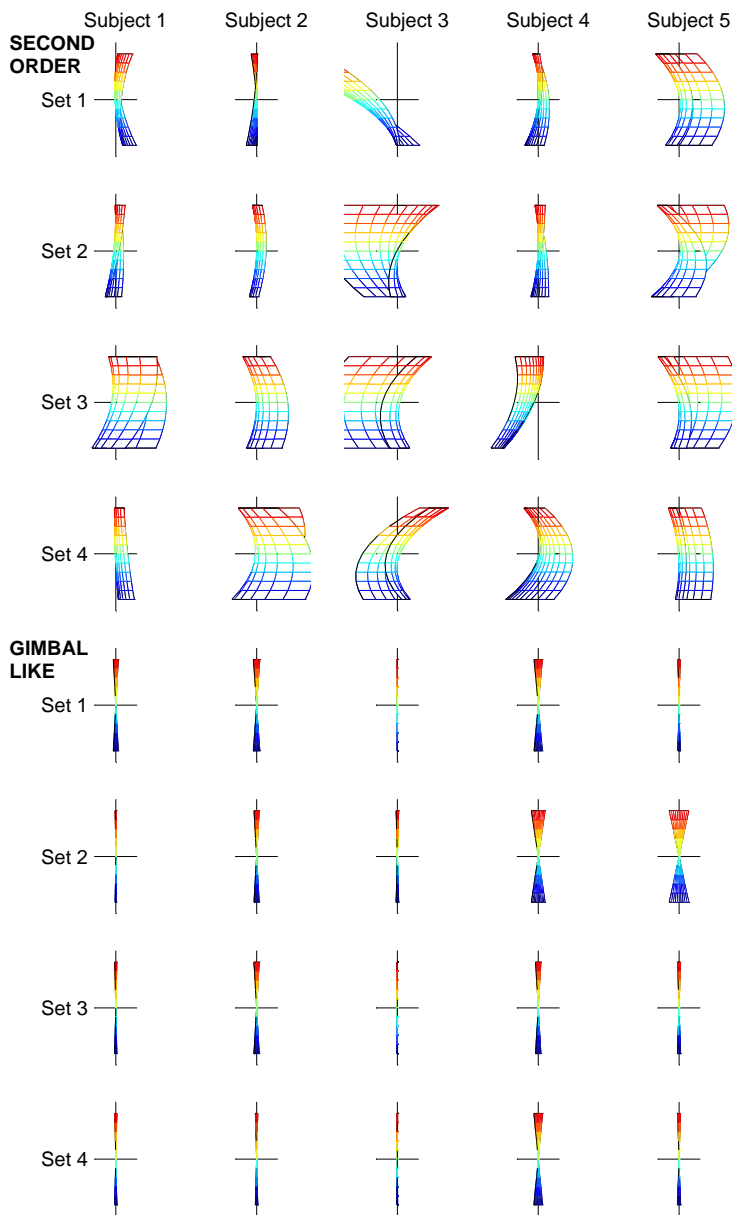


Figure 4.16: Side views of the fitted planes for the subjects 1-5 for forearm movements, for each set. The second order curves are the best fit to (3.3), while the gimbal-like are the best fit to (3.7). The curved nature of the second order surfaces can be seen, and within subjects, similar shaped surfaces are found, although they differ between subjects. The gimbal-like surfaces show very little twist, although the surfaces of Subject 4, which have the largest twist, all twist in the same direction

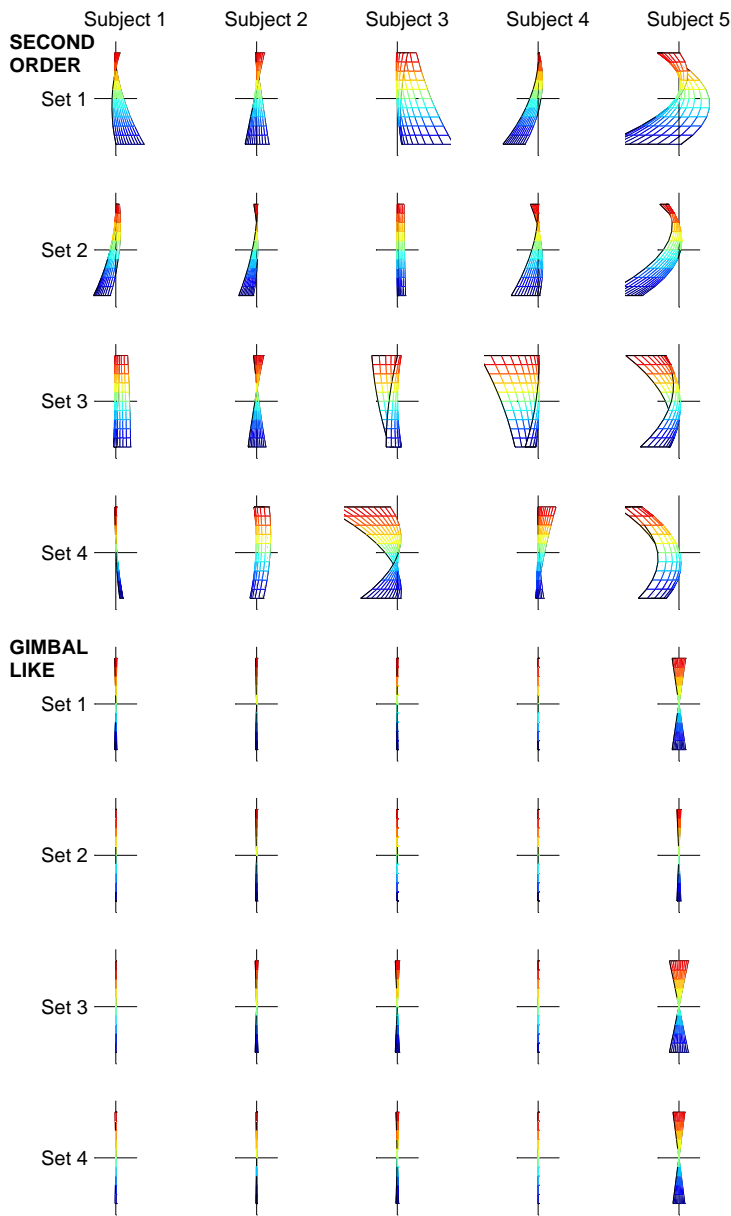


Figure 4.17: Side views of the fitted planes for the subjects 1-5 for upper arm movements, for each set. The second order curves are the best fit to (3.3), while the gimbal-like are the best fit to (3.7). The second order surfaces are curved to some extent, and a similar amount of twist can be seen in many of the surfaces. The twist of the gimbal-like surfaces is generally negligible - only Subject 5 shows a small amount of twist, all of which is in the same direction.

Subject		1	2	3	4	5
<b>Set 1:</b>						
Flat plane	whole WS	3.58°	3.54°	4.06°	3.28°	8.11°
	divided WS	2.79°	2.87°	3.28°	2.66°	5.94°
Second order	whole WS	3.40°	3.46°	3.90°	2.97°	7.99°
	divided WS	2.43°	2.65°	3.09°	2.61°	5.59°
Gimbal	whole WS	3.58°	3.50°	4.08°	3.05°	8.20°
	divided WS	2.98°	3.21°	3.67°	2.88°	7.23°
<b>Set 2:</b>						
Flat plane	whole WS	3.17°	3.81°	4.06°	4.48°	6.06°
	divided WS	2.42°	3.14°	3.13°	3.74°	4.92°
Second order	whole WS	3.12°	3.71°	3.36°	4.14°	5.53°
	divided WS	2.31°	2.88°	2.89°	3.46°	4.37°
Gimbal	whole WS	3.21°	3.77°	4.05°	4.20°	6.24°
	divided WS	3.00°	3.51°	3.58°	4.00°	5.82°
<b>Set 3:</b>						
Flat plane	whole WS	4.48°	4.06°	3.82°	3.85°	5.01°
	divided WS	3.09°	3.22°	3.04°	3.45°	3.74°
Second order	whole WS	4.30°	4.01°	3.51°	3.70°	4.82°
	divided WS	2.90°	3.08°	2.80°	3.20°	3.41°
Gimbal	whole WS	4.48°	4.07°	4.01°	3.93°	5.38°
	divided WS	3.61°	3.66°	3.71°	3.67°	4.82°
<b>Set 4:</b>						
Flat plane	whole WS	2.95°	4.06°	3.59°	5.09°	4.86°
	divided WS	2.40°	3.06°	2.88°	3.58°	4.14°
Second order	whole WS	2.83°	3.80°	3.32°	4.82°	4.75°
	divided WS	2.19°	2.98°	2.72°	3.34°	3.92°
Gimbal	whole WS	2.94°	4.12°	3.69°	5.27°	4.94°
	divided WS	2.80°	3.50°	3.33°	4.54°	4.58°

Table 4.5: Summary of thickness of different surfaces for forearm movements. The values represent the standard deviation of the distance from the surface in the  $r_x$  component. A comparison is made between the whole workspace, and the weighted average when divided into 9 equally sized (in  $r_y$  and  $r_z$ ) bins.

and 4.6.

From these tables, it can be seen that the thickness for the flat planes (see Figure 4.7) was significantly greater than that found in Liebermann (1998) (mean  $1.56^\circ$ ), while of a similar magnitude to that found in Hore

Subject		1	2	3	4	5
<b>Set 1:</b>						
Flat plane	whole WS	3.93°	1.99°	2.49°	1.94°	5.76°
	divided WS	3.10°	1.53°	2.08°	1.41°	4.33°
Second order	whole WS	3.60°	1.84°	2.46°	1.66°	5.47°
	divided WS	2.80°	1.47°	1.96°	1.31°	3.82°
Gimbal	whole WS	3.87°	1.95°	2.52°	2.33°	5.75°
	divided WS	3.38°	1.77°	2.24°	1.71°	5.41°
<b>Set 2:</b>						
Flat plane	whole WS	2.78°	2.37°	2.16°	2.77°	4.82°
	divided WS	2.12°	1.96°	1.93°	2.29°	3.48°
Second order	whole WS	2.70°	2.23°	2.14°	2.48°	4.54°
	divided WS	1.87°	1.82°	1.83°	2.18°	3.27°
Gimbal	whole WS	2.87°	2.37°	2.26°	4.12°	5.40°
	divided WS	2.70°	2.21°	2.05°	3.52°	4.52°
<b>Set 3:</b>						
Flat plane	whole WS	3.23°	2.65°	2.29°	2.44°	4.50°
	divided WS	2.25°	2.37°	2.05°	1.92°	3.44°
Second order	whole WS	3.12°	2.61°	2.27°	2.14°	4.33°
	divided WS	2.11°	2.23°	1.86°	1.79°	3.19°
Gimbal	whole WS	3.25°	2.63°	2.36°	2.77°	4.97°
	divided WS	2.55°	2.50°	2.19°	2.33°	4.12°
<b>Set 4:</b>						
Flat plane	whole WS	2.66°	2.80°	2.29°	2.25°	5.20°
	divided WS	2.18°	2.60°	2.01°	1.90°	3.74°
Second order	whole WS	2.61°	2.77°	2.24°	2.20°	4.88°
	divided WS	2.00°	2.36°	1.87°	1.75°	3.40°
Gimbal	whole WS	2.66°	2.81°	2.38°	2.57°	5.61°
	divided WS	2.41°	2.69°	2.16°	2.27°	5.18°

Table 4.6: Summary of thickness of different surfaces for upper arm movements. The values represent the standard deviation of the distance from the surface in the  $r_x$  component. A comparison is made between the whole workspace, and the weighted average when divided into 9 equally sized (in  $r_y$  and  $r_z$ ) bins.

et al. (1992). There was a small improvement for each subject for the fit to a second order surface (however, the fit to such a second order surface will never be worse than that to a flat plane). The lack of improvement for a second order fit may have been due to the magnitude of the rotations. Straumann et al. (1991) found that over a range of  $\pm 25^\circ$ , a flat plane (rather than a second order surface) constrained the rotation vectors of upper arm movements. Hore et al. (1992) found that over a range of  $\pm 30^\circ$ , the region of the twisted surface that is relevant is approximated well by a flat plane. This is similar to the range of orientations used in this experiment. This could explain why the twist may only have been noticeable if the range of rotations was larger.

The second order surfaces that were fitted generally had the same general shape (see Figure 4.16 and 4.17), due to similarity in the values of the curvature ( $g$  and  $j$ ) and the twist ( $h$ ) for each subject, although significant variation is seen between sets. Furthermore, variation is seen between subjects. For the forearm, the surfaces fit to the movements of subject 4 showed the closest fit to a Fick gimbal, and for the upper arm subject 5 showed surfaces with a small gimbal score. In general, however, the amount of twist shown when fit to a Fick gimbal was negligible, although it was usually twisted in the direction of a Fick gimbal (see Figure 4.18).

These results suggest that it is possible that a Fick gimbal strategy may be used for a larger range of rotations, but do not provide sufficient evidence. The lack of evidence may be attributed to the reasons mentioned above.

The lack of significant improvement in the thickness for a second order or gimbal surface rather than a flat plane, combined with the lack of consistency in the parameters leads to the conclusion that in general a flat plane is the best surface to use as a constraint on torsion.

The fit for the divided workspace was better than that for the entire workspace. When considering the second order surfaces, using a divided workspace gave a significantly better fit for all subjects (t-test at 0.2 significance level). This implies that by using local rules for the constraint of arm

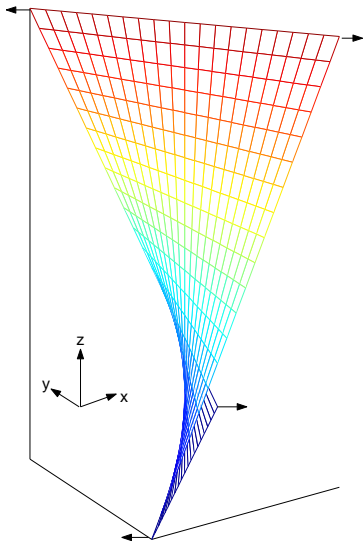


Figure 4.18: An example of a gimbal-like surface, where the twist is in the direction of a Fick gimbal (ie the gimbal score is negative). The upper left and lower right corner have positive torsion, while the other two corners have negative torsion. (The colours are an aid for judging the depth and have no additional meaning.)

orientations rather than a global rule, a better model for constraining the orientations can be found.

A summary of the thickness of the fit to a second order surface under a range of conditions can be found for the forearm (Table 4.7) and the upper arm (Table 4.8).

A comparison was made between the thickness of the plane if only stationary orientations are considered (i.e. those at the start and end points), and the thickness of the plane when the orientation at each time step is considered. These results can be found in Tables 4.7 and 4.8.

For a second order plane, for the forearm, the thickness of the plane for stationary movements was on average 14.3% less than that for all movements, while for the upper arm it was 19.0% less for stationary compared to all movements. These findings are similar to the results found in Admiraal et al. (2002) (they found a 9.5% improvement for the orientation of the upper arm). The t-test showed that the difference is significant for 3 of the 5 subjects at the 0.2 level for the forearm, and for all subjects (at the 0.2 level) for the upper arm.

	Subject	1	2	3	4	5
<b>Set 1:</b>						
All points	whole WS	3.40°	3.46°	3.90°	2.97°	7.99°
	divided WS	2.43°	2.65°	3.09°	2.61°	5.59°
Stationary	whole WS	2.84°	2.89°	3.82°	2.41°	7.57°
	divided WS	1.03°	1.28°	1.97°	1.84°	3.12°
Single step	whole WS	2.95°	2.91°	4.20°	2.03°	8.68°
	divided WS	1.71°	1.84°	2.35°	1.66°	4.59°
Double step	whole WS	3.25°	3.85°	3.52°	3.58°	6.56°
	divided WS	2.47°	2.64°	2.73°	2.98°	4.51°
<b>Set 2:</b>						
All points	whole WS	3.12°	3.71°	3.36°	4.14°	5.53°
	divided WS	2.31°	2.88°	2.89°	3.46°	4.37°
Stationary	whole WS	2.49°	3.03°	2.94°	3.59°	4.75°
	divided WS	1.24°	1.56°	2.30°	2.47°	2.32°
Single step	whole WS	2.80°	3.30°	3.32°	3.72°	5.33°
	divided WS	1.88°	2.13°	2.42°	2.58°	2.73°
Double step	whole WS	3.32°	3.64°	3.54°	4.53°	5.59°
	divided WS	2.36°	3.02°	2.82°	3.52°	3.81°
<b>Set 3:</b>						
All points	whole WS	4.30°	4.01°	3.51°	3.70°	4.82°
	divided WS	2.90°	3.08°	2.80°	3.20°	3.41°
Stationary	whole WS	3.93°	3.57°	3.43°	3.32°	4.16°
	divided WS	1.62°	1.94°	2.16°	2.62°	1.76°
Single step	whole WS	3.58°	3.43°	3.12°	3.04°	4.36°
	divided WS	2.64°	1.99°	2.40°	2.62°	2.50°
Double step	whole WS	3.51°	3.97°	3.61°	3.89°	5.15°
	divided WS	2.33°	3.20°	2.85°	3.33°	3.46°
<b>Set 4:</b>						
All points	whole WS	2.83°	3.80°	3.32°	4.82°	4.75°
	divided WS	2.19°	2.98°	2.72°	3.34°	3.92°
Stationary	whole WS	2.18°	3.48°	3.02°	3.49°	3.74°
	divided WS	1.06°	2.22°	2.30°	1.94°	2.19°
Single step	whole WS	2.47°	3.20°	2.52°	3.98°	3.98°
	divided WS	1.65°	2.13°	1.81°	2.52°	2.79°
Double step	whole WS	2.85°	4.18°	3.70°	5.40°	5.21°
	divided WS	2.21°	3.22°	2.92°	3.50°	4.17°

Table 4.7: Summary of thickness of second order surfaces for forearm movements. The values represent the standard deviation of the distance from the surface in the  $r_x$  component. A comparison is made between the whole workspace, and the weighted average when divided into 9 equally sized (in  $r_y$  and  $r_z$ ) bins.

	Subject	1	2	3	4	5
<b>Set 1:</b>						
All points	whole WS	3.60°	1.84°	2.46°	1.66°	5.47°
	divided WS	2.80°	1.47°	1.96°	1.31°	3.82°
Stationary	whole WS	2.83°	1.49°	1.89°	1.23°	4.40°
	divided WS	1.25°	0.71°	0.95°	0.76°	1.02°
Single step	whole WS	2.92°	1.64°	2.13°	1.47°	5.47°
	divided WS	2.05°	1.17°	1.55°	0.97°	2.87°
Double step	whole WS	3.66°	1.95°	2.61°	1.70°	5.07°
	divided WS	2.81°	1.43°	1.97°	1.34°	3.64°
<b>Set 2:</b>						
All points	whole WS	2.70°	2.23°	2.14°	2.48°	4.54°
	divided WS	1.87°	1.82°	1.83°	2.18°	3.27°
Stationary	whole WS	2.04°	1.83°	1.67°	2.11°	3.06°
	divided WS	0.74°	1.16°	1.35°	1.71°	1.35°
Single step	whole WS	2.03°	2.12°	1.80°	2.20°	4.00°
	divided WS	1.32°	1.62°	1.52°	1.95°	2.00°
Double step	whole WS	3.01°	2.22°	2.48°	2.57°	4.54°
	divided WS	2.00°	1.75°	1.94°	2.01°	2.99°
<b>Set 3:</b>						
All points	whole WS	3.12°	2.61°	2.27°	2.14°	4.33°
	divided WS	2.11°	2.23°	1.86°	1.79°	3.19°
Stationary	whole WS	2.31°	2.24°	1.82°	1.84°	3.14°
	divided WS	0.91°	1.45°	1.26°	1.51°	1.19°
Single step	whole WS	2.48°	2.30°	1.98°	1.89°	4.42°
	divided WS	1.78°	1.66°	1.54°	1.51°	2.77°
Double step	whole WS	3.20°	2.61°	2.39°	2.35°	3.73°
	divided WS	2.08°	2.17°	1.85°	1.90°	3.08°
<b>Set 4:</b>						
All points	whole WS	2.61°	2.77°	2.24°	2.20°	4.88°
	divided WS	2.00°	2.36°	1.87°	1.75°	3.40°
Stationary	whole WS	2.12°	2.50°	2.02°	1.95°	3.97°
	divided WS	1.11°	1.70°	1.48°	1.44°	1.34°
Single step	whole WS	2.14°	2.47°	1.88°	1.95°	5.07°
	divided WS	1.45°	1.97°	1.58°	1.42°	2.91°
Double step	whole WS	2.65°	2.98°	2.45°	2.43°	3.87°
	divided WS	1.97°	2.50°	1.97°	1.88°	2.97°

Table 4.8: Summary of thickness of second order surfaces for upper arm movements. The values represent the standard deviation of the distance from the surface in the  $r_x$  component. A comparison is made between the whole workspace, and the weighted average when divided into 9 equally sized (in  $r_y$  and  $r_z$ ) bins.

There was no significant difference in the thickness of the surfaces for orientations that were part of point to point trajectories compared to those that were part of double step movements. This can also be seen from the results in Tables 4.7 and 4.8. In some cases, the single step movements were better, while in others, the double step movements were better. These findings are similar to those of Minken et al. (1993), where it was found that highly curved eye movements produced as a result of the double step paradigm obeyed Listing's law equally as well as point to point movements.

The fit to the surfaces of rotation vectors for the upper arm was significantly better than for the forearm (by a t-test on the thickness of second-order surfaces at the 0.2 level). This suggests that upper arm movements are more constrained than forearm movements.

## 4.4 Discussion

In the results it has been shown that a surface can be fit to the rotation vectors for the forearm and upper arm during extended arm movements, and hence that a form of Donders' law is valid for such movements. A flat surface is a reasonable approximation to this surface, similar to results found for movements of the eye in a head fixed system (Tweed & Vilis, 1990b) and other studies of the extended arm (Liebermann, 1998). The thickness found for the surfaces, however, is larger than those found for the eye.

The thickness of the surfaces makes it difficult to differentiate further between the different models. A slightly better fit is achieved by using a second order surface, although the second order surfaces found were not consistent between sets and subjects. A significant improvement in the fit is also possible by considering the surfaces when the workspace is divided.

The results also seem to suggest that if considered over a larger workspace, the fit may be better to the rotation vectors reachable using a Fick gimbal with zero Fick torsional angle ( $\psi_F = 0$ ), similar to the findings in Hore et al. (1992). Experiments over a larger range of orientations would be necessary

to conclusively test this prediction. Such a system has the property that the wrist orientation with respect to the horizon, and with respect to the line of sight, remains constant. The absence of this finding in this experiment could also be due to the recording equipment or paradigm used, which may encourage such behaviour.

It was found that stationary orientations have less scatter from the Donders' surface than the orientations during the movement. In Admiraal et al. (2002), it is suggested that this may be due to errors in executing the motion plan because of difficulties in predicting the complex biomechanical properties of the arm, or because of differing delays from the central nervous system to different muscles.

In contrast, no significant difference was seen between single and double step movements. Linear superposition of the two control trajectories (in rotation vector space) would, in general, produce values of torsion different to those for a single step movement. As there is no difference seen, this suggests that superposition does not take place on the torsional component of the rotation vector, rather it is calculated in some other way. This issue will be further explored in Chapter 6.

The thicknesses of the surfaces are considerably larger than those found for eye movements. Examination of the variation in end point rotation vectors also showed that, in general, the torsional component contains more variation than the other components. These findings suggest that the torsional component is planned to a lesser degree than the other components.

In Soechting et al. (1995) it is claimed that Donders' law does not hold, but rather a minimum work strategy is employed. The work involved in producing torsional rotations is much smaller than that of rotations about the other axes. It is seen here that the thicknesses of the surfaces for the upper arm are less than those of the forearm. Rotations of the upper arm require more energy than the forearm, and hence this property may be a result of some sort of minimum work strategy.

Additionally, if the other components of the rotation were planned in or-

der to minimize work, and the torsion was just a byproduct of the generation of the other components, larger variation in the torsional component than the other components would have only a small effect on the minimum work principle. In this sense, the torsion would be less controlled than the other variables.

## Chapter 5

# Background on models of motor control

The planning of pointing movements in the brain can be modeled by an internal model - a set of theoretical computations that predict the motor commands necessary to perform a given motor event (Sabes, 2000). This chapter presents different models for the generation of pointing movements and saccades, examining their feasibility for use with extended arm pointing movements.

Point to point movements have been found to be repeatable and largely invariant in task space (Morasso, 1981; Flash & Hogan, 1985; Wolpert et al., 1995). A similar invariance in rotation vector or quaternion space has been seen in studies of head fixed eye saccades. The angular velocity of these movements show relatively little scatter for normal point to point saccades (Van Opstal, 2001). This repeatability suggests that some sort of model is used in the brain to generate these movements. A number of models and their implications for the subsequent generated trajectories will be presented.

## 5.1 Double step movements and the superposition strategy

The double step paradigm (Flash & Henis, 1991) can be used as a technique for testing different internal models. Models that may give satisfactory predictions for point to point movements will not necessarily provide accurate predictions when there is a change of plan mid-flight.

Flash & Henis (1991) found that the trajectory plan of double step movements in a plane could be modeled as the vectorial addition of the original trajectory plan (from the starting location to the first target) and a second trajectory plan (for the displacement from the first to the second target).

The trajectory plans that are added consist of bell-shaped velocity profiles. Similar velocity profiles were seen in a study of infant reaching movements (Von Hofsten, 1991). Here the movements consisted of a combination of “action units”, made up of acceleration and deceleration phases, while the path of each unit is fairly straight. As the infants grew older, the number of units decreased and they became straighter. This combination of action units is similar to the superposition of trajectory plans.

The tangential velocity while tracking moving targets can be modeled as the superposition of trajectory plans with bell-shaped tangential velocity profiles (Lee et al., 1997). This is based on the concept that a complex trajectory may be formed by the linear superposition of simple sub-movements.

The superposition strategy has also been considered for trajectory modification with robot manipulators (Gat-Falik & Flash, 1999). The benefit of this strategy is that it guarantees continuity in end effector / hand position and the first derivative with respect to time, without requiring knowledge of the hand position, velocity or acceleration at the time of the switch. The elementary units can also be planned independently in parallel, a strategy that can be implemented for use in robotics (Rogozin et al., 2001).

## 5.2 Abort-replan model

The abort-replan model (for example, in Hoff (1994)) is an alternative strategy for handling double step movements. It is based on generating a new trajectory plan after the target location is modified (or alternatively, generating the trajectory plan continuously as the movement progresses). The new trajectory plan is chosen such that the velocity and acceleration will be continuous with the old plan, but to end up at the new target location. To do this requires information about the current kinematic state. Feedback from vision and proprioception would be too slow to use, hence this model requires that efference copies of the current state be available.

## 5.3 Models for 2D movements in a plane

Flash & Henis (1991) presented a kinematic model for the generation of arm movements in a horizontal plane. Their model produces trajectories that minimize an objective function. It is known as the minimum-jerk model, and its cost function is the square of the magnitude of the jerk (rate of change of acceleration):

$$C = \frac{1}{2} \int_{t_0}^{t_f} \left( \left( \frac{d^3x}{dt^3} \right)^2 + \left( \frac{d^3y}{dt^3} \right)^2 \right) dt \quad (5.1)$$

$C$  is the cost,  $x$  and  $y$  are the time-varying hand positions,  $t_0$  is the time at the start of the movement, and  $t_f$  at the end of the movement.

By using the Euler-Lagrange equation, the unique solution for a movement from  $(x_0, y_0)$  to  $(x_f, y_f)$  beginning at time  $t_0$  and finishing at  $t_f$  is given by (Flash & Hogan, 1985):

$$\begin{aligned} x(t) &= x_0 + (x_f - x_0) (10\tau^3 - 15\tau^4 + 6\tau^5) \\ y(t) &= y_0 + (y_f - y_0) (10\tau^3 - 15\tau^4 + 6\tau^5) \end{aligned}, \text{ where } \tau = \frac{t - t_0}{t_f - t_0}. \quad (5.2)$$

The minimum-jerk model produces straight-line trajectories between the initial and final point, with a bell shaped velocity profile. The velocity can be

expressed as:

$$\begin{aligned}\dot{x}(t) &= 30\frac{A_x}{D}(\tau^2 - 2\tau^3 + \tau^4) \\ \dot{y}(t) &= 30\frac{A_y}{D}(\tau^2 - 2\tau^3 + \tau^4)\end{aligned}\tag{5.3}$$

where  $A_x = x_f - x_0$  and  $A_y = y_f - y_0$  are the amplitude in the  $x$  and  $y$  directions and  $D = t_f - t_0$  is the duration.

A simple model can be built to simulate such trajectories. From the current and desired position, the desired displacement vector  $d$  can be calculated:

$$\vec{d} = \begin{bmatrix} x_f - x_0 \\ y_f - y_0 \end{bmatrix} = \begin{bmatrix} A_x \\ A_y \end{bmatrix}\tag{5.4}$$

The displacement vector gives the amplitude of the movement. The duration of the movement is assumed here to be preset. A velocity profile for a unit amplitude,  $\sigma(t)$ , can be expressed as:

$$\sigma(t) = \frac{30}{D}(\tau^2 - 2\tau^3 + \tau^4)\tag{5.5}$$

The integral of (5.5) over the relevant time ( $0 \leq \tau \leq 1$ ) will be 1. Thus the velocity profile for an arbitrary amplitude  $\begin{bmatrix} A_x & A_y \end{bmatrix}'$  will be  $\vec{d} \cdot \sigma(t)$ . The velocity can then be integrated to give the position (with the movement beginning at the initial position). This model is illustrated in Figure 5.1. The construction of this model to include the generation of the movement by first producing the velocity profile was selected so it will be similar to models for saccade generation. This model will produce trajectories that satisfy equation (5.3).

A superposition scheme could be implemented with this model to handle trajectory modification. In parallel, the model would need to generate a trajectory from the initial to the first target, and the displacement from the first target to the second target - the output would be the vectorial summation (starting the second movement at the appropriate time) of the two generated trajectories. Due to the linear, commutative nature of the operations, the superposition could also be performed on the velocity  $(\dot{x}, \dot{y})$  and the same

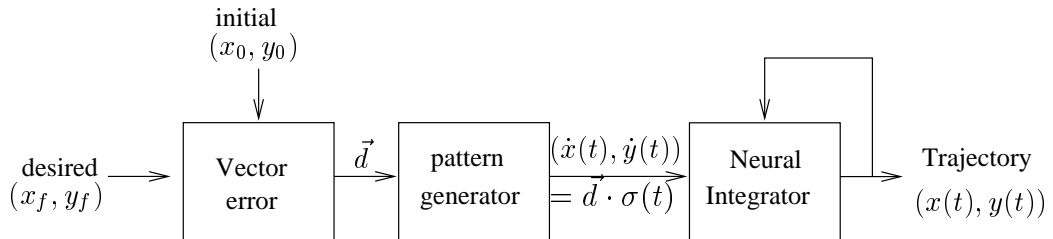


Figure 5.1: A 2D position based model. The desired displacement is calculated from the desired and current position by vector subtraction. The pattern generator then generates a smooth, bell shaped, velocity profile, which is integrated to produce the desired position.

result would be produced. In the generalization to a 3D rotational system, such assumptions cannot be made.

## 5.4 Models for saccade generation in the eye

A number of models have been presented for the generation of saccades in the oculomotor system (for example Tweed & Vilis, 1987; Van Opstal, 2001).

An analogous model to the one presented for 2D hand motions can be used for modeling point to point eye saccades. The rotation vector displacement  $\vec{d}_r$  can be calculated using vector subtraction. Note that this will *not* give the rotation from the initial orientation to the final orientation. The coordinate velocity ( $\vec{r}$ ) can then be calculated as  $\vec{r} = \vec{E} \cdot \sigma(t)$ , then integrated to give the current rotation vector. This model is shown in Figure 5.2.

This model will generate smooth trajectories, with single axis rotations. A single axis rotation is one where the entire rotation is about the same axis. This can be seen easily in angular velocity space, where a single axis rotation corresponds to a straight line that passes through the origin in angular velocity space (because the direction of the angular velocity vector is the axis of rotation). This model has a coordinate velocity of  $\vec{r} = \vec{d}_r \sigma(t)$ , and the rotation vector during the movement will be  $\vec{r} = \vec{r}_0 + \vec{d}_r \sigma(t)t$ . Using

equation (2.28), the angular velocity can be expressed as:

$$\begin{aligned}
\omega &= 2 \left( \frac{\vec{d}_r \sigma(t) + (\vec{r}_0 + \vec{d}_r \sigma(t)t) \times \vec{d}_r \sigma(t)}{1 + (\vec{r}_0 + \vec{d}_r \sigma(t)t) \cdot (\vec{r}_0 + \vec{d}_r \sigma(t)t)} \right) \\
&= 2 \left( \frac{\vec{d}_r \sigma(t) + (\vec{r}_0 \times \vec{d}_r \sigma(t)) + (\vec{d}_r \sigma(t)t \times \vec{d}_r \sigma(t))}{1 + (\vec{r}_0 + \vec{d}_r \sigma(t)t) \cdot (\vec{r}_0 + \vec{d}_r \sigma(t)t)} \right) \\
&= \frac{2\sigma(t)}{1 + (\vec{r}_0 + \vec{d}_r \sigma(t)t) \cdot (\vec{r}_0 + \vec{d}_r \sigma(t)t)} \left[ \vec{d}_r + \vec{r}_0 \times \vec{d}_r \right]
\end{aligned} \tag{5.6}$$

The angular velocity will hence always be in the same direction, but with the magnitude varying as a function of time. Hence, it is a single axis rotation.

The models presented for eye saccades have, however, generally been feedback models. Tweed & Vilis (1987) presented such a model, based on feeding back the current eye orientation. This model, adapted for rotation vectors, is presented in Figure 5.3.

The displacement that drives the feedback model is the rotation vector difference between the current and desired rotation:

$$\vec{d}_s = \vec{r}_f \circ \vec{r}_i^{-1} \tag{5.7}$$

This is different from the displacement vector  $\vec{d}_r = \vec{r}_f - \vec{r}_0$  used in the previous model. Here the displacement *is* equivalent to the rotation that would take

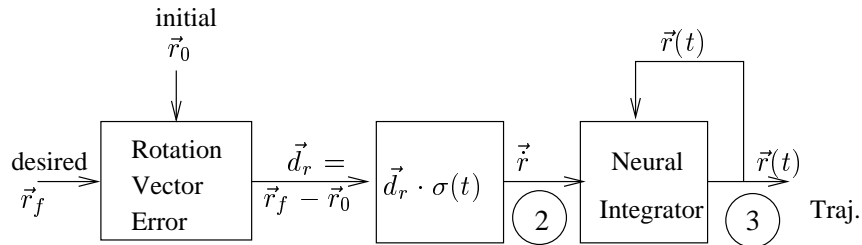


Figure 5.2: A 3D rotation vector model. The coordinate velocity  $\vec{r}$  is determined by  $\vec{d} \cdot \sigma(t)$ . A 3 dimensional “Neural Integrator” (Tweed & Vilis, 1987) gives the current orientation using feedback of the current orientation  $\vec{r}(t)$ .

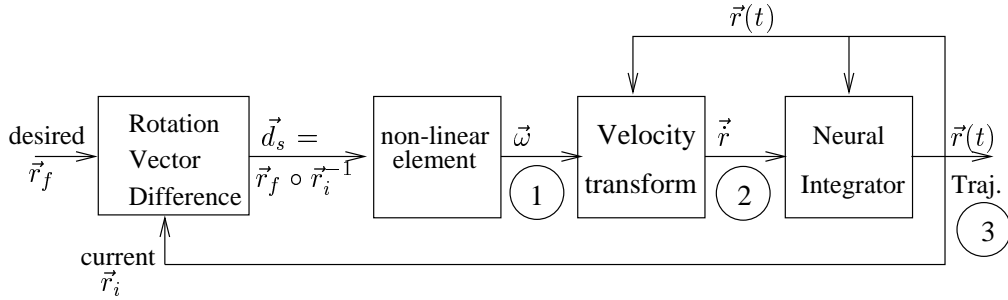


Figure 5.3: A 3D rotation vector model, based on Tweed & Vilis (1987). The current rotation vector displacement  $d_s$  is found (defined here as the rotation from the current orientation  $\vec{r}_i$  to the desired orientation  $\vec{r}_f$ ) and passed through a non-linear element to give the angular velocity. A 3 dimensional “Neural Integrator”, using feedback of the current orientation, outputs the trajectory plan, with the current orientation used to produce the updated error.

the current orientation to the desired orientation. The model will continue to work until the current orientation is the same as the desired orientation, when the rotation vector difference will be zero and it will stop.

In order to move towards the target, the axis of rotation needs to be in the direction of the displacement  $\vec{d}_s$ . This gives the direction of the angular velocity. The magnitude is determined by a non-linear element, sometimes referred to as a pulse generator. For eye saccades, there is evidence that this role is played by medium burst neurons (Van Gisbergen et al., 1981), which have a discharge rate relative to the saccade velocity. These bursts can be modeled using exponentials. A simple approximation can be made using (Tweed, 1997):

$$\vec{\omega} = \frac{a\vec{d}_s}{a + b|\vec{d}_s|} \quad (5.8)$$

where  $a$  and  $b$  are constants, and  $|\vec{d}_s|$  is the magnitude of the vector  $\vec{d}_s$ . Tweed (1997) notes that a more realistic model would use some combination of jerk, acceleration, velocity and position in determining the magnitude of

the angular velocity.

The implementation of the integrator can be performed using an intermediate step. The coordinate velocity can be calculated from the angular velocity (Van Opstal, 2001):

$$\dot{\vec{r}} = \frac{1}{2} (\vec{\omega} + \vec{\omega} \times \vec{r} + (\vec{\omega} \cdot \vec{r})\vec{r}) \quad (5.9)$$

The coordinate velocity can then be integrated separately for each component to give the trajectory in rotation vectors. Trajectories for point to point movements produced by this model will also be single axis rotations because the axis of rotation will be constant. The magnitude of the velocity will be determined by the form of the non-linear element.

## 5.5 Incorporation of Listing's law

The two previous models can be easily adapted to incorporate Listing's law. The input to the model is the desired gaze or pointing direction, which can be expressed as a unit vector  $e_r = [x \ y \ z]'$ . When a Listing's law constraint is applied (i.e. that  $r_x = 0$ ), then a pointing direction corresponds to a unique rotation vector. By solving equation (2.11) with this constraint, it is possible to find the unique rotation vector for a given pointing direction:

$$\begin{bmatrix} r_x \\ r_y \\ r_z \end{bmatrix} = \frac{(-1+x)}{y^2+z^2} \begin{bmatrix} 0 \\ z \\ -y \end{bmatrix} \quad (5.10)$$

An additional box to perform this transformation would then be added to the two models, but otherwise they would perform as before. A similar approach is used in Tweed & Vilis (1990b), where the desired gaze vector is transformed to desired eye orientation quaternion. Hence for a saccade generated using this movement, the start of the movement is assumed to be in Listing's plane, and the end of the movement is specified to be in Listing's plane. Although only these two positions are constrained to be in Listing's

plane, the intermediate positions will also be in Listing's plane. This is because a single axis rotation between two orientations that lie in Listing's plane has a straight line path in rotation vector space (Van Opstal, 2001), and so can be represented by the following equation

$$\vec{r}(t) = \vec{r}_1 + \sigma(t) \cdot (\vec{r}_2 - \vec{r}_1) \quad (5.11)$$

where  $\sigma(t)$  has an integral of 1 over the time of the movement (for example, equation (5.5) could be used). This does not generally hold when the constraint on the rotation vectors is a non-flat surface.

It should be noted that although the rotation vectors throughout the movement will lie in Listing's plane, the angular velocity axis for movements that do not begin or end at the primary position will have a tilt, i.e. they will not lie in Listing's plane. To ensure the rotation vectors remain in Listing's plane, the angular velocity axis is required to tilt out of Listing's plane by half the orthogonal deviation of gaze from the primary position. This is known as the *half-angle rule* (Crawford, 1998).

## 5.6 Trajectory modification with rotation vector models

While for the position based models, superposition could be performed at the position or velocity level, an analogous statement does not hold for rotation vectors. If a similar strategy of superposition is to be used for rotations, it can be performed at the level of angular velocity ( $\vec{\omega}$ ), coordinate velocity ( $\vec{\dot{r}}$ ) or rotation vector ( $\vec{r}$ ).

### Superposition of angular velocity ( $\vec{\omega}$ )

A test of superposition at the level of angular velocity can be performed with the model in Figure 5.3. First, the method of composing angular velocity needs to be considered.

The composition of angular velocity vectors is defined here as the angular velocity  $\vec{\omega}_3(t)$  such that it is equivalent to the angular velocity of the following rotation at each time step: first applying the rotation represented by  $\vec{\omega}_1(t)$ , and after time  $\tau$ , also afterwards applying the rotation represented by  $\vec{\omega}_2(t - \tau)$ .

For simplicity, the calculations will be performed using quaternions (see Appendix A) and later converted to rotation vectors. Consider a vector  $s_0$  that is rotated (at each time step) by the rotation represented by the quaternion  $q_1(t)$ . After a time  $\tau$ , after the rotation represented by  $q_1(t)$ , the rotation represented by  $q_2(t')$  is also applied. In the time scale of  $q_1(t)$ , the second rotation will be defined by  $q_2(t - \tau)$ , where the rotation for  $q_2(t)$  for where  $t < 0$  (ie no rotation) will be defined as the identity quaternion, that is, a rotation of zero radians about an arbitrary axis:

$$q_2(t) = 1 + \begin{bmatrix} 0 \\ 0 \\ 0 \end{bmatrix}, t < 0 \quad (5.12)$$

and so  $q_2^{-1}(t) = q_2(t)$  for  $t < 0$ .

The new position of the vector will be  $s(t)$ , defined by:

$$s(t) = q_2(t - \tau)q_1(t)s_0q_1^{-1}(t)q_2^{-1}(t - \tau) \quad (5.13)$$

Taking the time velocity gives

$$\begin{aligned} \dot{s}(t) &= \dot{q}_2(t - \tau)q_1(t)s_0q_1^{-1}(t)q_2^{-1}(t - \tau) + q_2(t - \tau)\frac{d}{dt}(q_1(t)s_0q_1^{-1}(t)q_2^{-1}(t - \tau)) \\ &= \dot{q}_2(t - \tau)q_1(t)s_0q_1^{-1}(t)q_2^{-1}(t - \tau) + q_2(t - \tau)\dot{q}_1(t)s_0q_1^{-1}(t)q_2^{-1}(t - \tau) \\ &\quad + q_2(t - \tau)q_1(t)s_0\frac{d}{dt}(q_1^{-1}(t)q_2^{-1}(t - \tau)) \\ &= \dot{q}_2(t - \tau)q_1(t)s_0q_1^{-1}(t)q_2^{-1}(t - \tau) + q_2(t - \tau)\dot{q}_1(t)s_0q_1^{-1}(t)q_2^{-1}(t - \tau) \\ &\quad + q_2(t - \tau)q_1(t)s_0\dot{q}_1^{-1}(t)q_2^{-1}(t - \tau) + q_2(t - \tau)q_1(t)s_0q_1^{-1}(t)\dot{q}_2^{-1}(t - \tau) \\ &= (\dot{q}_2(t - \tau)q_1(t) + q_2(t - \tau)\dot{q}_1(t))(s_0q_1^{-1}(t)q_2^{-1}(t - \tau)) \\ &\quad + (q_2(t - \tau)q_1(t)s_0)(\dot{q}_1^{-1}(t)q_2^{-1}(t - \tau) + q_1^{-1}(t)\dot{q}_2^{-1}(t - \tau)) \end{aligned} \quad (5.14)$$

Then using (2.18),(2.19) and (2.20):

$$\begin{aligned}
\dot{s}(t) &= (\dot{q}_2(t-\tau)q_1(t) - q_2(t-\tau)q_1(t)\dot{q}_1^{-1}(t)q_1(t))(s_0q_1^{-1}(t)q_2^{-1}(t-\tau)) \\
&\quad + (q_2(t-\tau)q_1(t)s_0)(-q_1^{-1}(t)\dot{q}_1(t)q_1^{-1}q_2^{-1}(t-\tau) + q_1^{-1}(t)\dot{q}_2^{-1}(t-\tau)) \\
&= (\dot{q}_2(t-\tau) - q_2(t-\tau)q_1(t)\dot{q}_1^{-1}(t))(q_1(t)s_0q_1^{-1}(t)q_2^{-1}(t-\tau)) \\
&\quad + (q_2(t-\tau)q_1(t)s_0q_1^{-1}(t))(-\dot{q}_1(t)q_1^{-1}q_2^{-1}(t-\tau) + \dot{q}_2^{-1}(t-\tau)) \\
&= (-q_2(t-\tau)\dot{q}_2^{-1}(t-\tau)q_2(t-\tau) - q_2(t-\tau)q_1(t)\dot{q}_1^{-1}(t) \\
&\quad q_2^{-1}(t-\tau)q_2(t-\tau))(q_1(t)s_0q_1^{-1}(t)q_2^{-1}(t-\tau)) \\
&\quad + (q_2(t-\tau)q_1(t)s_0q_1^{-1}(t))(-q_2^{-1}(t-\tau)q_2(t-\tau)\dot{q}_1(t)q_1^{-1} \\
&\quad q_2^{-1}(t-\tau) - q_2^{-1}(t-\tau)\dot{q}_2(t-\tau)q_2^{-1}(t-\tau))
\end{aligned} \tag{5.15}$$

Substituting back in (5.13):

$$\begin{aligned}
\dot{s}(t) &= (-q_2(t-\tau)\dot{q}_2^{-1}(t-\tau) - q_2(t-\tau)q_1(t)\dot{q}_1^{-1}(t)q_2^{-1}(t-\tau))s(t) \\
&\quad + s(t)(-q_2(t-\tau)\dot{q}_1(t)q_1^{-1}q_2^{-1}(t-\tau) - \dot{q}_2(t-\tau)q_2^{-1}(t-\tau)) \\
&= (\dot{q}_2(t-\tau)q_2^{-1}(t-\tau) + q_2(t-\tau)\dot{q}_1(t)q_1^{-1}(t)q_2^{-1}(t-\tau))s(t) \\
&\quad - s(t)(\dot{q}_2(t-\tau)q_2^{-1}(t-\tau) + q_2(t-\tau)\dot{q}_1(t)q_1^{-1}q_2^{-1}(t-\tau))
\end{aligned}$$

and from (2.22)

$$= 2(\dot{q}_2(t-\tau)q_2^{-1}(t-\tau) + q_2(t-\tau)\dot{q}_1(t)q_1^{-1}(t)q_2^{-1}(t-\tau)) \times s(t) \tag{5.16}$$

Hence by (2.24), the angular velocity  $\vec{\omega}_3$  can be expressed as

$$\vec{\omega}_3(t) = 2(\dot{q}_2(t-\tau)q_2^{-1}(t-\tau) + q_2(t-\tau)\dot{q}_1(t)q_1^{-1}(t)q_2^{-1}(t-\tau)) \tag{5.17}$$

Using equation (2.25):

$$\vec{\omega}_3(t) = \vec{\omega}_2(t-\tau) + q_2(t-\tau)\vec{\omega}_1q_2^{-1}(t-\tau) \tag{5.18}$$

Now expanding the expression using (A.2):

$$\begin{aligned}
& q_2(t - \tau) \circ \vec{\omega}_1(t) \circ q_2^{-1}(t - \tau) \\
&= [\{-\vec{q}_2(t - \tau) \cdot \vec{\omega}_1(t)\} + q_{20}(t - \tau)\vec{\omega}_1(t) + \vec{q}_2(t - \tau) \times \vec{\omega}_1(t)] \circ q_2^{-1}(t - \tau) \\
&= \{-q_{20}^{-1}(t - \tau)(\vec{q}_2(t - \tau) \cdot \vec{\omega}_1(t)) - (q_{20}(t - \tau)\vec{\omega}_1(t) + \vec{q}_2(t - \tau) \times \vec{\omega}_1(t)) \cdot \vec{q}_2^{-1}(t - \tau)\} \\
&\quad - (\vec{q}_2(t - \tau) \cdot \vec{\omega}_1(t))\vec{q}_2^{-1}(t - \tau) + q_{20}^{-1}(t - \tau)(q_{20}(t - \tau)\vec{\omega}_1(t) + \vec{q}_2(t - \tau) \times \vec{\omega}_1(t)) \\
&\quad + (q_{20}(t - \tau)\vec{\omega}_1(t) + \vec{q}_2(t - \tau) \times \vec{\omega}_1(t)) \times \vec{q}_2^{-1}(t - \tau) \\
&= \{q_{20}(t - \tau)[\vec{q}_2(t - \tau) \cdot \vec{\omega}_1(t) - \vec{q}_2(t - \tau) \cdot \vec{\omega}_1(t)] + (\vec{q}_2(t - \tau) \times \vec{\omega}_1(t)) \cdot \vec{q}_2(t - \tau)\} \\
&\quad + (\vec{q}_2(t - \tau) \cdot \vec{\omega}_1(t))\vec{q}_2(t - \tau) + q_{20}^2(t - \tau)\vec{\omega}_1(t) + q_{20}(t - \tau)(\vec{q}_2(t - \tau) \times \vec{\omega}_1(t)) \\
&\quad - q_{20}(t - \tau)(\vec{\omega}_1(t) \times \vec{q}_2(t - \tau)) - (\vec{q}_2(t - \tau) \times \vec{\omega}_1(t) \times \vec{q}_2(t - \tau)) \\
&= \{\vec{q}_2(t - \tau) \times \vec{\omega}_1(t)\} \cdot \vec{q}_2(t - \tau) + q_{20}^2(t - \tau)\vec{\omega}_1(t) + 2q_{20}(t - \tau)(\vec{q}_2(t - \tau) \times \vec{\omega}_1(t)) \\
&\quad + (\vec{q}_2(t - \tau) \cdot \vec{\omega}_1(t))\vec{q}_2(t - \tau) - \vec{q}_2(t - \tau) \times \vec{\omega}_1(t) \times \vec{q}_2(t - \tau)
\end{aligned}$$

substituting using (A.4), and noting that  $(\vec{a} \times \vec{b}) \cdot \vec{a} = 0$

$$\begin{aligned}
&= q_{20}^2(t - \tau)(\vec{\omega}_1(t) + 2(\vec{r}_2(t - \tau) \times \vec{\omega}_1(t)) + (\vec{r}_2(t - \tau) \cdot \vec{\omega}_1(t))\vec{r}_2(t - \tau) \\
&\quad - \vec{r}_2(t - \tau) \times \vec{\omega}_1(t) \times \vec{r}_2(t - \tau))
\end{aligned} \tag{5.19}$$

In the above calculations, because it is assumed that  $q_2(t - \tau)$  is a unit quaternion, then  $q_{20} = q_{20}^{-1}$  and  $\vec{q}_2(t - \tau) = -\vec{q}_2^{-1}(t - \tau)$ . The scalar part disappeared as expected, because it is an angular velocity. The final expression can hence be written as:

$$\begin{aligned}
\vec{\omega}_3(t) &= \omega_2(t - \tau) + \frac{\vec{\omega}_1(t) + 2(\vec{r}_2(t - \tau) \times \vec{\omega}_1(t)) + (\vec{r}_2(t - \tau) \cdot \vec{\omega}_1(t))\vec{r}_2(t - \tau)}{1 + \vec{r}_2(t - \tau) \cdot \vec{r}_2(t - \tau)} \\
&\quad - \frac{\vec{r}_2(t - \tau) \times \vec{\omega}_1(t) \times \vec{r}_2(t - \tau)}{1 + \vec{r}_2(t - \tau) \cdot \vec{r}_2(t - \tau)}
\end{aligned} \tag{5.20}$$

Superposition of angular velocity could be performed using (5.20) at the point marked by 1 in Figure 5.3. Superposition at this point is problematic, because the tilt in the angular velocity necessary to remain in Listing's plane is a function of the current orientation. Superposition of the tilts in general

will not give the required tilt for the double step movement. Minken et al. (1993) explained that every combination of angular velocity commands will fail to generate the required tilting under all circumstances. This is because the current orientation is also needed. An example of performing superposition using (5.20) is shown in Figure 5.4. Significant violations of Listing's law can be seen in such a case. Minken et al. (1993) made a number of suggestions to get around this problem. One suggestion was to use the coordinate velocity  $\vec{r}$  rather than the angular velocity  $\vec{\omega}$ .

### Superposition of coordinate velocity

Superposition of coordinate velocity could take place at the point marked 2 in Figure 5.2 or at the point marked 2 in Figure 5.3. If the superposition was performed using the feedback model (Figure 5.3), then the rotation vectors from the original (control) trajectories would need to be used. This would involve using an efference copy of the predicted rotation vector for a point to point movement rather than feeding back the actual rotation vector.

Superposition of coordinate velocity is much simpler - regular vector addition can be used. The results of superposition of coordinate velocity on the same data sets as before can also be seen in Figure 5.4.

When superposition is performed on coordinate velocity, Listing's law is not violated during double step trajectories. The torsional component of the coordinate velocity  $\dot{r}_x$  is always zero because Listing's law means that  $r_x(t)$  is always zero, and hence the summation of coordinate velocities will also have a torsional component of zero. This in turn means that the torsional component of the rotation vector  $r_x(t)$  will remain unchanged, that is, it will always be zero. This holds only for the special case of Listing's law where  $\dot{r}_x = 0$  throughout the workspace.

It should be noted that this model and the angular velocity based model will give similar trajectories for point to point movements, where both follow Listing's law. The difference can only be seen in the double step case.

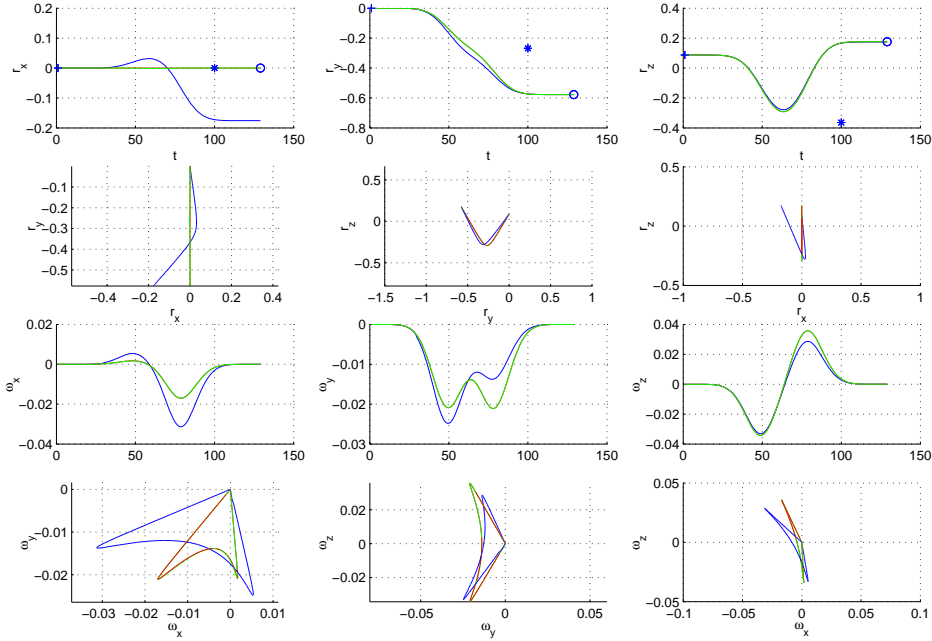


Figure 5.4: An example of superposition of different quantities. The first and third rows show the rotation vectors and angular velocity in components plotted against time. The second and fourth rows show the rotation vectors and angular velocity from the top, back and side views. The blue lines indicate superposition of angular velocity ( $\omega$ ). It can be seen that non-zero torsion is introduced (the blue line in the upper-left graph has non-zero values), indicating violations of Listing's law due to the incorrect tilt. In contrast, superposition of coordinate velocity (red) and rotation vectors (green) (the red and green partially obscure each other) give equivalent results - zero torsion is maintained throughout. For superposition of these quantities, the angular velocity axis has the appropriate tilt introduced as a result of the torsion being zero.

### Superposition of rotation vectors

Superposition could also take place after the entire trajectory has been generated, at the level of rotation vectors (marked by 3 in Figure 5.2 or Figure 5.3). This could take place using rotation vector composition, defined in Equation

(2.8).

Initially, just the first rotation  $\vec{r}_1(t)$  takes place. When the second rotation  $\vec{r}_2(t - \tau)$  begins (at time  $\tau$ ), then they are combined according to:

$$\vec{r}(t) = \vec{r}_2(t - \tau) \circ \vec{r}_b^{-1} \circ \vec{r}_1(t) \quad (5.21)$$

where  $\vec{r}_1(t)$  defines the rotation vector as a function of time for rotating from  $\vec{r}_a$  to  $\vec{r}_b$ , and  $\vec{r}_2(t)$  is the rotation vector as a function of time for a movement from  $\vec{r}_b$  to  $\vec{r}_c$ . This defines the result of rotating first by the rotation represented by  $\vec{r}_1(t)$ , followed by that represented by  $\vec{r}_2(t - \tau)$ . The rotation by  $\vec{r}_b^{-1}$  is necessary, because  $\vec{r}_2(t)$  implicitly includes a rotation to  $\vec{r}_b$ . Although both rotations introduce zero torsion, the superposition of them does not generally have zero torsion - this is due to the cross product in (2.8). An example of superposition of rotation vectors with the same initial data is shown in Figure 5.4, although the small torsional component is difficult to see in the diagram. At the end of the movement, unlike with the angular velocity, the torsion returns to zero. This is because Equation (5.21) at the end of the movement ( $t_f$ ) will equal:

$$\begin{aligned} \vec{r}(t_f) &= \vec{r}_c \circ \vec{r}_b^{-1} \circ \vec{r}_b \\ &= \vec{r}_c \end{aligned} \quad (5.22)$$

Hence the orientation at the end of the movement will be  $\vec{r}_c$ , which is in Listing's plane. So while the torsion during the movement does not obey Listing's law during superposition of rotation vectors, it does at the start and end of the movement.

## 5.7 Incorporation of Donders' law for non-flat surfaces

In Chapter 4, it was suggested that for extended arm pointing movements, the rotation vectors describing the orientations throughout the movement may be constrained to a curved rather than a flat surface.

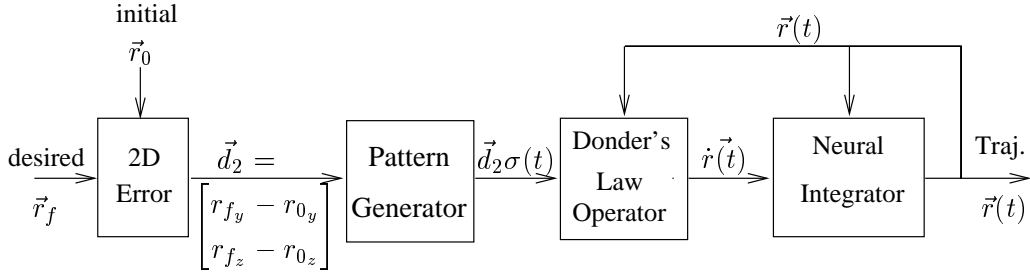


Figure 5.5: A 3D coordinate velocity model. In this model, the Donders' law operator is applied after calculation of the required 2D error for each time step. Unlike in the Listing's law case, the operator is dependent on the current position.

The models presented so far will fail to produce trajectories that satisfy Donders' law for constraints other than Listing's law. This is because they are based on setting the initial and final points to satisfy Donders' law, and assuming that the intermediate points will also satisfy it. While this is true for Listing's law, it is not generally true for Donders' law.

An alternative model is presented where the Donders' law constraint is shifted so that it is applied throughout the movement. This model is an adaption of the model in Figure 5.2. The model in Figure 5.3 could also be modified for this condition, but would be more complicated, and the model presented here will be suitable to test superposition.

This model uses a two dimensional displacement ( $\vec{d}_2$ ) rather than a three dimensional displacement. The two dimensional rotation vector desired displacement is defined as:

$$\vec{d}_2 = \begin{bmatrix} r_{fy} - r_{0y} \\ r_{fz} - r_{0z} \end{bmatrix} \quad (5.23)$$

The pattern generator generates the current displacement,  $\vec{d}_2\sigma(t)$ , so that at time  $t$  it needs to move  $\vec{d}_2\sigma(t)$  towards the target. The necessary coordinate velocity is then generated to ensure adherence to Donders' law, using the current orientation. A diagram of this model is shown in Figure 5.5.

While this model produces single step trajectories that satisfy Donders' law, an additional problem is introduced. The Donders' operator is dependent on the current position, hence the superposition of two quantities, generated at different orientations to the current position, will not generally result in the correct torsion being specified.

Superposition of angular velocity and rotation vectors were shown to be problematic even with a flat plane. Superposition of coordinate velocity also produces the wrong answer when considering this more general case.

For example, if a gimbal-like system is used for Donders' law (see Chapter 3), where the constraint on torsion is

$$r_x = s(r_y r_z) \quad (5.24)$$

then this will lead to a constraint on coordinate velocity of (by taking the time derivative):

$$\dot{r}_x = s(\dot{r}_y r_z + r_y \dot{r}_z). \quad (5.25)$$

Hence performing superposition of the torsional components of two control coordinate velocities  $\dot{r}_{x_1}$  and  $\dot{r}_{x_2}$  will give:

$$\begin{aligned} \dot{r}_{x_1} + \dot{r}_{x_2} &= s(\dot{r}_{y_1} r_{z_1} + \dot{r}_{y_2} r_{z_2} + r_{y_1} \dot{r}_{z_1} + r_{y_2} \dot{r}_{z_2}) \\ &= \dot{r}_{x_3} - s(\dot{r}_{y_1} r_{z_2} + \dot{r}_{y_2} r_{z_1} + r_{y_2} \dot{r}_{z_1} + r_{y_1} \dot{r}_{z_2}) \\ &\neq \dot{r}_{x_3} \end{aligned} \quad (5.26)$$

This will only give the necessary coordinate velocity torsional component ( $\dot{r}_{x_3}$ ) if  $s = 0$  - this is if a Listing's plane is used as the Donders' law constraint.

However, the bracketed terms in (5.26) are close to zero if the overlap (the time that both control trajectories are operating) is not large. With a small overlap, the torsion generated is very close to that required to satisfy the Fick gimbal constraint. However, with a large overlap, the velocities will be significant during the overlap and hence large variations will be seen. In both situations though, the final torsion will be as required.

An alternate strategy would be to perform superposition on only the  $\dot{r}_y$  and  $\dot{r}_z$  components of the movements. Then the  $\dot{r}_x$  component would be set

using the appropriate Donders' law constraint. This would clearly guarantee that Donders' law is satisfied. The movement would be effectively planned in 2 dimensions, with the torsional constraint only applied at the final stage.

For example, for a Fick rule, a form of superposition could be defined for coordinate velocity such that it would always produce the correct torsion by rearranging equation 5.26:

$$\dot{r}_{x_3} = \dot{r}_{x_1} + \dot{r}_{x_2} + s(\dot{r}_{y_1}r_{z_z} + \dot{r}_{y_2}r_{z_1} + r_{y_2}\dot{r}_{z_1} + r_{y_1}\dot{r}_{z_2}) \quad (5.27)$$

However, performing the superposition would then require the rotation vectors of both control trajectories as well as their coordinate velocities.

Performing superposition in terms of  $\dot{r}_y$  and  $\dot{r}_z$  does not guarantee that the correct final target location is reached. The position of the end effector in space is a function of all three components of the rotation vector, not just the torsional component. This is because the  $r_x$  component is related to a rotation about a space fixed axis (pointing straight ahead), rather than an arm fixed axis. Hence the value of the  $r_x$  component also affects the position of the end effector and not just the angle of rotation about its own axis.

## 5.8 Models in Fick coordinates

The only solution that seems to remain is to plan the motion in two dimensions, and then constrain the torsion. A representation is required that will ensure that the primary goal, the pointing direction of the end effector, will be achieved. Fick coordinates can be used for this purpose - the  $\theta_F$  and  $\phi_F$  angles (described in Figure 2.2) specify the pointing direction of the end effector, while the rotation about its own axis is specified only by the  $\psi_F$  angle. A model can be described where the trajectory is first generated in terms of  $\theta_F$  and  $\phi_F$ , hence the 2D displacement vector  $d_F$  can be defined as

$$\vec{d}_F = \begin{bmatrix} \theta_f - \theta_0 \\ \phi_f - \phi_0 \end{bmatrix} \quad (5.28)$$

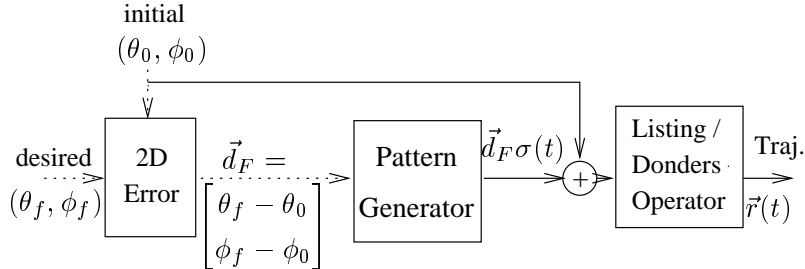


Figure 5.6: Two-dimensional Fick angles model. The error from the initial pointing direction to the desired pointing direction is calculated in two-dimensional Fick coordinates, then passed to the pattern generator. This occurs instantaneously (shown by the dotted lines). The pattern generator produces a trajectory plan in two dimensional Fick coordinates as a function of time, then at the last stage the torsion is specified to satisfy Donders’ law with the output being the appropriate rotation vector. The solid lines show the parts of the model that operate throughout the movement.

This leads to a model where the trajectory is first generated in 2D in terms of  $\theta_F$  and  $\phi_F$ . Then the necessary rotation vector to satisfy Donders’ law at each point is generated. This model is shown in Figure 5.6.

Superposition using such a model could be performed by adding the trajectory plans generated in 2D Fick coordinates before the Donders’ law constraint is applied. This superposition will ensure that the pointing direction is correct, while the torsion will be fixed after the superposition to satisfy Donders’ law. This is shown in Figure 5.7.

Note that superposition of 3-dimensional Fick coordinates  $(\theta_F, \phi_F, \psi_F)$  would fail in general, because the Donders’ law constraints are dependent on the position. The exception to this rule would be when  $\psi_F$  is exactly zero - ie if the “Fick rule” were exactly followed then superposition could be performed in Fick coordinates (because  $\psi_F$  would always be zero). This is analogous to superposition with coordinate velocity with a Listing’s law rule.

A variation of this model could be constructed where feedback of two dimensional Fick coordinates is used. The Donders’ law constraint would

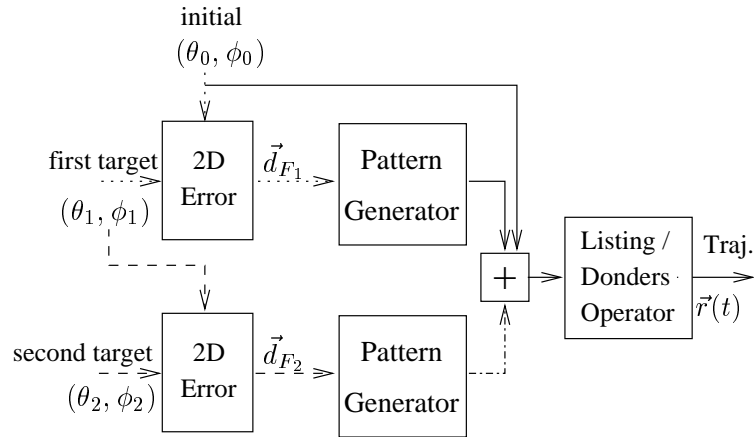


Figure 5.7: Two-dimensional Fick angles model with superposition. This is an extension of the model shown in Figure 5.6. At the time when the movement deviates from the initial plan (after the target has jumped), the error from the first target to the second target will be calculated. The events occurring at this time are shown with the dashed lines. A trajectory plan in 2D Fick coordinates from the first target to the second target will then be generated, shown by the dash-dotted line. This is added to the trajectory plan of the first movement and only at the last stage is the Donders’ law constraint applied. The solid lines show the parts of the model that operate throughout the entire movement.

still need to be applied as the last step as with the superposition model. This alternative still ensures that Donders’ law is applied throughout the movement.

## 5.9 Three-dimensional “Velocity box” model

While the previous models constrained the orientation in order to apply Donders’ law, it is possible to achieve adherence to Donders’ law through velocity constraints (Ceylan et al., 2000).

The input to such a model is the desired two-dimensional Fick angle dis-

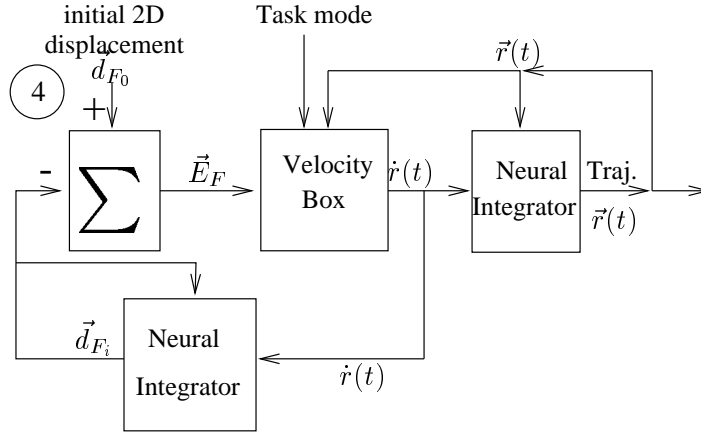


Figure 5.8: A 3D “Velocity box” feedback model. The model takes the desired 2D Fick angle displacement as the input. Throughout the movement, the current displacement (initially  $\vec{0}$ ), is compared with the desired displacement, generating the error (5.29). A coordinate velocity is generated in the velocity box that will reduce the error and satisfy certain velocity constraints (for example, to satisfy Listing’s law), which is then integrated to give the rotation vector trajectory.

placement as specified in Equation (5.28). The use of the desired displacement as the input rather than the desired orientation is based on findings that the superior colliculus, which is believed to generate the motor commands, encodes the displacement as the input for trajectory generation (Tweed & Vilis, 1990b). This model is shown in Figure 5.8.

Feedback of the current coordinate velocity is used to update the current displacement. The current displacement is compared to the desired displacement, and the difference is the 2D error signal ( $\vec{E}_F$ ), defined to be:

$$\vec{E}_F = d_{F_f} - d_{F_i} \quad (5.29)$$

The direction of the coordinate velocity will be set to reduce the error, while under certain velocity constraints, as suggested by Ceylan et al. (2000).

The magnitude of the coordinate velocity will be generated in a similar way to the model presented in Figure 5.3. This will be integrated to give the

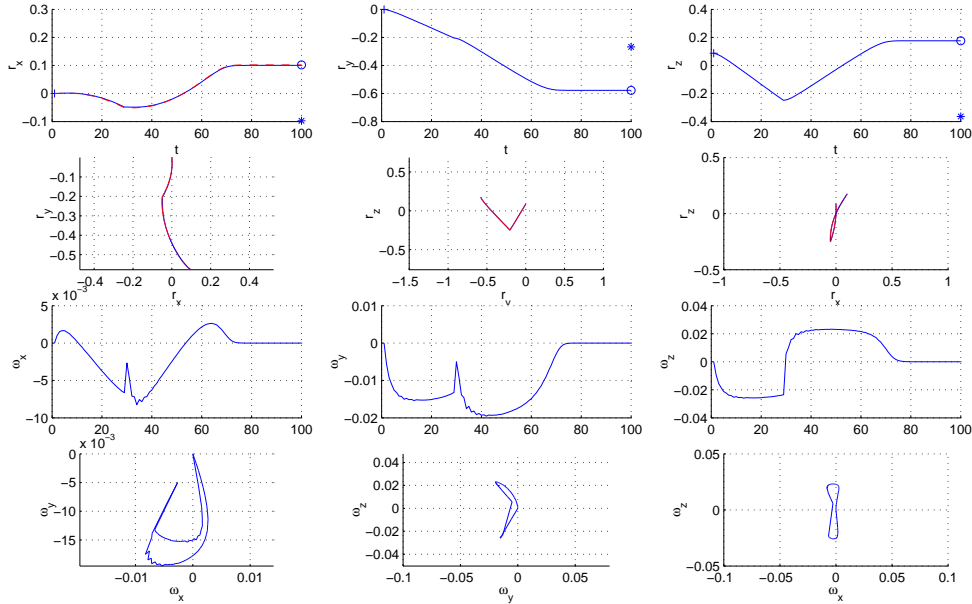


Figure 5.9: An example of superposition using the “Velocity box” feedback model, with a Fick gimbal with zero torsion. The first and third rows show the time development of the rotation vectors and the angular velocity vectors, while the second and fourth row show them from top, back and side views. The trajectories produced by the model (blue) have values of torsion that match the values required by Donders’ law (indicated by the dotted red line).

rotation vector which is required to perform the movement.

The velocity box model can incorporate constraints for Donders’ law. For example, to constrain orientations to a Fick gimbal with zero Fick torsional angle, the angular velocity vector must lie in a plane whose normal vector is the current vector position rotated into the horizontal plane (Ceylan et al., 2000). A simulation of this model for a double step case can be seen in Figure 5.9.

This model will fit the required values of torsion throughout the movement as predicted by the Fick gimbal rule. This is because the velocity constraints are applied after the superposition has taken place. The use of velocity constraints rather than orientation constraints is advantageous because it

allows nonholonomic <sup>1</sup> constraints such as “minimum rotation” to also be implemented (Ceylan et al., 2000).

The conversion from Fick coordinates to coordinate velocity will be explained in more detail in Chapter 6. Implementation of the velocity box for more general situations can also be performed. The difficulties in doing this in angular velocity space are explained in Appendix B.

Constraints can be specified more simply in terms of coordinate velocity rather than angular velocity. For example, for the Fick gimbal rule, first take the time derivative of (3.7):

$$\begin{aligned} \dot{r}_1 &= s(\dot{r}_2 r_3 + r_2 \dot{r}_3) \\ \Rightarrow \dot{r}_1 - s r_3 \dot{r}_2 - s r_2 \dot{r}_3 &= 0 \end{aligned} \tag{5.30}$$

Then the normal vector to the plane of coordinate velocity vectors will be  $\begin{bmatrix} 1 & -s r_3 & -s r_2 \end{bmatrix}'$ . For Listing’s law, this simply becomes  $\begin{bmatrix} 1 & 0 & 0 \end{bmatrix}'$  which is no longer dependent on the position (because we are now in coordinate velocity space rather than angular velocity space). The coordinate velocity necessary to adhere to any gimbal score can now be easily calculated. A similar procedure can be performed with a more general second order surface. Constraints that need to be in terms of angular velocity (such as minimum rotation, defined as  $N = f$ ) can be easily converted to coordinate velocity using (5.9).

## 5.10 Conclusions

Eye saccades and extended arm movements that observe a flat Listing’s law constraint can be modeled by a number of models for simple point to point trajectories. This is because Listing’s law holds during a single axis rotation between two points in Listing’s plane. Two classes of models have been considered - models where the entire movement is planned from the beginning,

---

<sup>1</sup>A nonholonomic constraint on velocity is one that cannot be integrated to give a constraint on orientation.

and feedback models where the current orientation (or an efference copy of it) is compared to the desired orientation and the error between them reduced throughout the movement.

During double step movements, the situation is more complex as in general these movements will not be single axis rotations.

Superposition of the coordinate velocity ( $\vec{r}$ ) will produce double step movements that satisfy Listing's law due to the constant zero torsional component ( $\dot{r}_x = 0$ ), while superposition of angular velocity  $\vec{\omega}$  will fail to produce trajectories that satisfy Listing's law. Superposition of the rotation vectors  $\vec{r}$  will not produce trajectories that satisfy Listing's law, although at the end points the correct torsional values will be produced, and during the movement, the torsion will be close to that dictated by Listing's law.

When the surface for constraining the rotation vectors is not flat, the situation is more complicated than for the flat Listing's plane. Even for point to point movements, the constraint on torsion cannot just be set at the beginning and the end of the movement, but must be constrained throughout the movement.

A solution to this problem is to perform superposition in two dimensions, using, for example, the  $\theta_F$  and  $\phi_F$  angles from the Fick angle representation. Superposition in these coordinates can be performed, with the torsional component constrained after superposition has taken place.

An alternate method for constraining orientation is to constrain the velocity. Donders' law constraints can be expressed in terms of velocity constraints, as well as nonholonomic constraints that cannot be expressed only in terms of orientation. Again the constraints must be placed in what is essentially the last step to ensure that the orientations produced by this model can satisfy the various Donders' law constraints.

There are two fundamental questions that remain regarding the models used for the generation of extended arm movements. Is the fundamental mechanism used for generating arm movements a feedback system or based on superposition at some level? Secondly, are the constraints needed for

Donders' law applied at the level of orientation or velocity? While an analysis of double step movements may shed light on the first question, analysis of the produced movements may be insufficient to differentiate between the two methods for constraining torsion.

# Chapter 6

## Models of motion planning for extended arm pointing movements

### 6.1 Introduction

This chapter describes an experiment designed to test the predictive powers of models for describing extended arm movements. As background, the form of trajectories in position and orientation space of single step and double step movements were examined. Then the predictions of several models for describing double step movements were compared. A comparison was made between a superposition and an abort-replan model, between the use of different Donders' law constraints, and between models that operate in orientation space compared to coordinate velocity space.

### 6.2 Methods

The experimental setup is the same as described in Chapter 4.

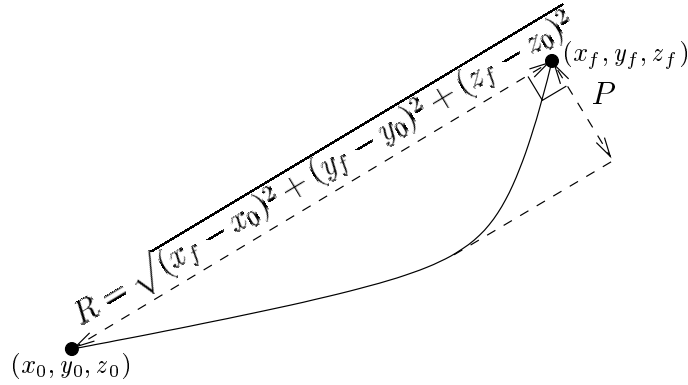


Figure 6.1: A measure of curvature from Smit & Van Gisbergen (1990), defined as  $C = \frac{P}{R}$ . A negative sign indicates the deviation (in the y-z plane) was in the counterclockwise direction, a positive sign in the clockwise direction.

### 6.2.1 Techniques of analysis

First, the unperturbed (single step) trajectories were analyzed. The shapes of the trajectories were considered in both task space, and in rotation vector space. The curvature of the saccades was measured using the measure described in Smit & Van Gisbergen (1990):

$$C = P/R \quad (6.1)$$

where  $R$  is the amplitude of the straight line connecting the start and the end of the movement,  $P$  is the largest perpendicular deviation from this line, and  $C$  is the curvature (see Figure 6.1). The invariance of the velocity and angular velocity was compared, using principal components analysis (PCA) for functions, based on Ramsay & Silverman (1997) using the accompanying Matlab software (Ramsay, 2001). Principal components analysis for functions identifies the strongest modes of variation in the variables by finding a weight function that maximizes a measure of this variation. Each principal component is orthogonal to all other components so that each component shows something new, and has a score to indicate how much of the variation it accounts for.

Velocity and angular velocity are analyzed rather than position or orienta-

tion because they ignore shifts between the starting positions of movements. The variations in the velocity and angular velocity within and between subjects were considered.

Initially, the trajectories of the double step movements were considered in two dimensions in Fick notation, using  $\theta_F$  and  $\phi_F$ . This uniquely defines the pointing direction of the arm, but not the torsion. The following analysis was performed simultaneously in the  $\theta_F$  and  $\phi_F$  components on each double step movement.

A superposition scheme similar to that in Flash & Henis (1991) was used.

1. A point-to-point trajectory was selected from the control movements, that after being appropriately time-scaled to coincide with the trajectory being tested, is the closest (in terms of mean distance) during the first tenth of the duration of the movement. The selection of the closest control movement was necessary because of significant variation in the starting positions of the movements. This trajectory was called the first control movement ( $\theta_1(t)$ ).
2. The first significant deviation in velocity profiles between the first control movement and the test movement was found.
3. The second control movement was found by scaling in time and space the mean of single step movements from the first target to the second target so that it began at the time the first control movement ended at the location of the end of the first control movement, and finished at the time of the end point of the movement at the location of the end point of the double step movement. This was called the second control movement ( $\theta_2(t)$ ).
4. From the time of the first significant deviation, the trajectory produced by the superposition model was defined as the addition of the first control movement, and the difference of the second control movement

from its starting position. i.e.

$$\theta(t) = \begin{cases} \theta_1(t) & 0 \leq t < t_1 \\ \theta_1(t) + \theta_2(t - t_1) - \theta_b & t_1 \leq t \leq t_2 \\ \theta_b & t_2 \leq t \leq t_1 \\ \theta_2(t - t_1) & t_2 \leq t \leq t_3, t_1 \leq t \leq t_3 \end{cases} \quad (6.2)$$

where  $\theta(t)$  is the Fick angle at time  $t$ ,  $\theta_b$  is the Fick angle at the end of the first control movement,  $t_1$  is the time at the first significant deviation between the first control movement and the test movement,  $t_2$  is the time at the end of the first control movement,  $t_3$  is the time at the end of movement and  $t$  is the time such that  $0 \leq t \leq t_3$  throughout the movement.

Note that if there is no overlap (i.e. the first control movement ends before  $t_1$ ) then the Fick angle remains at  $\theta_b$  from  $t_2$  until  $t_1$ .

5. As an alternative scheme, the abort-replan strategy will be tested, based on the techniques presented in Henis (1991). A 5th order polynomial will be fitted such that the Fick angle, velocity and acceleration at the start of the movement are equal to those of the trajectory being tested at the time of the first significant deviation. The angle at the end of the predicted movement needs to be equal to the angle at the end of the movement being tested, and the velocity and acceleration are assumed to be zero at the end of the movement. The unique 5th order polynomial that satisfies these constraints can be expressed as

$$\begin{aligned} \theta_{a-r}(t) = & \left(6\theta_c - 6\theta_d - 3\dot{\theta}_d - \frac{1}{2}\ddot{\theta}_d\right) \left(\frac{t - t_1}{t_3 - t_1}\right)^5 \\ & + \left(-15\theta_c + 15\theta_d + 8\dot{\theta}_d + \frac{3}{2}\ddot{\theta}_d\right) \left(\frac{t - t_1}{t_3 - t_1}\right)^4 \\ & + \left(10\theta_c - 10\theta_d - 6\dot{\theta}_d - \frac{3}{2}\ddot{\theta}_d\right) \left(\frac{t - t_1}{t_3 - t_1}\right)^3 \\ & + \frac{1}{2}\ddot{\theta}_d \left(\frac{t - t_1}{t_3 - t_1}\right)^2 + \dot{\theta}_d \left(\frac{t - t_1}{t_3 - t_1}\right) + \theta_d \end{aligned} \quad (6.3)$$

where  $\theta_{a-r}(t)$  is the predicted Fick angle of the abort-replan model (valid for  $t_1 \leq t \leq t_3$ ),  $\theta_c$  is the Fick angle at the end of the trajectory (time  $t_3$ ),  $\theta_d$  is the Fick angle at the time of the first significant deviation between the first control and the test movement ( $t_1$ ), and  $\dot{\theta}$  and  $\ddot{\theta}$  represent the first and second derivatives with respect to time. The entire predicted movement can be expressed as:

$$\theta(t) = \begin{cases} \theta_1(t) & 0 \leq t < t_1 \\ \theta_{a-r}(t) & t_1 \leq t \leq t_3 \end{cases} \quad (6.4)$$

The two trajectories in terms of  $\theta_F$  and  $\phi_F$  were compared to the experimental double step trajectories. The error is defined as the distance between the prediction of the model and experimental data summed over the sample points, divided by the distance of the experimental data from the start of the movement summed over the sample points:

$$E_F = \frac{\sum_i \sqrt{(\theta_{m_i} - \theta_{e_i})^2 + (\phi_{m_i} - \phi_{e_i})^2}}{\sum_i \sqrt{(\theta_{e_i} - \theta_{e_1})^2 + (\phi_{e_i} - \phi_{e_1})^2}} \quad (6.5)$$

where  $\theta_{m_i}$  and  $\theta_{e_i}$  are the relevant Fick coordinates at time  $i$  for the model and experimental data respectively, where  $i = 1$  refers to the time at the start of the movement. The sum is performed over the time points where the movement is sampled.

6. The models were also be extended to 3D rotation vector space. To do this, the rotation vectors were generated from the Fick angles, which can be performed using equation (2.13). However, this equation requires the Fick torsional angle  $\psi_F$ , which is unknown. A constraint can be placed on the torsion using Donders' law. Equation (2.13) provides three equations, while the Donders' law constraint provides a fourth. A second order surface, where the constraint is equation (3.3), and a Listing's law constraint ( $r_x = 0$ ) were tested. The constants generated in fitting the surfaces in Chapter 4 were used for the second order surface.

This gives four unknowns,  $r_x$ ,  $r_y$ ,  $r_z$  and  $\psi_F$ , and four equations. Note that the  $r_y$  and  $r_z$  values for a given pointing direction are not unique. It is not clear if there is an analytic solution to find these variables - hence the solution was found numerically, using the Levenberg-Marquardt method (Jacobs, 1977). The predicted rotation vectors will be compared to those from the experimental data, using a similar error measure to before:

$$E_r = \frac{\sum_i \sqrt{(r_{x_{mi}} - r_{x_{ei}})^2 + (r_{y_{mi}} - r_{y_{ei}})^2 + (r_{z_{mi}} - r_{z_{ei}})^2}}{\sum_i \sqrt{(r_{x_{ei}} - r_{x_{e1}})^2 + (r_{y_{ei}} - r_{y_{e1}})^2 + (r_{z_{ei}} - r_{z_{e1}})^2}} \quad (6.6)$$

where  $r_{x_{mi}}$  and  $r_{x_{ei}}$  are the rotation vector component  $r_x$  of the model and the experimental data at time  $i$ .

A similar algorithm will be followed to test the “velocity box” model.

1. The time derivative of the Fick angles will be calculated.
2. The conversion to coordinate velocity vectors is achieved using Equation (2.15). An additional equation is specified by the constraint on velocity, as explained in Chapter 5. In this case, the constraint is the time derivative of the second order surface (3.3):

$$\dot{r}_x = e\dot{r}_y + f\dot{r}_z + 2g\dot{r}_y r_y + h(\dot{r}_y r_z + \dot{r}_z r_y) + 2j\dot{r}_z r_z \quad (6.7)$$

In this case there are five unknowns ( $\dot{r}_x, \dot{r}_y, \dot{r}_z, \psi, \dot{\psi}$ ) (the value of  $r_x, r_y$  and  $r_z$  are assumed to be known from feedback, according to the velocity box model), but only four equations. A fifth equation can be written relating  $\psi$  to the current orientation.

The rotation to a given arm orientation can be decomposed into two rotations - one which rotates the arm to the desired position, and another which rotates the arm about its own axis to give the desired value of torsion. The first rotation is equivalent to the first two terms in the equation for a rotation in Fick coordinates (2.5), while the second is

equivalent to the rotation by the Fick torsional angle  $\psi$  about the pointing direction of the arm. This can be expressed as the composition of two rotation vectors:

$$\vec{r}_{\text{total}} = \vec{e}_r \tan\left(\frac{\psi}{2}\right) \circ \vec{n} \tan\left(\frac{\alpha}{2}\right) \quad (6.8)$$

where  $\vec{r}_{\text{total}}$  is the rotation vector representing the combined (total) rotation to the current arm position from the reference position,  $\vec{e}_r$  is a unit vector in the direction of the pointing direction,  $\vec{n}$  is the unit vector that is the axis of rotation for a rotation from the reference position to  $\vec{e}_r$ , while  $\alpha$  is the angle of rotation about that axis that takes the arm to its current pointing direction (from the reference position).

This expression can be expanded using the rule for rotation vector composition (2.8):

$$\vec{r}_{\text{total}} = \frac{\vec{e}_r \tan\frac{\psi}{2} + \vec{n} \tan\frac{\alpha}{2} + \vec{e}_r \tan\frac{\psi}{2} \times \vec{n} \tan\frac{\alpha}{2}}{1 - (\vec{e}_r \tan\frac{\psi}{2}) \cdot (\vec{n} \tan\frac{\alpha}{2})}$$

Note that  $\vec{n}$  and  $\vec{e}_r$  are orthogonal, so their dot product will be zero

$$\Rightarrow \vec{r}_{\text{total}} = \vec{e}_r \tan\frac{\psi}{2} + \frac{\vec{e}_0 \times \vec{e}_r}{|\vec{e}_0 \times \vec{e}_r|} \tan\frac{\alpha}{2} + \vec{e}_r \tan\frac{\psi}{2} \times \frac{\vec{e}_0 \times \vec{e}_r}{|\vec{e}_0 \times \vec{e}_r|} \tan\frac{\alpha}{2} \quad (6.9)$$

Let the reference position be a unit vector pointing straight ahead ( $\vec{e}_0 = [1 \ 0 \ 0]'$ ) and the current pointing direction will be defined as  $\vec{e}_r = [x \ y \ z]'$ , where  $\sqrt{x^2 + y^2 + z^2} = 1$ . Then

$$\vec{e}_0 \times \vec{e}_r = \begin{bmatrix} 0 \\ -z \\ y \end{bmatrix} \quad \text{and} \quad \vec{e}_r \times (\vec{e}_0 \times \vec{e}_r) = \begin{bmatrix} y^2 + z^2 \\ -xy \\ -xz \end{bmatrix} \quad (6.10)$$

Equation (6.9) is a three element vector equation - we will look at just

the first component ( $r_x$ ):

$$\begin{aligned} r_x &= x \tan \frac{\psi}{2} + \tan \frac{\psi}{2} \tan \frac{\alpha}{2} \frac{y^2 + z^2}{\sqrt{y^2 + z^2}} \\ \Rightarrow \tan \frac{\psi}{2} &= \frac{r_x}{x + \sqrt{y^2 + z^2} \tan \frac{\alpha}{2}} \end{aligned} \quad (6.11)$$

The angle  $\alpha$  is the angle between  $\vec{e}_r$  and  $\vec{e}_0$ , and hence can be expressed as

$$\alpha = \arccos(\vec{e}_0 \cdot \vec{e}_r) = \arccos(x) \quad (6.12)$$

Using the identity

$$\tan \frac{\alpha}{2} = \pm \sqrt{\frac{1 - \cos \alpha}{1 + \cos \alpha}} \quad (6.13)$$

the value of  $\psi$  can now be found

$$\psi = 2 \arctan \left( \frac{r_x}{x \pm \sqrt{y^2 + z^2} \sqrt{\frac{1-x}{1+x}}} \right) \quad (6.14)$$

With the five equations, a numerical solution for  $\vec{r}$  can be found at each time step. The rotation vectors can be calculated by integrating  $\vec{r}$ . The rotation vector at the beginning of the movement was assumed to be the same as that from the experiment. The rotation vectors calculated were then compared to the experimental data as before using Equation (6.6).

## 6.3 Results

### 6.3.1 Analysis of control movements

When considered in three-dimensional position space, such as in the coordinate system described in Figure 2.1, extended arm movements span the surface of a sphere (centered at the shoulder), and hence a point to point

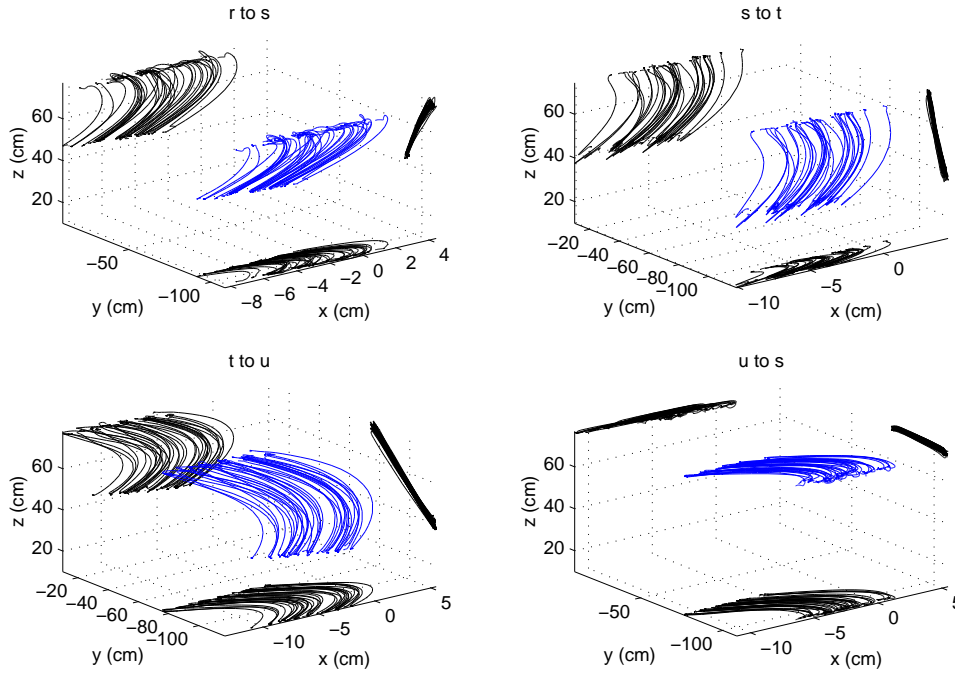


Figure 6.2: Trajectories of the control movements for subject 3. The black lines show the projections onto the  $x$ - $y$ ,  $y$ - $z$  and  $x$ - $z$  planes.

movement can not be a straight line in the workspace. This can be seen in the control movements – those for subject 3 are shown in Figure 6.2. The results for the other subjects can be found in Appendix D. The paths for the same control movement are all very similar - the main cause of variability here is variation in the  $x$  coordinate, which may be caused by small translations of the shoulder (although it should be noted that the scale of the axes are not uniform, and so the variation in the  $x$  component is quite small).

The trajectories, as expected, are curved, although the projection onto the  $y - z$  plane shows nearly straight paths in this plane. While a geodesic is the shortest path between two points on a sphere, straight paths in the  $y - z$  plane are *not*, in general, geodesics. A straight line projection in the  $y - z$  plane means that there is a plane that passes through a straight line in the  $y - z$  plane and the path. If the path were a geodesic, then there

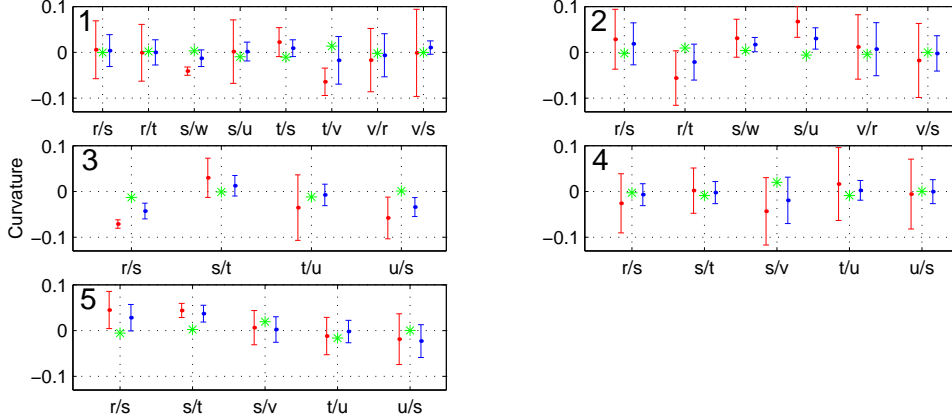


Figure 6.3: Curvature of the control movements (position). Each graph represents one subject. The points show the mean, and the error bars the standard deviation of the curvature (defined in (6.1)) of each point to point movement for each subject. Red shows the value calculated for all three coordinates, blue is just the movements in the  $y$ - $z$  plane. The green points mark the curvature of a geodesic between the two points.

must also be a plane that passes through the path and the origin. If it were a geodesic, these two planes must intersect along the path, but the intersection of two planes will not be a curve, and so in general such a movement is not a geodesic (purely vertical movements are an exception to this rule because the two planes are the same). However the range of movements being considered was sufficiently small that the projection of a geodesic in the  $y - z$  plane was very close to a straight line.

A summary of the curvature of all the movements for all subjects is shown in Figure 6.3, along with the curvature if the movement were a geodesic. The geodesic was found by taking the relevant portion of the intersection of the sphere of reachable points for the extended arm, and a plane that includes the start and end points and the centre of the sphere.

The diagonal movement  $r \rightarrow s$  shown in Figure 6.2 has some curvature, more than is expected if it were a geodesic. However, the direction of the

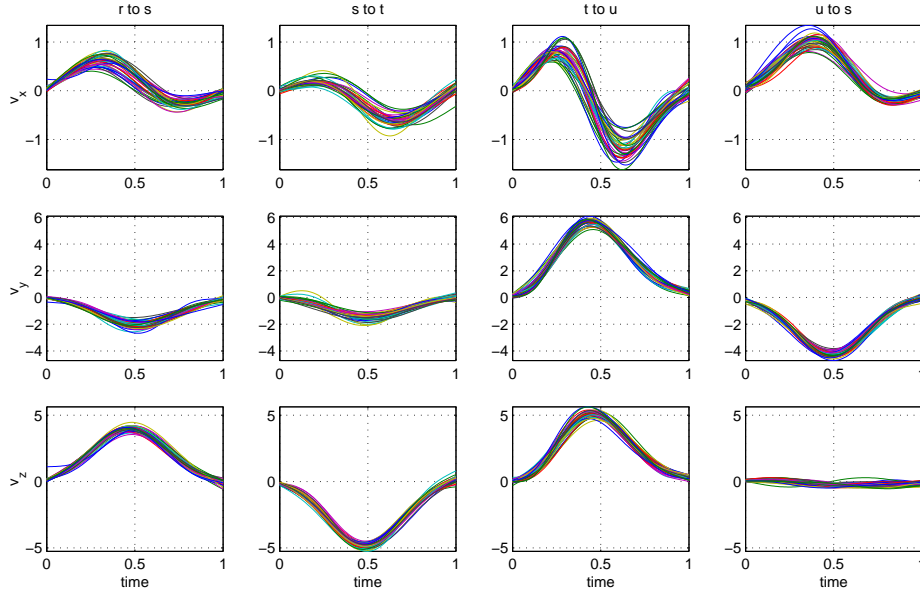


Figure 6.4: Subject 3: Velocity during control movements.

curvature is not consistent across subjects (for example, subject 3 has curvature with a similar magnitude but in the opposite direction). In general, the curvature of the position is generally quite small, less than 0.1. Most of the curvature is found due to variation in  $x$  values. When the curvature is calculated for the projection in the  $y - z$  plane, significantly smaller values are found, although often larger than that required for a geodesic, and even curved in the opposite direction. For many of the movements, the mean is close to zero, with positive and negative curvature found. This suggests that for these movements, the curvature is a result of errors rather than a consequence of the motor plan. Higher curvature is seen in a few cases - for example,  $s \rightarrow v$  for subject 4 and  $r \rightarrow s$  for subjects 3 and 5, these are all diagonal movements.

Invariant velocity profiles were found across the control movements, after being appropriately time scaled. The velocity profiles for all the control movements for subject 3 are shown in Figure 6.4. The profiles for the other subjects can be found in Appendix G.

In the  $v_y$  and  $v_z$  components, a bell shaped velocity profile is seen, which is fairly invariant between movements (which have been time scaled, with the velocity also scaled to ensure the integral of the graph remains constant). In the  $v_x$  component, a reverse in the direction of the velocity is seen - this is because the movements take place on a sphere.

To compare the variation in the control movements, principal components analysis was performed. The analysis of the velocity of one set of control trajectories, that for Subject 5, movement  $r \rightarrow s$ , is shown in Figure 6.5.

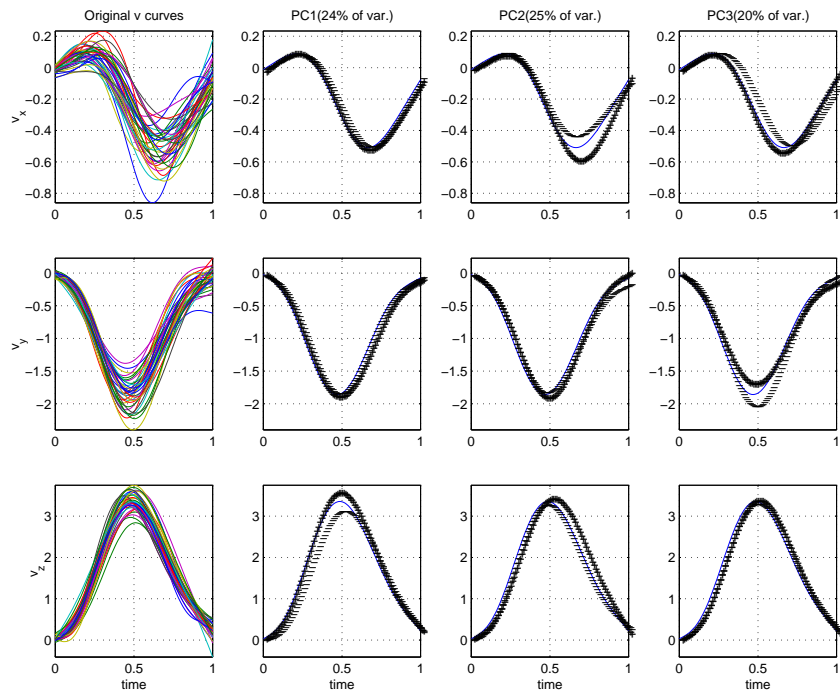


Figure 6.5: Principal Components Analysis of the velocity for Subject 5, movements from  $r$  to  $s$ . The blue lines are the mean, shown with the addition(+) and subtraction (-) of a suitable multiple of each Principal component curve (Ramsay & Silverman, 1997).

The principal components analysis of these movements shows that much of the variation is due to difference in the amplitude - 24% of the variation is due to differences in amplitude mostly in the  $v_z$ , 20% to amplitude differences

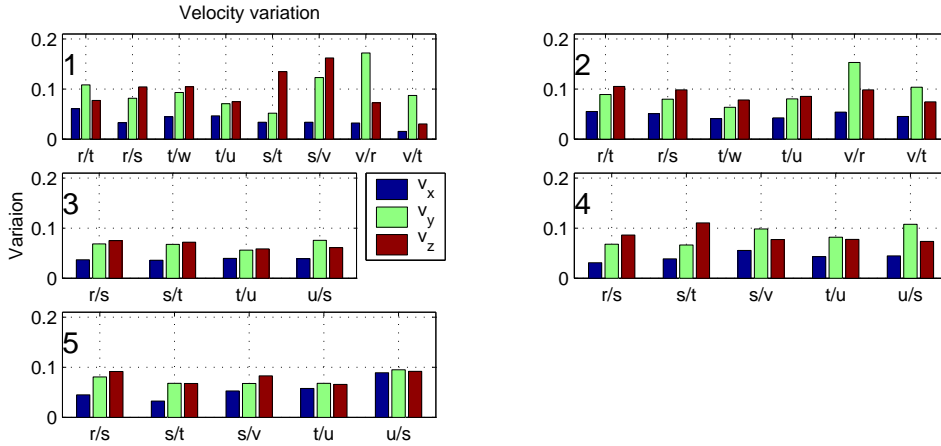


Figure 6.6: Inter-movement variation of the velocity of the control movements. The bars show the magnitude of the area of the graph of the standard deviation as a proportion of the area of the (absolute value of the) mean.

mostly in the  $v_y$  component, and 25% due to amplitude differences mostly in the  $v_x$  component. It should be noted that the variation is in the amplitude rather than the timing of the peaks - these are probably due to small errors in locating the start or end points. In summary, the velocity profiles (here for 37 control movements) for this control movement are largely invariant. Similar results are found for other movements and subjects. The variation in the different components is summarized for all the subjects in Figure 6.6.

Throughout all the movements, the variation in the  $v_x$  component is the smallest - this is probably because with extended arm movements, there is little room for variation in this direction.

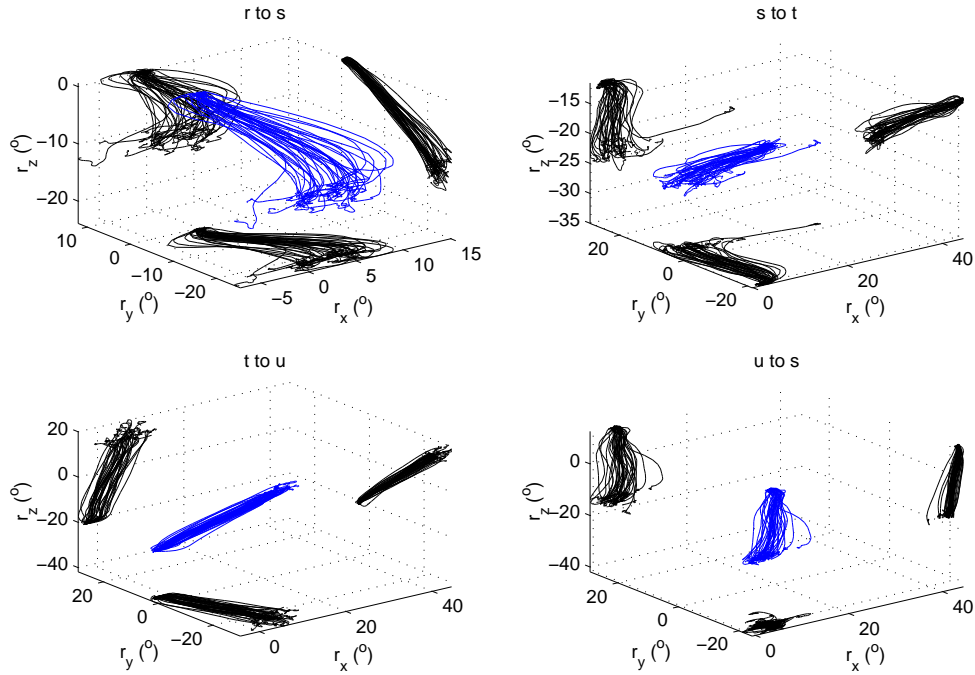


Figure 6.7: Trajectories of the forearm for control movements of subject 3 in rotation vector space. The black lines show the projections onto the  $r_x - r_y$ ,  $r_y - r_z$  and  $r_x - r_z$  planes.

When the control trajectories are considered in rotation vector space, a different picture emerges. The control movements for subject 3 in rotation vector space are displayed for the forearm (Figure 6.7) and the upper arm (Figure 6.8). The trajectories for the other subjects can be found in Appendices E and F.

Less uniformity is seen when the movements are considered in rotation vector space rather than three-dimensional position space. Curvature is seen for the rotation vectors. The curvature of all the movements is summarized in Figure 6.9.

Some movements show highly curved trajectories in rotation vector space (for example the upper arm rotation of subject 5, movement  $r \rightarrow s$ ). These suggest that single axis rotations are not used here. The curvature differs

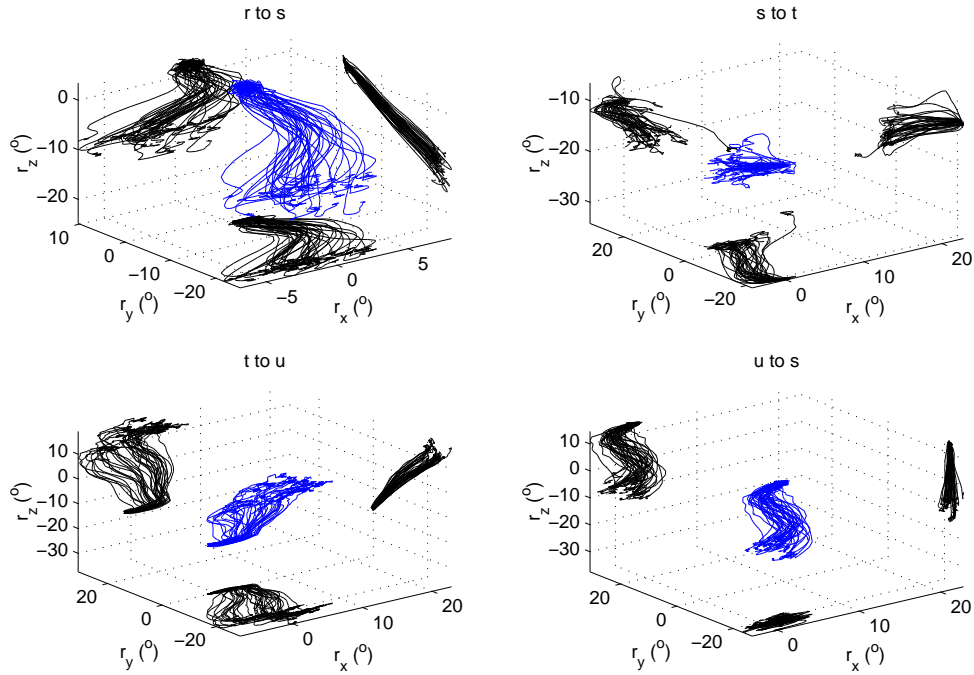


Figure 6.8: Trajectories of the upper arm for control movements of subject 3 in rotation vector space. The black lines show the projections onto the  $r_x - r_y$ ,  $r_y - r_z$  and  $r_x - r_z$  planes.

between the upper arm and forearm orientations in some of the movements. An inspection of the graphs shows that this is primarily due to differences in the  $r_x$  component.

The angular velocity for the upper arm and forearm for subject 2 are shown in Figures 6.10 and 6.11. The profiles for the other subjects can be found in Appendices H and I.

The variation in the different components of the angular velocity is summarized in Figure 6.12. Here it can be seen that in general the variation in  $r_x$  is greater than that for the other components. This effect is more noticeable in forearm that in upper arm rotations.

This difference can be highlighted with an example, that of Subject 5 for movement  $t \rightarrow u$  (for 37 control movements). The principal components

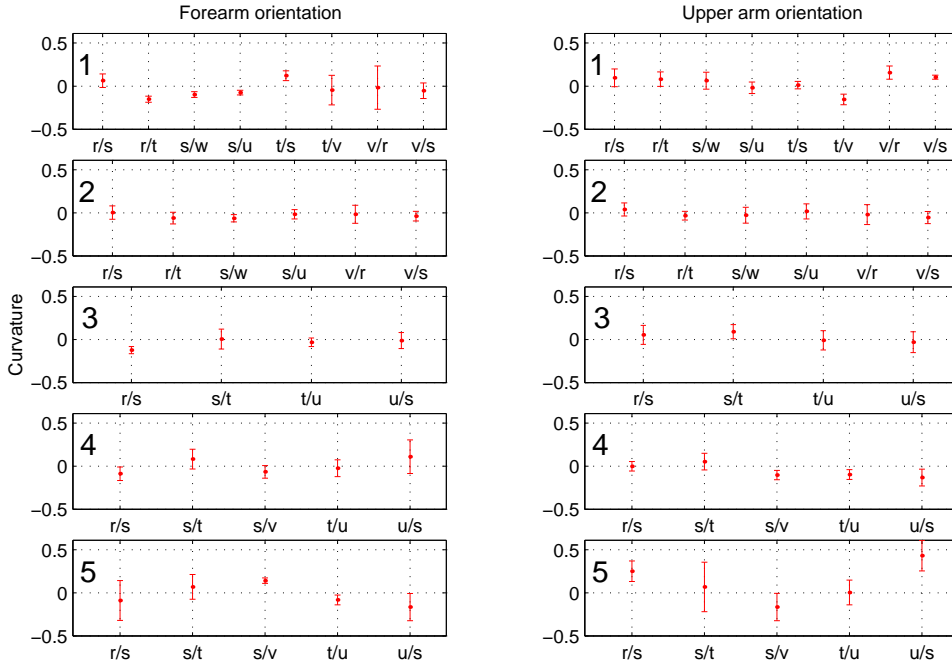


Figure 6.9: Curvature of the control movements in rotation vector space. Each row represents one subject. The points show the mean, and the error bars the standard deviation of the curvature (defined in (6.1)) of each point to point movement for each subject in rotation vector space.

analysis of these movements for the forearm and upper arm are plotted in Figures 6.13 and 6.14. In both sets of movements, the  $\omega_y$  and  $\omega_z$  components are bell shaped, nearly symmetric and largely invariant. However, the  $\omega_x$  component shows a great deal of variation in the forearm movements. PCA shows that the principal components PC1 and PC2 shown in Figure 6.13 are mostly due to large variations in  $\omega_x$  - together these two components account for 58% of the variation. For the upper arm, while the variation in the  $\omega_x$  component is more than that for the other components, it is of a smaller proportion than for the forearm. Similar results are seen for the other movements of subject 5, and for the other subjects.

Looking at movements in rotation vector space provides a more complete

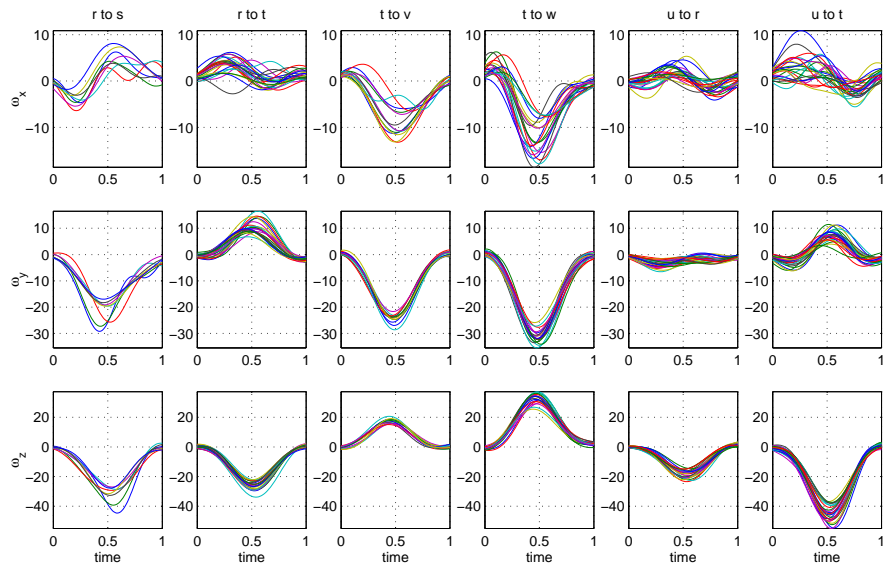


Figure 6.10: Subject 2: Forearm angular velocity during control movements.

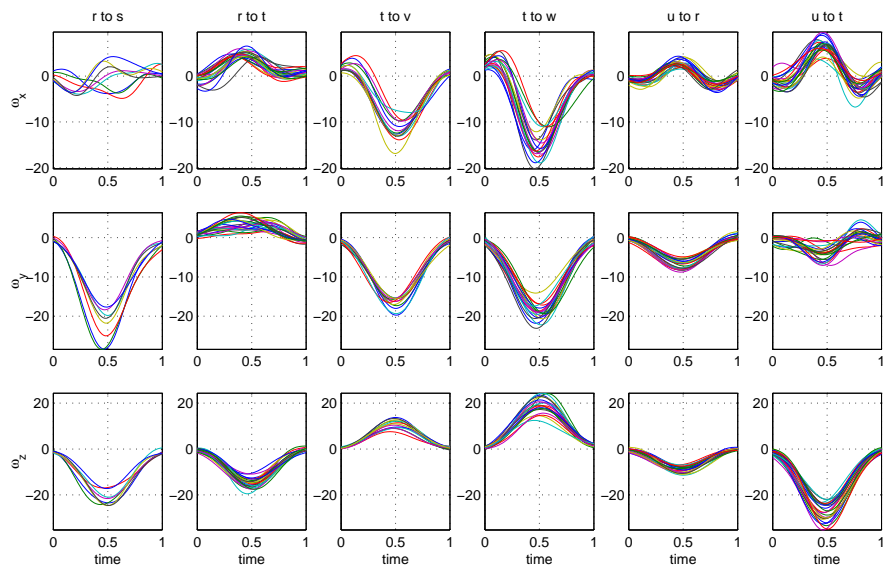


Figure 6.11: Subject 2: Upper arm angular velocity of control movements.

description of the arm's posture for extended arm movements than position space. The torsional component  $\omega_x$  of the angular velocity shows much more

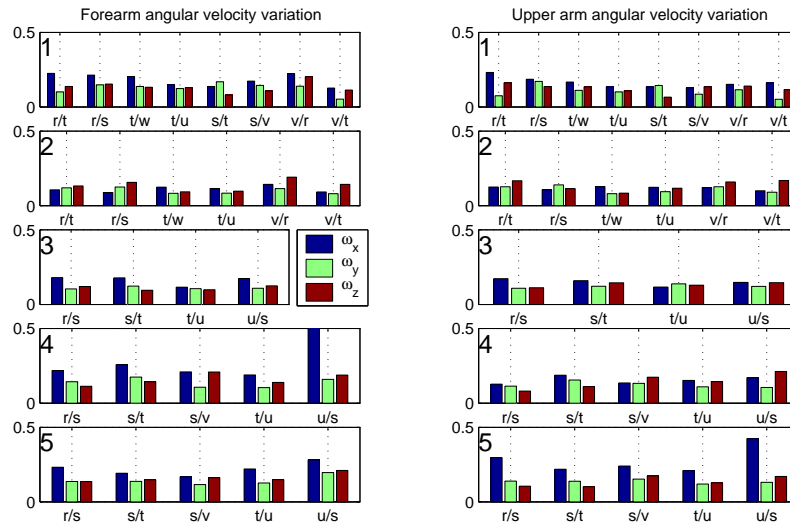


Figure 6.12: Inter-movement variation of control movement angular velocity. The bars are the magnitude of the area under the standard deviation graph as a proportion of the area under the (absolute value of the) mean.

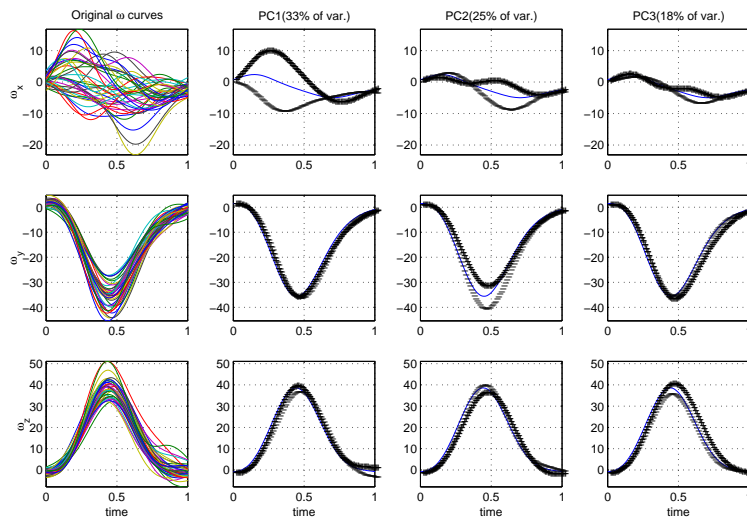


Figure 6.13: Principal Components Analysis of the angular velocity of forearm control movements for Subject 5, movements from  $t$  to  $u$ .

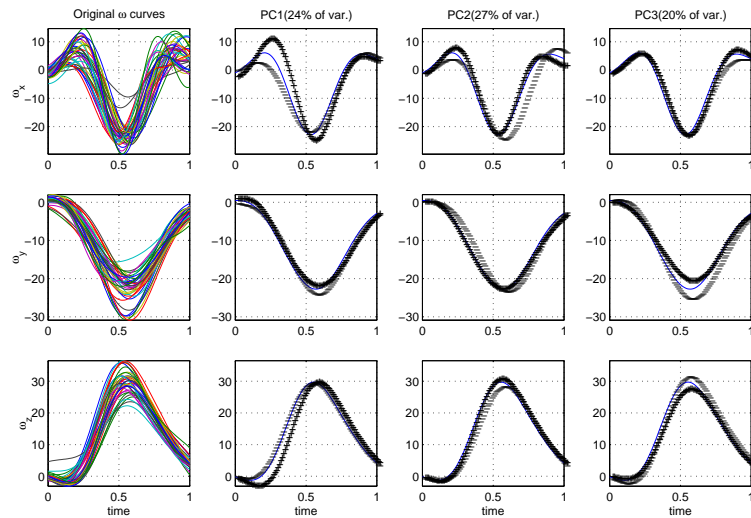


Figure 6.14: Principal Components Analysis of the angular velocity of upper arm control movements for Subject 5, movements from  $t$  to  $u$ .

variation than the other components (especially for movements of the forearm) - this information can not be seen by only looking at the movements in position space.

### 6.3.2 Analysis of double step movements

Initially, the trajectories were analyzed in two dimensions, using the Fick coordinates  $\theta_F$  and  $\phi_F$  (but not  $\psi_F$ ). Two models were tested - the superposition model, and an abort-replan model. The results of these predictions, along with the actual trajectories are plotted for Subject 3, Set 1 for the forearm (Figures 6.15, 6.17, and 6.19) and the upper arm (Figures 6.16, 6.18, 6.20).

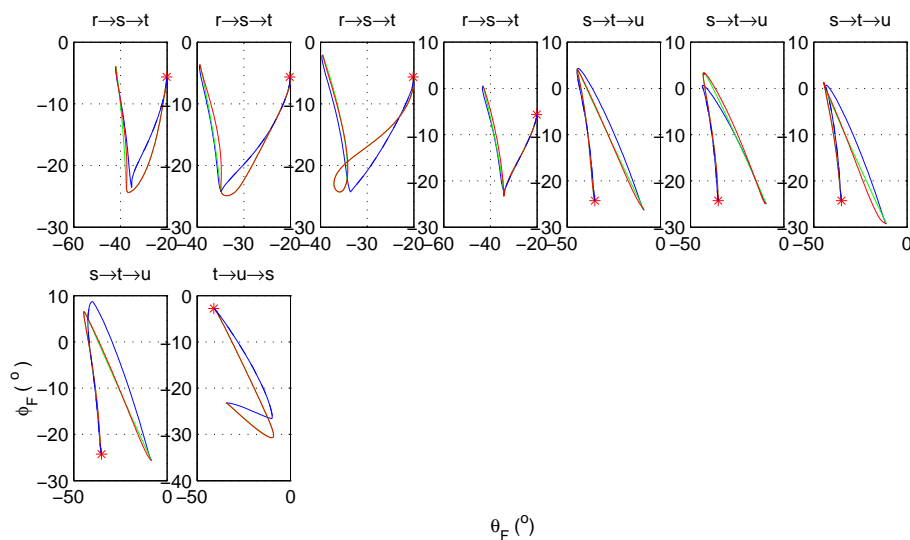


Figure 6.15: Predicted and actual two dimensional trajectories for small overlap (less than 0.2) for the forearm for Subject 3, Set 1 plotted in the  $\theta_F$ (horizontal axis) -  $\phi_F$ (vertical axis) plane. The red line shows the actual movement, the solid blue line the prediction from the superposition scheme, the dashed blue line the first control movement and the green line the prediction from the abort-replan scheme.

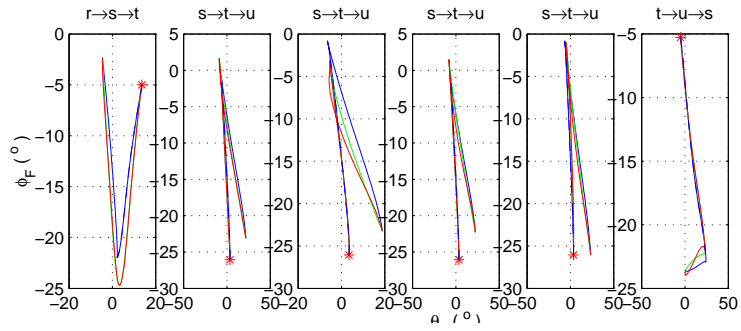


Figure 6.16: Predicted and actual 2D Fick trajectories for small overlap (less than 0.2) for the upper arm. See Fig. 6.15 for an explanation of the colours.

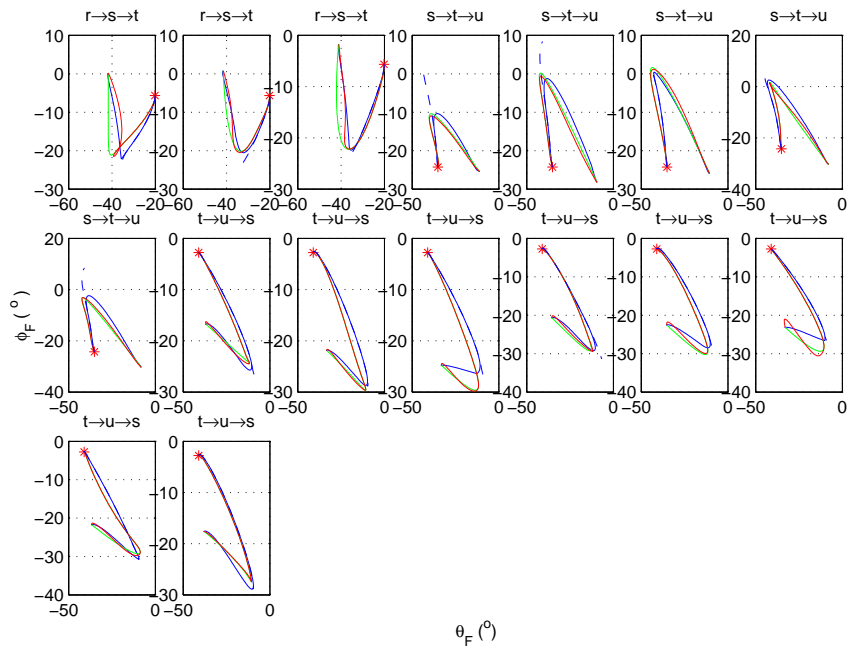


Figure 6.17: Predicted and actual 2D Fick trajectories for medium overlap (between 0.2 and 0.6) for the forearm for Subject 3, Set 1. See Fig. 6.15 for an explanation of the colours.

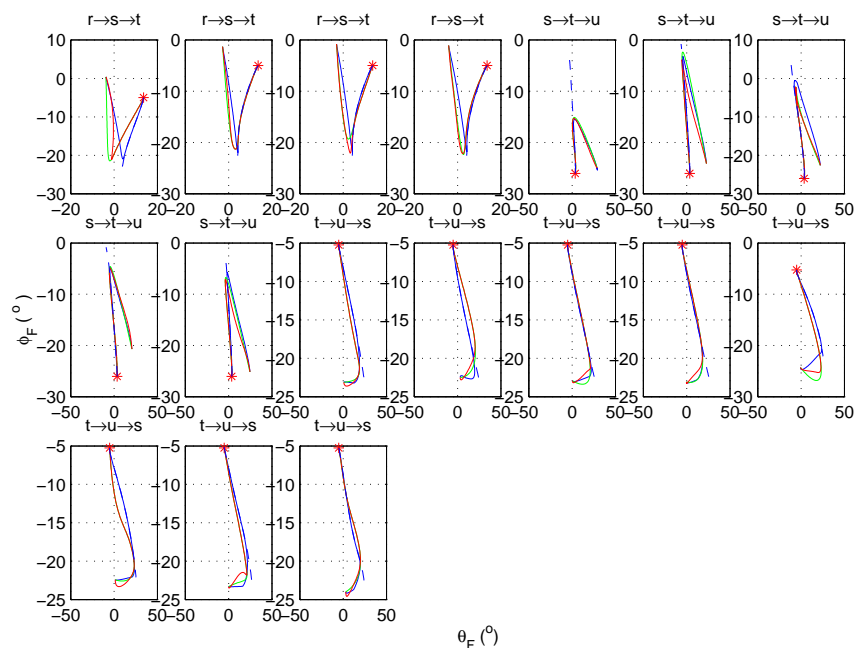


Figure 6.18: Predicted and actual 2D Fick trajectories for medium overlap (between 0.2 and 0.6) for the upper arm for Subject 3, Set 1. See Fig. 6.15 for an explanation of the colours.

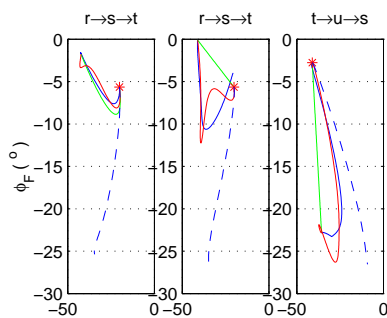


Figure 6.19: Predicted and actual 2D Fick trajectories for large overlap (greater than 0.6) for the forearm for Subject 3, Set 1. See Fig. 6.15 for an explanation of the colours.

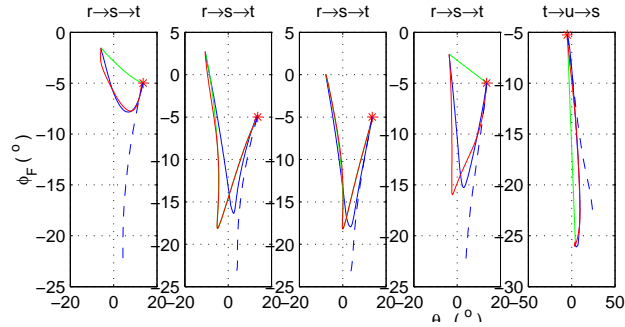


Figure 6.20: Predicted and actual 2D Fick trajectories for large overlap (greater than 0.6) for the upper arm for Subject 3, Set 1. See Fig. 6.15 for an explanation of the colours.

For ease of comparison, the movements were divided into 3 groups, based on the “overlap” - this is defined as, assuming superposition takes place, the proportion of time (of the complete movement) that the two control trajectories are operating at the same time. They were divided into those with small or no overlap (overlap less than or equal to 0.2), those with moderate overlap (overlap between 0.2 and 0.6), and those with large overlap (overlap greater than 0.6). Different behaviour can be seen in the different cases.

When there is no or small overlap, the combined trajectory consists of a movement to the first target, followed by a movement from the first to the second target, either with a pause between the movements (if there is no overlap), or with the second movement starting slightly before the end of the first movement. The difference between the predictions of the abort-replan and the superposition schemes is negligible for such movements.

Where there is a moderate overlap (between 0.2 and 0.6), a more curved trajectory can be seen near the end of the first control trajectory. The addition of the start of the second control movement causes a smooth turn to the second target rather than a sharp point. Again, the predictions from both schemes are very similar, and give predictions close to the actual trajectories.

For large overlaps (greater than 0.6), the trajectory of the double step

movement very quickly deviates from that of the first control movement, and highly curved trajectories are generated. In some of these cases, a large difference is seen between the prediction of the superposition and the abort-replan scheme. The superposition scheme in these cases provides a much better approximation to the trajectory. This is because the trajectory does not take the most direct path (while taking into account smoothness of velocity and acceleration), as would be the case if an abort-replan scheme were used. The graphs of large overlap for the other subjects are displayed in Appendix J.

The errors in predicting the trajectories for the two schemes for Subject 3 are summarized in Figure 6.21. The results for the other subjects can be found in Appendix K.

The results have been presented grouped by ISI. Movements with large overlaps are only seen for small ISIs. When the ISI is 300ms or above, there are generally no large overlaps found (an exception is found in Subject 2). This is because of the reaction time - the first movement would be completed or nearly completed before the target jumps and the modification can take place.

Both of the models considered operate in two dimensional Fick coordinate space. The summary of the errors show that in these coordinates both models have good predictive powers when there is no, small or moderate overlap. Both models produce very similar predictions for such overlaps. The predictions of the superposition model are in general slightly worse for large overlaps compared to smaller overlaps, however they are much better than the predictions of the abort-replan model. Hence only the superposition model provides good predictions throughout the entire range of overlaps for movements considered in terms of  $\theta_F$  and  $\phi_F$ .

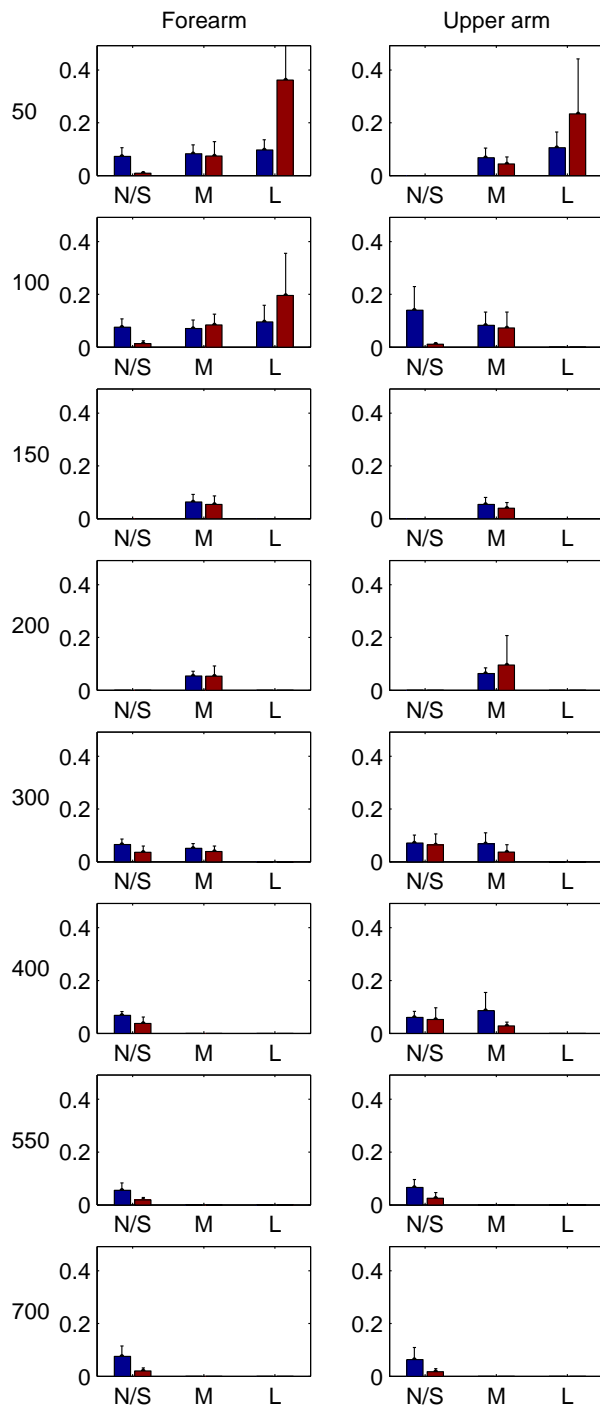


Figure 6.21: Summary of errors of two dimensional models for subject 3. The height of the bars represent the mean, and the length of the errors bars the standard deviation of the error between the actual trajectory and the prediction of the models, for the superposition model (in blue), and the abort-replan model (in red). The results are divided into those with no or small (N/S) overlap (less than 0.2), with moderate (M) overlap (between 0.2 and 0.6), and large (L) overlap (greater than 0.6). The left column shows the results for the forearm and the right for the upper arm. Each row presents the results for the ISI time shown at the left of the column. Similar results are seen for no, small and moderate overlap, while the superposition model performs better for large overlaps.

The rotation vectors equivalent to the Fick angles generated by the superposition scheme were then calculated, under the assumption of Donders' Law. Two Donders' law conditions were tested - Listing's law ( $r_x = 0$ ), and a second order surface. The rotation vectors for Subject 3, Set 1 are shown for the forearm (Figure 6.22) and the upper arm (Figure 6.23).

These graphs are plotted in components ( $r_x, r_y$  and  $r_z$ ) against time. The results for the other subjects for the cases with large overlap are displayed in Appendix L.

The predicted  $r_y$  (green) and  $r_z$  (red) components are quite similar for all the planning schemes. Slightly different results are found in these components depending on the Donders' law constraint because these values are not unique for given values of  $\theta_F$  and  $\phi_F$  but depend also on the torsion of the arm. Significant variation, however, can be seen in the  $r_x$  component.

The errors in rotation vector space for Subject 3 are summarized in Figure 6.24. The results for the other subjects can be found in Appendix M.

From Figure 6.24, for forearm movements, considerable errors can be seen with all the planning schemes - this is due mostly to errors in the  $r_x$  component, as can be seen in Figure 6.22. For the forearm, the Listing's law scheme produces more accurate predictions, despite the finding that a second order surface was a better fit to the data. The process of fitting the reference position rotated the rotation vectors such that the rotation vectors are distributed evenly about the  $r_y - r_z$  plane - meaning that on average  $r_x = 0$  is a good prediction of the torsion. The second order surface, which can have a large range of  $r_x$  especially at the edges of the workspace, may be a poor approximation in parts of the workspace. This may explain why using Listing's law may on average give a better fit.

For subject 3, the results for the upper arm showed better results than that for the forearm. This is in line with the finding in Chapter 4 that the thickness of the Donders' surfaces were less for the forearm than the upper arm. Still, significant deviations are seen. An example of this can be seen in Figure 6.22. The movements that begin and end at  $s$  have different torsional

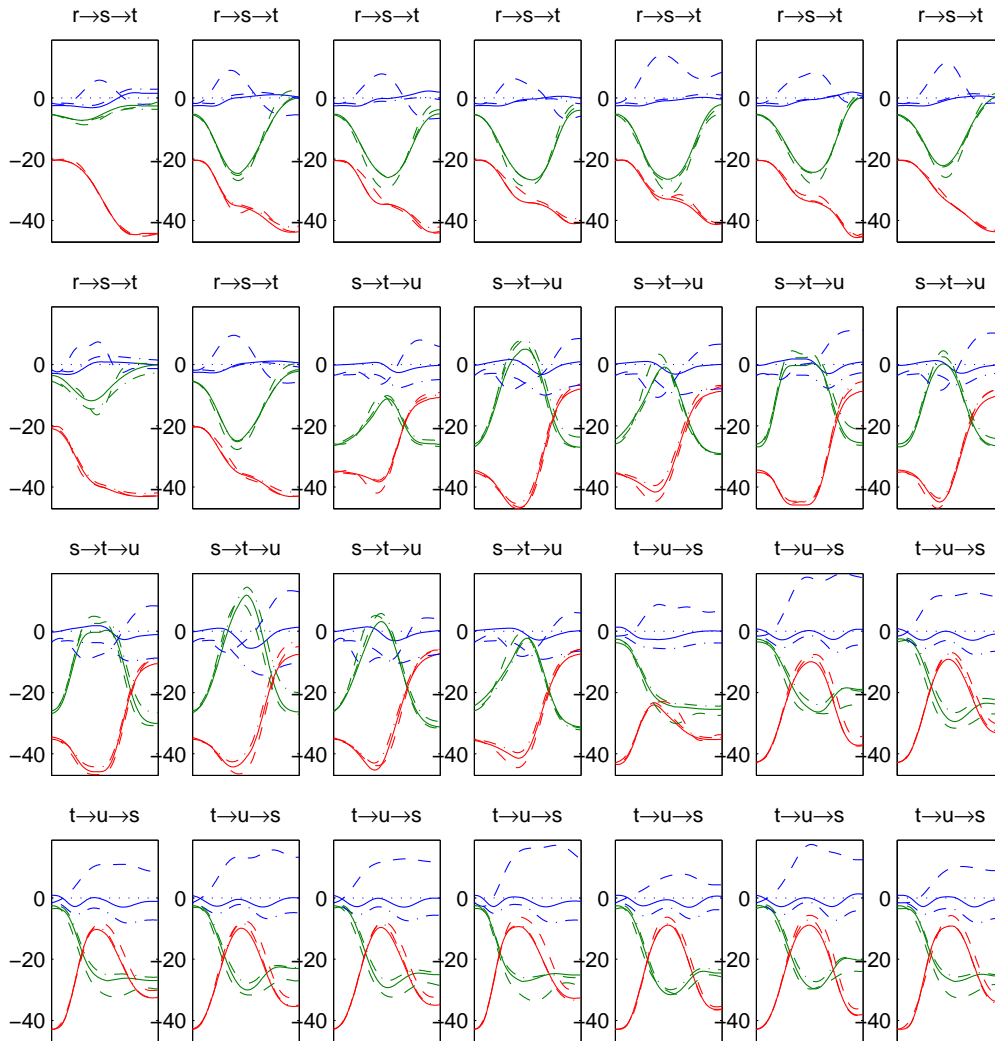


Figure 6.22: Rotation vectors (in degrees) during double step movements for the forearm for Subject 3, Set 1, in components -  $r_x$  (blue),  $r_y$  (green) and  $r_z$  (red). The dashed lines shows the experimental data, the solid line the prediction with a second order surface Donders' constraint on orientation, the dotted line the prediction of a Listing's law constraint on orientation (only the  $r_x$  component shown) and the dotted-dash line the prediction for a second order surface constraint on coordinate velocity.

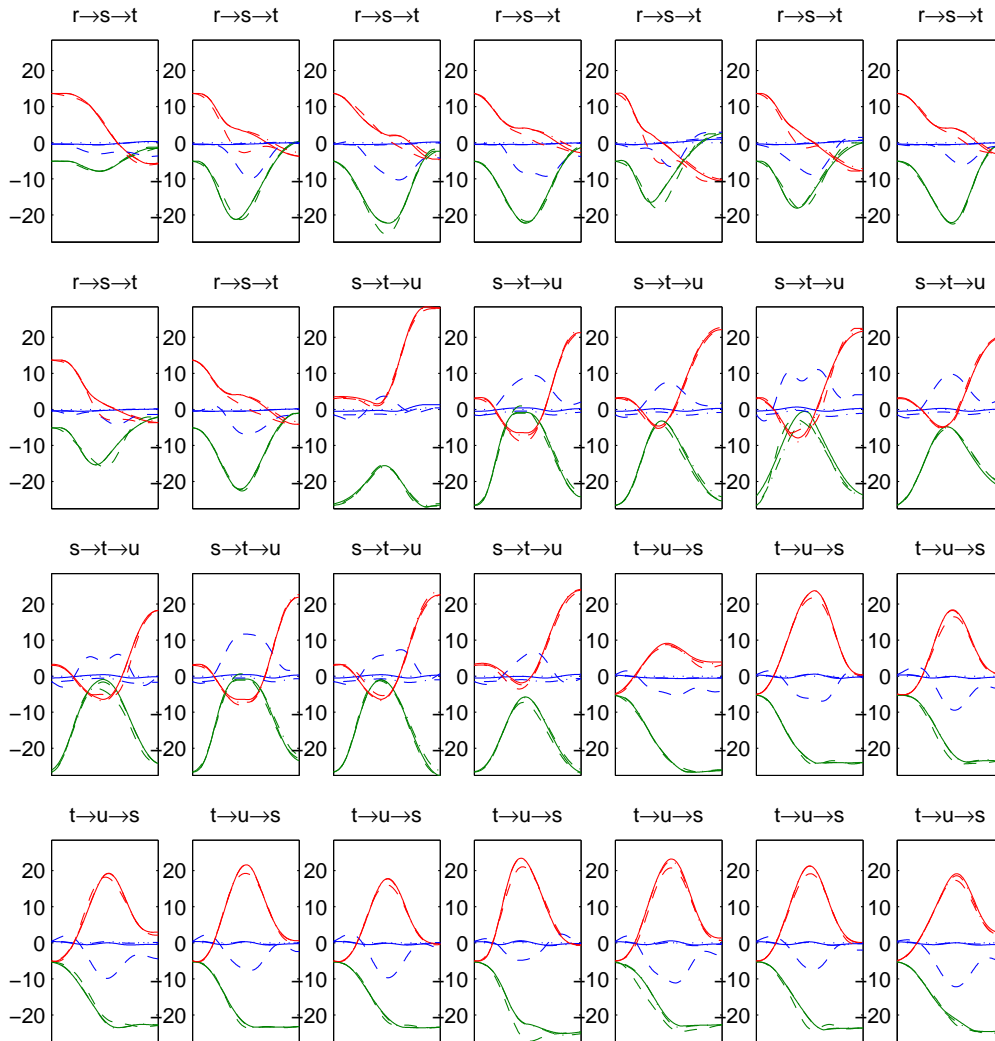


Figure 6.23: Rotation vectors (in degrees) during double step movements for the upper arm for Subject 3, Set 1 in components. See Figure 6.22 for an explanation of the colours.

values. (This can also be seen from Figure C.2).

However, the other subjects did not show significant differences between the forearm and the upper arm. For subject 4, the results for the forearm appear to be better than those for the upper arm.

The results for the model where the constraint was placed on velocity

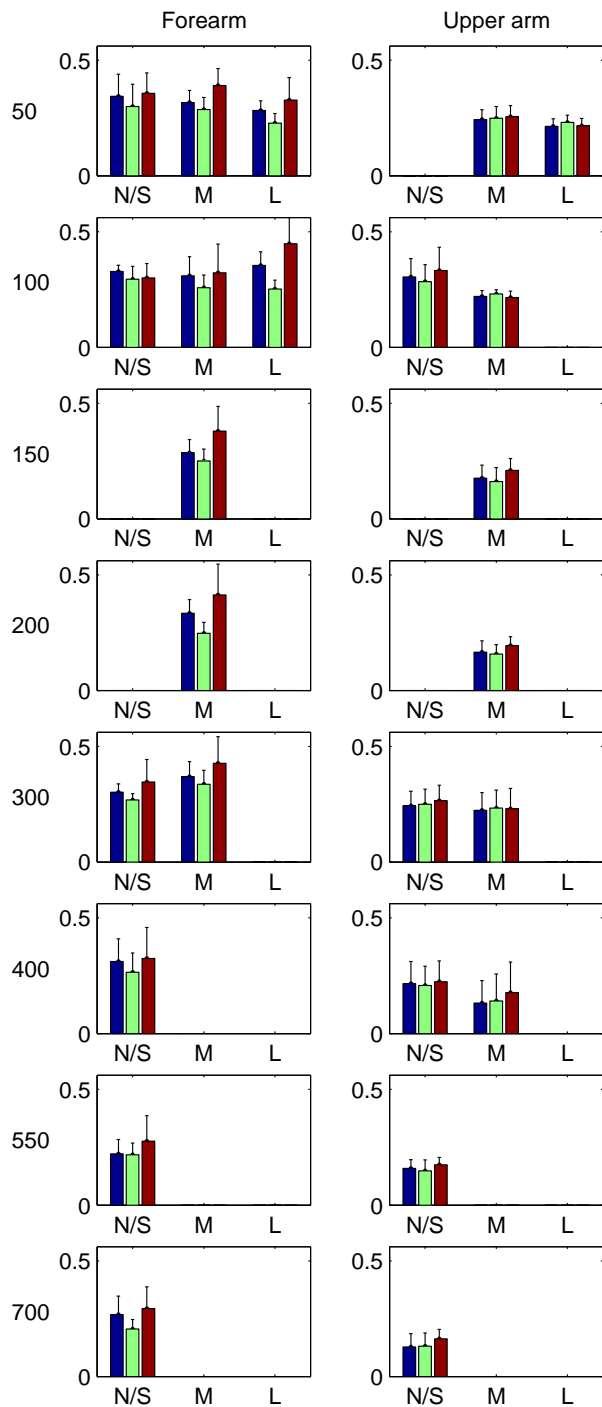


Figure 6.24: Summary of errors of three dimensional models for Subject 3. The height of the bars is the mean, and the error bars length the standard deviation of the error between the actual trajectory and the predictions, with different Donders' law constraints on the orientation - a second order surface constraint (blue), a Listing's law constraint (green), and a constraint on the coordinate velocity (red). The results are divided into those with no or small (N/S) overlap (less than 0.2), moderate (M) overlap (between 0.2 and 0.6), and large (L) overlap (greater than 0.6). The left column shows the forearm results, and the right the upper arm, and each row the results for the ISI shown. Similar results are seen for many of the trials, while for some the Listing plane constraint shows better results.

were also shown on the same figures. These are very close to the results for the second order surface, because using the velocity does not give any further information, and the velocity constraint suffers from the same problems as the constraints on the orientation do.

## 6.4 Discussion

The point-to-point control movements generally showed invariant characteristics. In velocity space, the movements in the  $v_y$  and  $v_z$  components were bell shaped and nearly symmetric. As the length of the arm is fixed throughout the movement, the  $v_x$  component is a function of the other two components, and so in general did not show bell shaped velocity profiles.

The paths were found to be close to geodesics, which can account for some of the curvature observed. However, curvature of greater magnitude than that expected for a geodesic was found, and the direction of the curvature varied between subjects. The highest values of curvature were found for diagonal movements. Atkeson & Hollerbach (1985) found that during unconstrained vertical movements, curved rather than straight movements are produced and suggested that this may be related to difficulties in handling gravity - this may explain the curvature seen in some of the cases.

In Desmurget et al. (1997), it was suggested that curvature is greater in unconstrained than compliant movements. Although this is not a compliant movement, a constraint is placed on the movements by the extended arm requirement. However, although curvature greater than that predicted by a geodesic movement was found, unlike in their study the direction of the curvature was not consistent. This suggests that the curvature seen here is a result of errors rather than a strategy. The movements seen here had invariant characteristics in hand space - this feature they saw only in compliant hand movements. It may be that the extended arm constraint, which reduces the available workspace, causes the movements to have similar properties to compliant hand movements. This in turn may mean that the results found here can not be extrapolated to general, unconstrained three-dimensional arm movements.

Some of the rotation vectors describing the movements were found to be highly curved, meaning that single axis rotations are not, in general, used. This was in contrast to the nearly straight line path seen with the position.

In angular velocity space, bell shaped profiles were seen in  $\omega_y$  and  $\omega_z$ ,

however the torsional component  $\omega_x$  showed a significant amount of variation. The torsional component ( $\omega_x$ ) of the angular velocity can vary without significantly affecting the final pointing direction. The variation in the torsional component of the angular velocity was found to be greater for the forearm than for the upper arm.

The results for the double step trajectories show that the movements can be well modeled in two dimensional Fick coordinates using a superposition model, where the trajectory consists of the vector addition of the trajectory in Fick coordinates from the start to the first target, and a trajectory consisting of the difference in Fick coordinates from the first to the second target. While an abort-replan model provides good predictions when the overlap is small, this model fails for larger overlaps.

Evidence of the use of the difference from the first to the second target was seen in a study of double step movements in the horizontal plane. Boulinguez et al. (2001) found that when there is a gap between the extinction of the first target and the presentation of the second target, it is likely that different processes are used compared to when there is no gap between the two targets. They proposed that this is because information from the retinal error (the difference from the first to the second target) would be available in the no-gap case, but unavailable when there is a gap. The movements that could make use of this information (which the superposition model uses) had a reduced length of time before the first observable correction in the arm trajectory.

Some of the errors seen for superposition of trajectories may have been due to what is known as averaged trajectories. These are trajectories that rather than beginning to move towards the first or the second target, instead move towards some intermediate point. Henis (1991) showed that for movements in a horizontal plane a modified version of the superposition model can be used to predict the trajectories of these movements. It may be possible to use a similar procedure with these movements to produce a more accurate model.

The extension of the model to rotation vectors provides reasonable pre-

dictions, but with significant errors seen in the torsional component ( $r_x$ ). The amount of variation seen is a small fraction of the possible values that the arm could take. The errors in torsion appear to be due to the selection of different torsional values for the start and end of the movements.

In this task, successful completion is achieved by having the arm end up in the correct pointing direction. The value of torsion is not important in achieving this goal. This may mean that the value of torsion is less controlled than the other variables, and the values of torsion seen are by-products of processes acting on the other variables. Scholz et al. (2000) suggested that for each task, a set of relevant task variables can be defined, which can then be combined to form a UCM (“uncontrolled manifold”). A relevant task variable for this task would be the vector of the pointing direction of the arm. For other examples, they showed that the variation in the joint configurations parallel to the set of appropriate task variables had a UCM that showed significantly less variability to the joint configurations that were perpendicular. This may provide an explanation of why the variation in torsion is much greater than in the other components - it does not however give a way of predicting torsion.

The constraints on the orientation used in the models require knowledge of the current pointing direction. The use of feedback for trajectory generation is problematic because of the slow speed of sensory feedback loops. Proprioceptive or visual feedback is too slow to allow it be used. It is a fundamental requirement of feedback models that some information about the current state is available in order to plan the current action. A solution to this problem may be found by the use of a forward model (Kawato, 1999). This is where the current state of the arm is predicted for a given action, based on learning from previous movements. This allows a feedback model to be implemented, using the current predicted arm location for feedback. This could be realized using a hybrid model (Desmurget & Grafton, 2000; Sabes, 2000), which begins with a feed-forward motor plan, which is then corrected by using the forward model as the movement progresses. The forward model

itself may be corrected using visual and proprioceptive feedback.

No significant difference was seen between using constraints on orientation or on velocity. Constraints on coordinate or angular velocity rather than on rotation vectors do have some advantages. There is more invariance in angular velocity than in rotation vector paths, and more varied, nonholonomic, constraints can be placed on the angular velocity than the orientation (Ceylan et al., 2000). From these results, it is not possible to determine whether constraints are placed on orientation or coordinate or angular velocity.

The movement plans that have been considered have all been based on kinematics alone. This assumption is based on the invariance seen in the velocity profiles. However dynamics clearly must play a role in movement planning. These models implicitly assume that the dynamics would be planned after the path. A more realistic model may be one that is planned on a combination of kinematic and dynamic factors (Soechting & Flanders, 1998).

# Chapter 7

## Summary

This work studied models for the generation of extended arm movements. Different surfaces were compared for their ability to describe permissible arm orientations throughout the movement. Additionally, two models, the superposition and the abort-replan models, were compared and tested for their success in predicting the trajectories of double step movements.

When considered in rotation vector space, the end points show more variation in the torsional component ( $r_x$ ) than the other components. This increased variation is also seen throughout the movements. While the profiles of the angular velocity are invariant in the horizontal ( $\omega_y$ ) and vertical ( $\omega_z$ ) components, the torsional component ( $\omega_x$ ) shows considerable variation. The variation in the torsion is generally greater for the forearm than the upper arm, suggesting that the forearm torsion is less planned than that of the upper arm.

Despite this variation, it is possible to fit surfaces to the rotation vectors representing the movements. These surfaces can act as a constraint on the values that the rotation vectors can take. This constraint is known as Donders' law. A flat plane, where  $r_x = 0$  provides the best overall fit, although for each set of movements, a second order surface gives a closer fit, but not one that is consistent across sets of movements or between subjects. The orientations reachable by a Fick gimbal system with zero torsional component

were also considered as a surface, but this showed no improvement over a flat plane.

Dividing the workspace into smaller subspaces and then fitting the surfaces separately for each of the subspaces produces a significantly better fit. The fit of surfaces to orientations only at stationary locations was also significantly better than the fit to orientations sampled throughout the movement. This suggests that the Donders' law constraints may be applied only at the endpoints. However, the fit of the surfaces during single step and double step movements (which are much more curved than single step movements) was similar. It seems that the same strategy for constraining torsion is used in both cases.

When considered in position space, the movements were invariant, and showed bell shaped velocity profiles in the  $y$  and  $z$  coordinates. Some curvature was seen, but not with a consistent pattern, suggesting that it was due to errors. Similar invariance is also seen when the trajectories are considered in two dimensional Fick coordinates ( $\theta_F$  and  $\phi_F$ ), where the torsional component is not considered.

Superposition in two dimensional Fick coordinates provides a good description of the double step trajectories, whereas the abort-replan scheme fails when the deviation of the double step movement from a movement from the initial location to the first target occurs soon after the movement onset. The fundamental difference between the two methods is that the superposition strategy is based on the combination of two movement plans constructed in advance, while the abort-replan is based on feedback of the current orientation.

The extension to a full three dimensional orientation model also requires information about the current orientation. The appropriate rotation vector was selected to be in the correct pointing direction and satisfy a Donders' law constraint. This produced trajectories where the torsion was a reasonable approximation to the predictions but did not follow them closely. It was not possible to determine from the results whether these constraints are applied

in terms of orientation, or angular or coordinate velocity.

Extended arm movements appear to be planned in two dimensions, perhaps in two dimensional Fick coordinates ( $\theta_F$  and  $\phi_F$ ). Subsequently, double step trajectories can be well modeled using superposition in two dimensions. The torsional component appears to be planned to a lesser extent and independently from the other two dimensions.

# Bibliography

Admiraal M., Medendorp W. & Gielen C. (2002). Three-dimensional head and upper arm orientations during kinematically redundant movements and at rest. *Experimental Brain Research*, 142:181–192.

Arun K., Huand T. & Blostein S. (1987). Least-squares fitting of two 3-d point sets. *IEEE Transactions on Pattern Analysis and Machine Intelligence*, PAMI-9(5):698–700.

Atkeson C. & Hollerbach J. (1985). Kinematic features of unrestrained vertical arm movements. *Journal of Neuroscience*, 5(9):2318–2330.

Boulinguez P., Blouin J. & Nougier V. (2001). The gap effect for eye and hand movements in double-step pointing. *Experimental Brain Research*, 138:352–358.

Ceylan M., Henriques D., Tweed D. & Crawford J. (2000). Task-dependent constraints in motor control: Pinhole goggles make the head move like an eye. *Journal of Neuroscience*, 20(7):2719–2730.

Craig J. (1986). *Introduction to Robotics*. Addison-Wesley, Reading, MA.

Crawford J. (1998). Listing’s law: what’s all the hubbub? In Harris & Jenkin (1998).

Desmurget M. & Grafton S. (2000). Forward modeling allows feedback control for fast reaching movements. *Trends in Cognitive Sciences*, 4(11):423–431.

- Desmurget M., Jordan M., Prablanc C. & Jeannerod M. (1997). Constrained and unconstrained movements involve different control strategies. *Journal of Neurophysiology*, 77:1644–1650.
- Desmurget M., Pélisson D., Rossetti Y. & Prablanc C. (1998). From eye to hand: Planning goal-directed movements. *Neuroscience and Biobehavioral Reviews*, 22:761–788.
- Desmurget M. & Prablanc C. (1997). Postural control of three-dimensional prehension movements. *Journal of Neurophysiology*, 77:452–464.
- Flash T. (1987). The control of hand equilibrium trajectories in multi-joint arm movements. *Biological Cybernetics*, 57:257–274.
- Flash T. & Henis E. (1991). Arm trajectory modification during reaching towards visual targets. *Journal of Cognitive Neuroscience*, 3:220–230.
- Flash T. & Hogan N. (1985). The coordination of arm movements: An experimentally confirmed mathematical model. *Journal of Neuroscience*, 5(7):1688–1703.
- Gat-Falik T. & Flash T. (1999). The superposition strategy for arm trajectory modification in robotic manipulators. *IEEE Transactions on Systems, Man and Cybernetics*, 29:83–95.
- Georgopoulos A., Kalaska J. & Massey J. (1981). Spatial trajectories and reaction times of aimed movements: Effects of practice, uncertainty, and change in target location. *Journal of Neurophysiology*, 46(4):725–743.
- Gielen C., Vrijenhoek E., Flash T. & Neggers S. (1997). Arm position constraints during pointing and reaching in 3-d space. *Journal of Neurophysiology*, 78:660–673.
- Glenn B. & Vilis T. (1992). Violations of listing’s law after large eye and head gaze shifts. *Journal of Neurophysiology*, 68(1):309–318.

- Grea H., Desmurget M. & Prablanc C. (2000). Postural invariance in three-dimensional reaching and grasping movements. *Experimental Brain Research*, 134(2):155–162.
- Harris L. & Jenkin M., eds. (1998). *Vision and Action*. Cambridge University Press, Cambridge.
- Haslwanter T. (1995). Mathematics of three-dimensional eye rotations. *Vision Research*, 35(12):1727–1739.
- Henis E. (1991). *Strategies Underlying Arm Trajectory Modification During Reaching Towards Visual Targets*. Ph.D. thesis, Weizmann Institute of Science.
- Henn V. (1997). History of three-dimensional eye movement research. In M. Fetter, T. Haslwanter, H. Misslisch & D. Tweed, eds., *Three Dimensional Kinematics of Eye, Head, and Limb Movements*, pages 3–14. Harwood Academic Publishers, Amsterdam.
- Hoff B. (1994). A model of duration in normal and perturbed reaching movement. *Biological Cybernetics*, 71:481–488.
- Hollerbach J. (1982). Computers, brains and the control of movement. *Trends in Neurosciences*, 5:189–192.
- Hore J., Watts S. & Vilis T. (1992). Constraints on arm position when pointing in three dimensions: Donder’s law and the fick gimbal strategy. *Journal of Neurophysiology*, 68(2):374–383.
- Jacobs D., ed. (1977). *The State of the Art in Numerical Analysis*. Academic Press, London.
- Kawato M. (1999). Internal models for motor control and trajectory planning. *Current Opinion In Neurobiology*, 9:718–727.
- Kreyszig E. (1993). *Advanced Engineering Mathematics, 7th edition*. John Wiley & Sons, New York.

- Lee D., Port N. & Georgopoulos A. (1997). Manual interception of moving targets II. On-line control of overlapping sub-movements. *Experimental Brain Research*, 116:421–433.
- Liebermann D. (1998). *Intrinsic joint kinematic strategies for planning reaching and pointing movements towards 3-dimensional targets*. Ph.D. thesis, Weizmann Institute of Science.
- Luttgens K. & Hamilton N. (1997). *Kinesiology: Scientific Basis of Human Motion, 9th Ed.*. Madison, WI: Brown & Benchmark.
- Miller L., Theeuwes M. & Gielen C. (1992). The control of arm pointing movements in three dimensions. *Experimental Brain Research*, 90:415–426.
- Minken A., Van Opstal A. & Van Gisbergen J. (1993). Three-dimensional analysis of strongly curved saccades elicited by double-step stimuli. *Experimental Brain Research*, 93:521–533.
- Morasso P. (1981). Spatial control of arm movements. *Experimental Brain Research*, 42:223–227.
- Murray R., Zexiang L. & Sastry S. (1994). *A Mathematical Introduction to Robotic Manipulation*. CRC Press, Boca Raton, FL.
- Paulignan Y., Frak V., Yoni Y. & Jeannerod M. (1997). Influence of object position and size on human prehension movements. *Experimental Brain Research*, 114(2):226–234.
- Ramsay J. (2001). *Matlab and S-PLUS Functions for Functional Data Analysis*. McGill University.
- Ramsay J. & Silverman B. (1997). *Functional data analysis*. Springer-Verlag, New York.
- Rogozin V., Edan Y. & Flash T. (2001). A real-time trajectory modification algorithm. *Robotica*, 19(4):395–405.

- Sabes P. (2000). The planning and control of reaching movements. *Current Opinion in Neurobiology*, 10:740–746.
- Scholz J., Schöner G. & Latash M. (2000). Identifying the control structure of multijoint coordination during pistol shooting. *Experimental Brain Research*, 135:382–404.
- Smit A. & Van Gisbergen J. (1990). An analysis of curvature in fast and slow human saccades. *Experimental Brain Research*, 81:335–345.
- Söderkvist I. & Wedin P. (1993). Determining the movements of the skeleton using well-configured markers. *Journal of Biomechanics*, 26(12):1473–1477.
- Soechting J., Buneo C., Herrmann U. & Flanders M. (1995). Moving effortlessly in three dimensions: Does donder’s law apply to arm movement? *Journal of Neuroscience*, 15(9):6271–6290.
- Soechting J. & Flanders M. (1993). Parallel, interdependent channels for location and orientation in sensorimotor transformations for reaching and grasping. *Journal of Neurophysiology*, 70:1137–1150.
- Soechting J. & Flanders M. (1998). Movement planning: kinematics, dynamics, both or neither? In Harris & Jenkin (1998).
- Soechting J. & Lacquaniti F. (1981). Invariant characteristics of a pointing movement in man. *The Journal of Neuroscience*, 1(7):710–720.
- Soechting J. & Lacquaniti F. (1983). Modification of trajectory of a pointing movement in response to a change in target location. *Journal of Neurophysiology*, 49(2):548–564.
- Straumann D., Haslwanter T., Hepp-Reymond M. & Hepp K. (1991). Listing’s law for eye, head and arm movements and their synergistic control. *Experimental Brain Research*, 86:209–215.

Theeuwen M., Miller L. & Gielen C. (1993). Are the orientations of the head and arm related during pointing movements? *Journal of Motor Behavior*, 25(3):242–250.

Tweed D. (1997). Three-dimensional models of the human eye-head saccadic system. *Journal of Neurophysiology*, 77:654–666.

Tweed D., Cadera W. & Vilis T. (1990). Computing three-dimensional eye position quaternions and eye velocity from search coil signals. *Vision Research*, 30(1):97–110.

Tweed D. & Vilis T. (1987). Implications of rotational kinematics for the oculomotor system in three dimensions. *Journal of Neurophysiology*, 58(4):832–849.

Tweed D. & Vilis T. (1990a). Geometric relations of eye position and velocity vectors during saccades. *Vision Research*, 30(1):111–127.

Tweed D. & Vilis T. (1990b). The superior colliculus and spatiotemporal translation in the saccadic system. *Neural Networks*, 3:75–86.

Uno Y., Kawato M. & Suzuki R. (1989). Formation and control of optimal trajectory in human multijoint arm movement. minimum torque-change model. *Biological Cybernetics*, 61(2):89–101.

Van Gisbergen J., Robinson D. & Gielen S. (1981). A quantitative analysis of generation of saccadic eye movements by burst neurons. *Journal of Neurophysiology*, 45(3):417–442.

Van Opstal A. (1993). Representation of eye position in three dimensions. In A. Berthoz, ed., *Multisensory Control of Movement*, pages 27–41. Oxford University Press.

Van Opstal A. (2001). The gaze control system. In L. van Hemmen, E. Domanj & J. Cowan, eds., *Models of Neural Networks IV*. Springer Verlag, New York.

Von Hofsten C. (1991). Structuring of early reaching movements: A longitudinal study. *Journal of Motor Behavior*, 23(4):280–293.

Wolpert D.M., Ghahramani Z. & Jordan M.I. (1995). Are arm trajectories planned in kinematic or dynamic coordinates? An adaptation study. *Experimental Brain Research*, 103(3):460–470.

# Appendix A

## Quaternions

Quaternions are four-dimensional structures, that have some useful properties in relation to fixed axis rotations. A quaternion is defined as

$$q = \cos\left(\frac{\theta}{2}\right) + \sin\left(\frac{\theta}{2}\right) \vec{n} \quad (\text{A.1})$$

where  $\vec{n}$  is the axis of rotation and  $\theta$  the size of the rotation (from some reference point). Note that this gives a scalar component, called  $q_0$ , and a 3 element vector component, called  $\vec{q}$ .

The multiplication of two quaternions is achieved by the following rule Haslwanter (1995):

$$q \circ p = q_0 p_0 - \vec{q} \cdot \vec{p} + (q_0 \vec{p} + p_0 \vec{q} + \vec{q} \times \vec{p}) \quad (\text{A.2})$$

Note also that the product, or composition, of two quaternions gives another quaternion. This product gives the rotation made up of a rotation from reference position by  $p$  followed by a rotation by  $q$ .

Quaternions have the elegant property that the rotation of a vector initially at  $s_0$  by the rotations represented by  $q(t)$  can be described by the quaternion product

$$s(t) = q(t) \circ s_0 \circ q^{-1}(t) \quad (\text{A.3})$$

Quaternions are related to rotation vectors by the simple relationship

$$\begin{aligned}\vec{r} &= \frac{\vec{q}}{q_0} \\ \Rightarrow \vec{q} &= q_0 \vec{r} \\ \Rightarrow \dot{\vec{q}} &= \dot{q}_0 \vec{r} + q_0 \dot{\vec{r}}\end{aligned}\tag{A.4}$$

Here we will use normalized quaternions (that is,  $|q| = \sqrt{q_0^2 + \vec{q} \cdot \vec{q}} = 1$ ), and hence the inverse  $q^{-1}$  of a quaternion can be written as

$$q^{-1} = q_0 - \vec{q}\tag{A.5}$$

## Appendix B

# Setting the velocity rules with the “Velocity box” model

The velocity box model presented in Chapter 6 has the option of setting the gimbal score ( $s$ ). For example, a score of  $-1$  refers to a Fick gimbal with the Fick torsional component set to zero, whereas a score of zero refers to a flat Listing’s plane rule. This leads to the question of how these constraints can be applied using velocity rather than orientation constraints to allow a more general operator (using velocity constraints allows the use of nonholonomic constraints).

In Ceylan et al. (2000), it is explained that the Fick pattern is achieved by rotating  $f$  (a unit vector in the gaze / pointing direction) into the horizontal plane. In the paper, it is suggested that this be achieved by normalizing (making its length 1)  $N_{\text{fick}} = k \times (f \times k)$ , where  $k$  is a body fixed vector pointing up and  $N_{\text{fick}}$  is the normal vector to the plane of permissible angular

velocity vectors. Equivalently:

$$\begin{aligned}
N_{\text{fick}} &= a(k \times (f \times k)) \\
&= a((k \cdot k)f - (k \cdot f)k) \\
&= a\left(f - \begin{bmatrix} 0 \\ 0 \\ f_3 \end{bmatrix}\right) \\
&= a \begin{bmatrix} f_1 \\ f_2 \\ 0 \end{bmatrix} \\
&= \frac{1}{\sqrt{f_1^2 + f_2^2}} \begin{bmatrix} f_1 \\ f_2 \\ 0 \end{bmatrix}
\end{aligned} \tag{B.1}$$

where  $a$  is the scalar required to normalize the vector. Similarly, they explain that for a Helmholtz pattern is achieved by rotating  $f$  into the sagittal plane (ie normalizing  $N_{\text{Helmholtz}} = j \times (f \times j)$ ). This can also be expressed as

$$N_{\text{Helmholtz}} = \frac{1}{\sqrt{f_1^2 + f_3^2}} \begin{bmatrix} f_1 \\ 0 \\ f_3 \end{bmatrix} \tag{B.2}$$

Furthermore, they stated that the normal to the velocity plane for Listing's law is halfway between the two previously mentioned normals, that is, it bisects the angle between  $N_{\text{Helmholtz}}$  and  $N_{\text{Fick}}$ . They stated that this is equivalent to  $N_{\text{Listing}} = f + i$  normalized. This is the half angle rule (Van Opstal, 2001). If these two formulations are equivalent, then (where  $d$  and  $e$  are the appropriate scalars to normalize):

$$\begin{aligned}
&d(N_{\text{Fick}} + N_{\text{Helmholtz}}) = e(f + i) \\
\Rightarrow d \left( \frac{1}{\sqrt{f_1^2 + f_2^2}} \begin{bmatrix} f_1 \\ f_2 \\ 0 \end{bmatrix} + \frac{1}{\sqrt{f_1^2 + f_3^2}} \begin{bmatrix} f_1 \\ 0 \\ f_3 \end{bmatrix} \right) &= \frac{1}{\sqrt{(f_1 + 1)^2 + f_2^2 + f_3^2}} \begin{bmatrix} f_1 + 1 \\ f_2 \\ f_3 \end{bmatrix}
\end{aligned} \tag{B.3}$$

Considering just the second component, then:

$$\begin{aligned}\frac{d}{\sqrt{f_1^2 + f_2^2}} f_2 &= \frac{1}{\sqrt{(f_1 + 1)^2 + f_2^2 + f_3^3}} f_2 \\ \Rightarrow \frac{d}{\sqrt{f_1^2 + f_2^2}} &= \frac{1}{\sqrt{(f_1 + 1)^2 + f_2^2 + f_3^3}}\end{aligned}\tag{B.4}$$

and just the third component:

$$\begin{aligned}\frac{d}{\sqrt{f_1^2 + f_3^2}} f_3 &= \frac{1}{\sqrt{(f_1 + 1)^2 + f_2^2 + f_3^3}} f_3 \\ \Rightarrow \frac{d}{\sqrt{f_1^2 + f_3^2}} &= \frac{1}{\sqrt{(f_1 + 1)^2 + f_2^2 + f_3^3}}\end{aligned}\tag{B.5}$$

Then from (B.4) and (B.5),

$$\begin{aligned}\frac{d}{\sqrt{f_1^2 + f_2^2}} &= \frac{d}{\sqrt{f_1^2 + f_3^2}} \\ \Rightarrow f_1^2 + f_2^2 &= f_1^2 + f_3^2 \\ \Rightarrow f_2 &= \pm f_3\end{aligned}\tag{B.6}$$

Now the left hand side of (B.3) can be more succinctly expressed as:

$$d(N_{\text{Fick}} + N_{\text{Helmholtz}}) = \frac{d}{\sqrt{f_1^2 + f_2^2}} \begin{bmatrix} 2f_1 \\ f_2 \\ f_3 \end{bmatrix}\tag{B.7}$$

This allows  $d$  to be easily calculated (it is the normalizing factor):

$$\begin{aligned}\frac{d}{\sqrt{f_1^2 + f_2^2}} \sqrt{4f_1^2 + f_2^2 + f_3^2} &= 1 \\ \Rightarrow d &= \frac{\sqrt{f_1^2 + f_2^2}}{\sqrt{4f_1^2 + 2f_2^2}}\end{aligned}\tag{B.8}$$

Now (B.3) and (B.7) can be rewritten as

$$d(N_{\text{Fick}} + N_{\text{Helmholtz}}) = \frac{1}{\sqrt{4f_1^2 + 2f_2^2}} \begin{bmatrix} 2f_1 \\ f_2 \\ f_3 \end{bmatrix}\tag{B.9}$$

Now looking back at the second component in (B.3), we can see that

$$\begin{aligned}
\frac{1}{\sqrt{4f_1^2 + 2f_2^2}} &= \frac{1}{\sqrt{(f_1 + 1)^2 + 2f_2^2}} \\
\Rightarrow 4f_1^2 + 2f_2^2 &= (f_1 + 1)^2 + 2f_2^2 \\
\Rightarrow 3f_1^2 - 2f_1 - 1 &= 0 \\
\Rightarrow f_1 &= 1 \text{ or } -\frac{1}{3}
\end{aligned} \tag{B.10}$$

Substitution of  $f_1 = \frac{1}{3}$  into (B.3) causes a contradiction, and hence the only solution is for  $f_1 = 1$ . As  $f$  is a unit vector, this implies that it is the

vector  $f = \begin{bmatrix} 1 \\ 0 \\ 0 \end{bmatrix}$ . This is the vector that is pointing straight ahead - ie, the reference position. This is the unique position where the normal to the Fick

and Helmholtz velocity planes will be the same (equal to  $\begin{bmatrix} 1 \\ 0 \\ 0 \end{bmatrix}$ ), which is also

the normal vector for Listing's law at this point, being the reference position. Hence the stated conclusion that (B.3) is true is actually only the case in the special case of the reference position.

The continuum between a Fick gimbal and a Helmholtz gimbal in terms of orientation can be expressed by the gimbal score (3.7). To build a realistic "Velocity box" model, it would be necessary to be able to express positions in the continuum as velocity constraints and not just the extreme cases. Previous experimental results, for example Ceylan et al. (2000), have shown gimbal scores can vary and are not limited to -1, 1 and 0 (representing a Fick gimbal, Helmholtz gimbal and Listing's law).

One option is to set three normal vectors (the one defined by Listing's law (the half angle rule), the normal for a Fick gimbal, and the normal for a Helmholtz gimbal) and then interpolate between them for twist scores between these values. It is not possible to just interpolate between the value for a Fick gimbal and a Helmholtz gimbal for the reasons described previously. It

is unclear if in such a scheme  $\alpha$  corresponds to the twist score  $s$ .

$$N(\alpha, f) = \begin{cases} N_{\text{Listing}} - \alpha(N_{\text{Fick}} - N_{\text{Listing}}) & \text{if } \alpha < 0 \\ N_{\text{Listing}} + \alpha(N_{\text{Helmholtz}} - N_{\text{Listing}}) & \text{if } \alpha > 0 \end{cases} \quad (\text{B.11})$$

An alternative approach would be to use coordinate velocity constraints. This method was explained in Chapter 5.

## Appendix C

# Spread of rotation vectors at end points

The following graphs show the spread of the rotation vectors at each of the start / end points. The graph for Subject 1 is shown in the main body of the text (Figure 4.5). The rows represent the targets  $R$ ,  $S$ ,  $T$ ,  $U$ ,  $V$  (and  $W$  for subject 2).

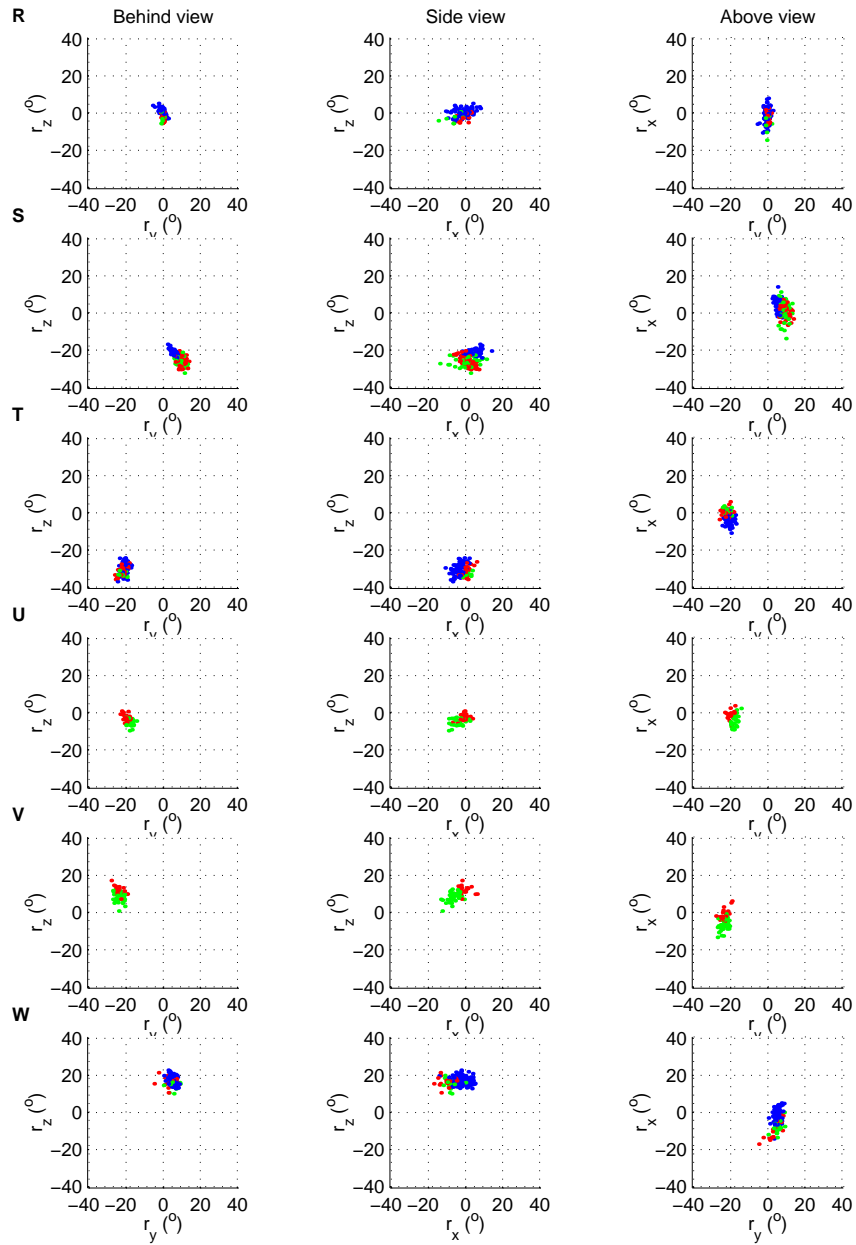


Figure C.1: End point spread of forearm rotation vectors for subject 2, Green denotes double step movements and red control movements ending at a particular point, blue denotes movements starting at that point.

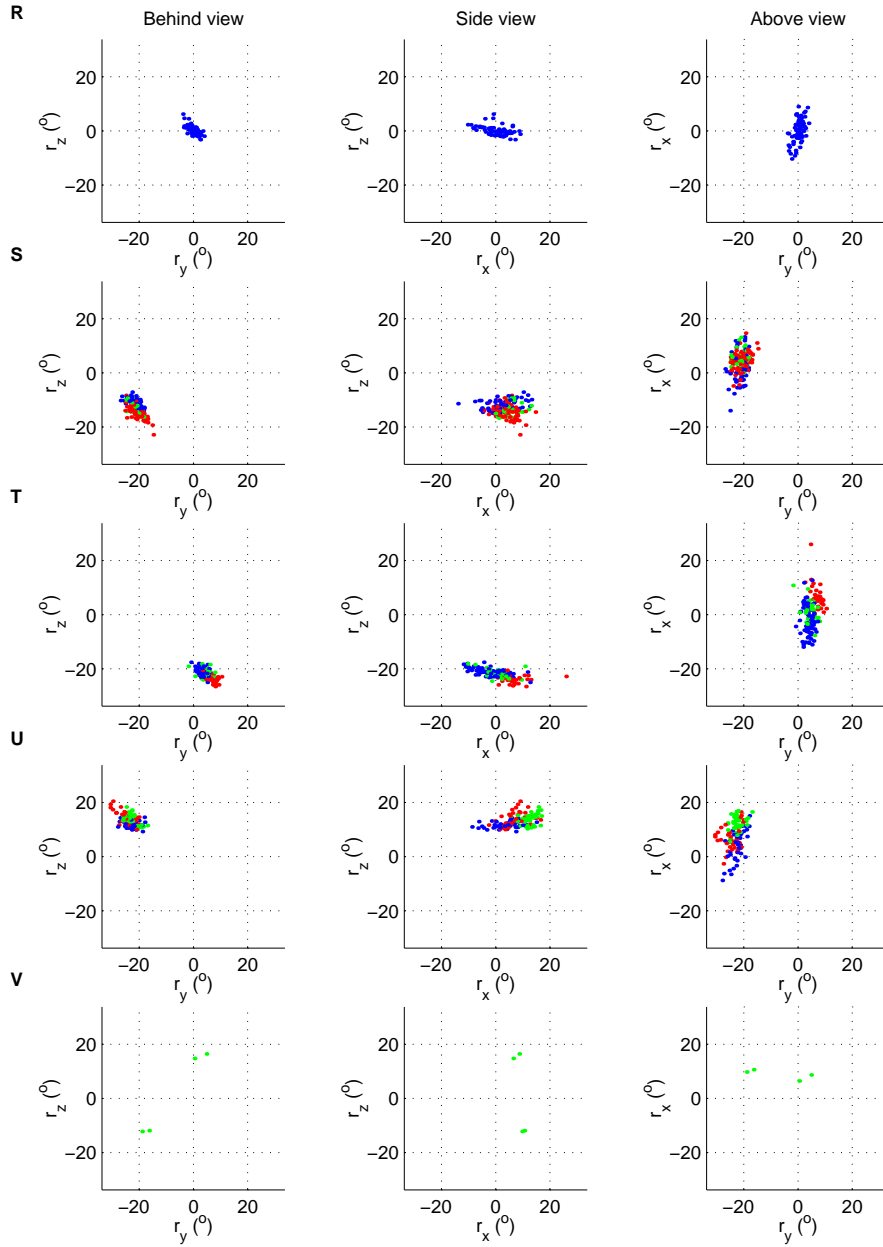


Figure C.2: End point spread of forearm rotation vectors for subject 3, Green denotes double step movements and red control movements ending at a particular point, blue denotes movements starting at that point.

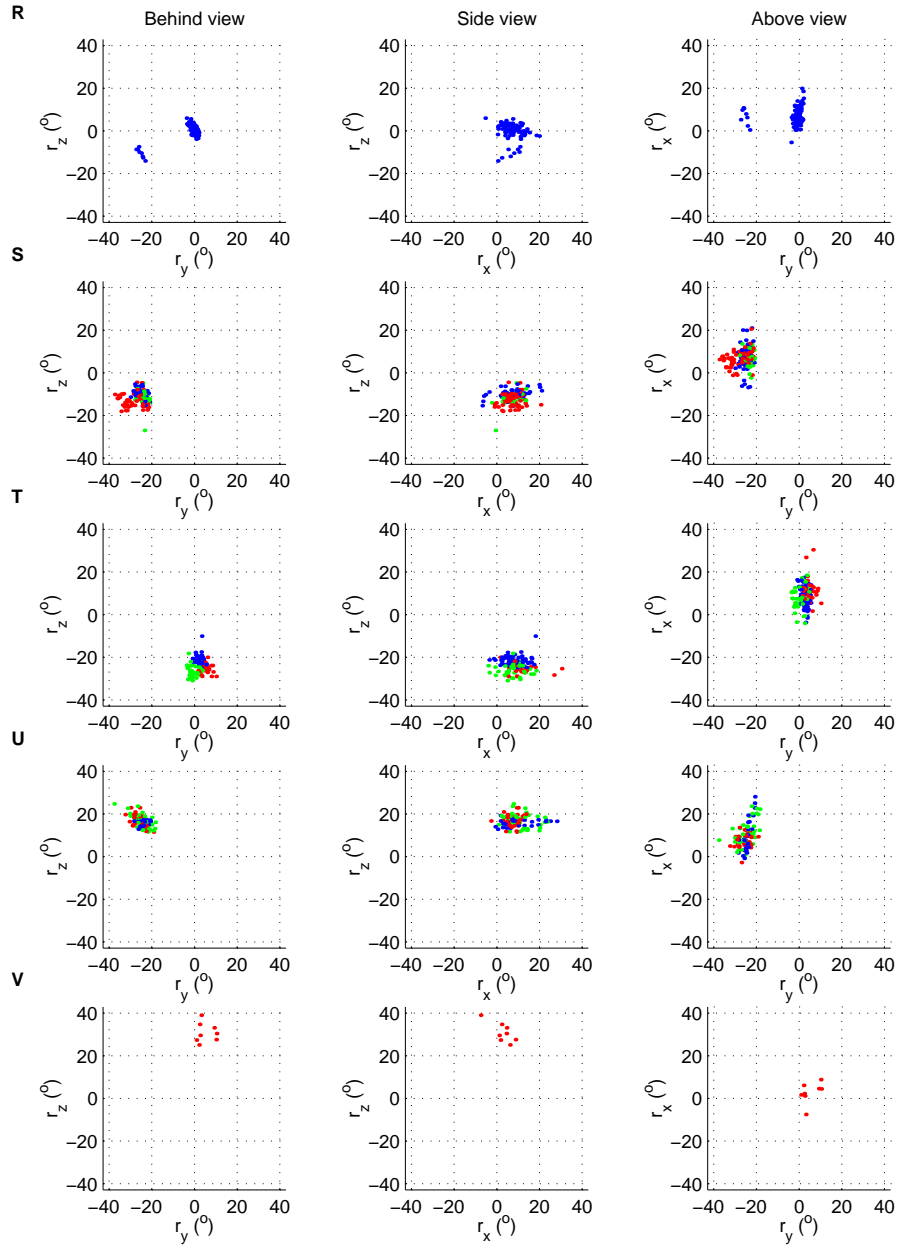


Figure C.3: End point spread of forearm rotation vectors for subject 4, Green denotes double step movements and red control movements ending at a particular point, blue denotes movements starting at that point.

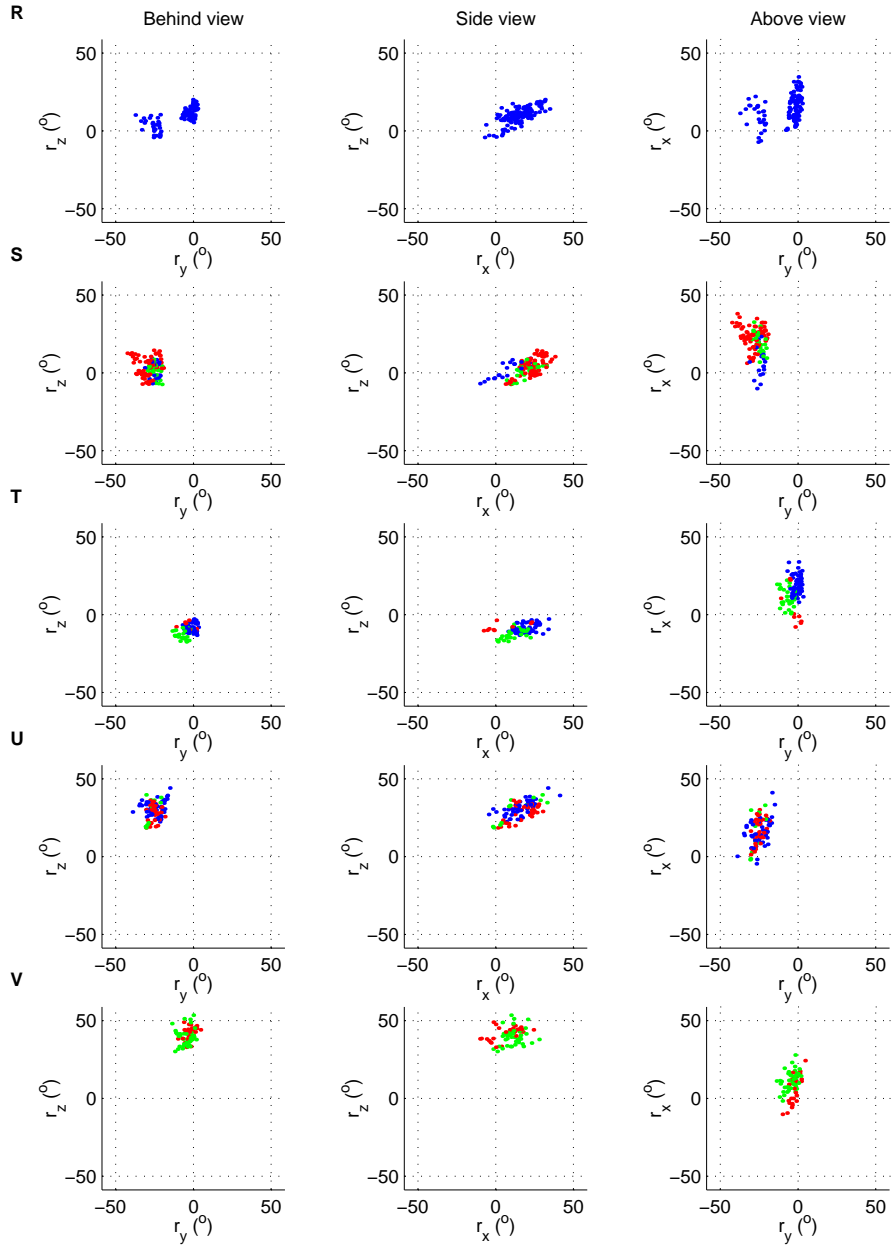


Figure C.4: End point spread of forearm rotation vectors for subject 5, Green denotes double step movements and red control movements ending at a particular point, blue denotes movements starting at that point.

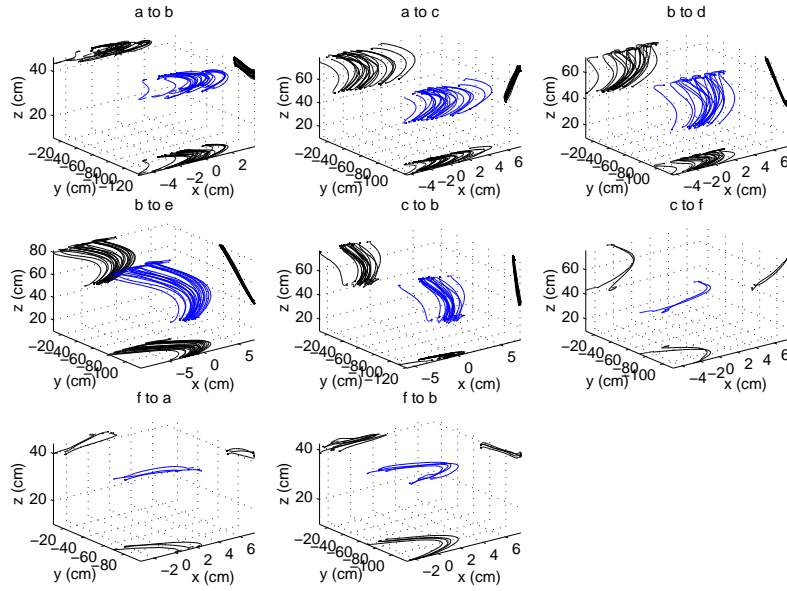


Figure D.1: Trajectories of the control movements for Subject 1.

## Appendix D

### Paths of control movements (position)

The paths of the control movements are shown here for all subjects except subject 3 (this is shown in Figure 6.2).

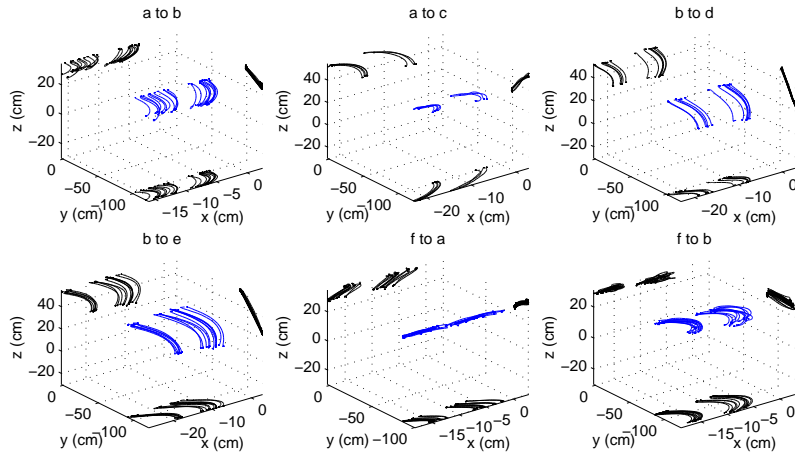


Figure D.2: Trajectories of the control movements for Subject 2.

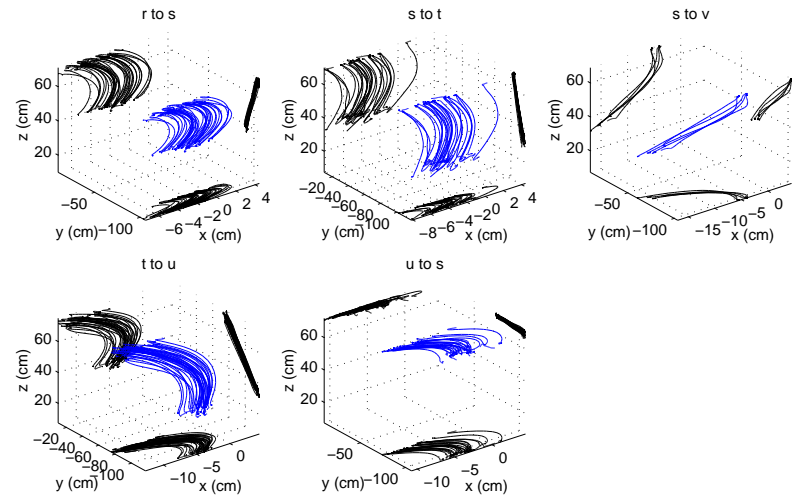


Figure D.3: Trajectories of the control movements for Subject 4.

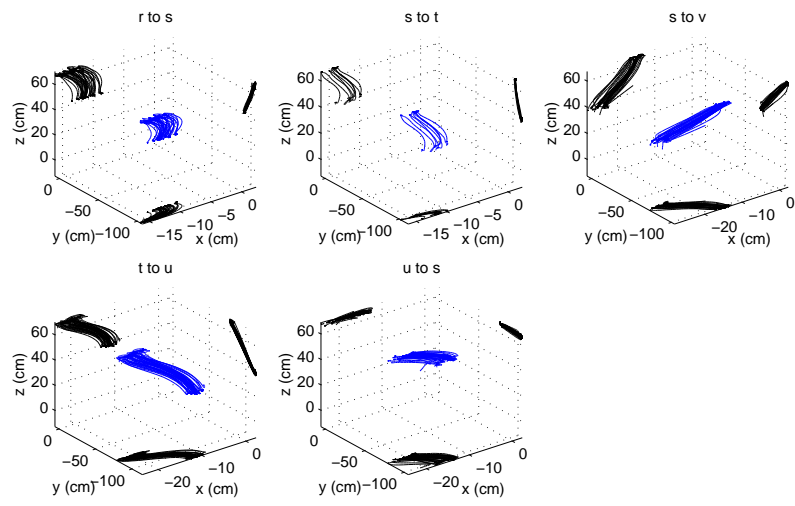


Figure D.4: Trajectories of the control movements for Subject 5.

# Appendix E

## Trajectory of forearm control movements (orientation)

The orientations of the control movements for forearm movements are shown here for all subjects except subject 3 (this is shown in Figure 6.7).

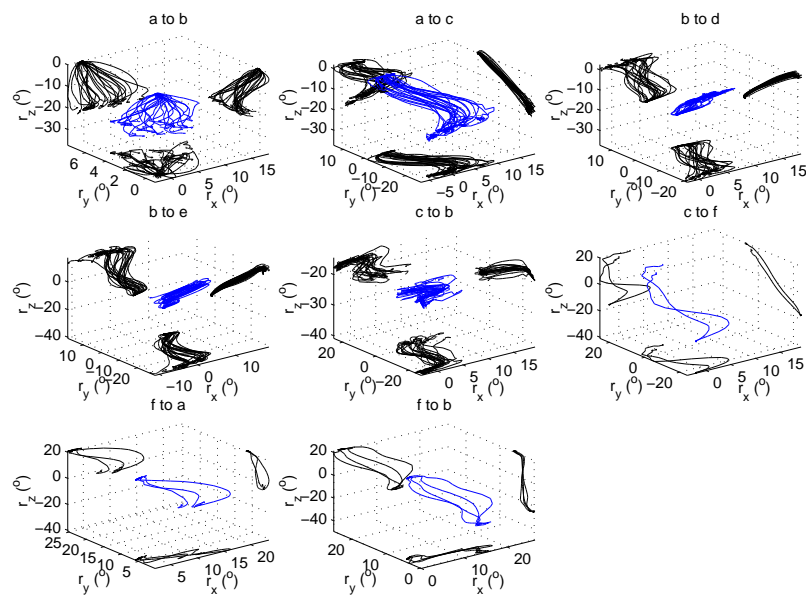


Figure E.1: Trajectories of the forearm control movements (orientation) for Subject 1.

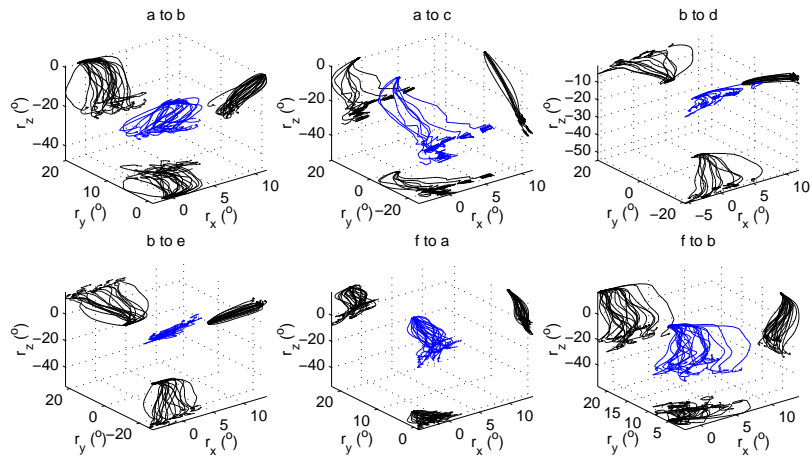


Figure E.2: Trajectories of the forearm control movements (orientation) for Subject 2.

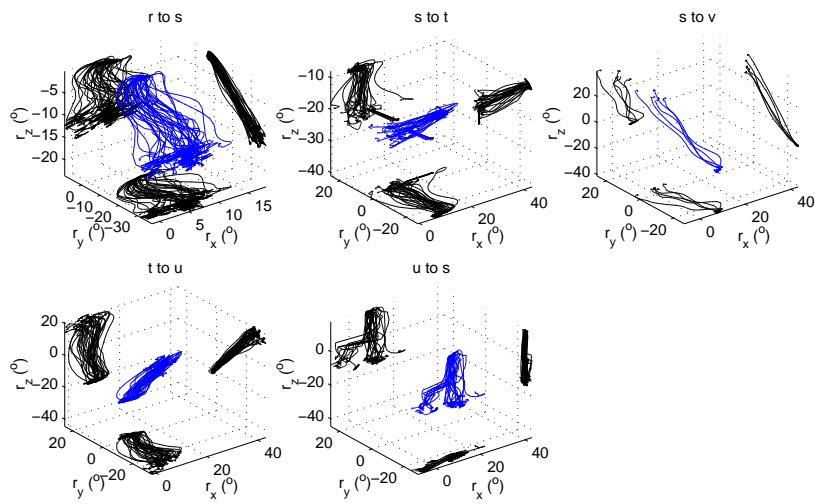


Figure E.3: Trajectories of the forearm control movements (orientation) for Subject 4.

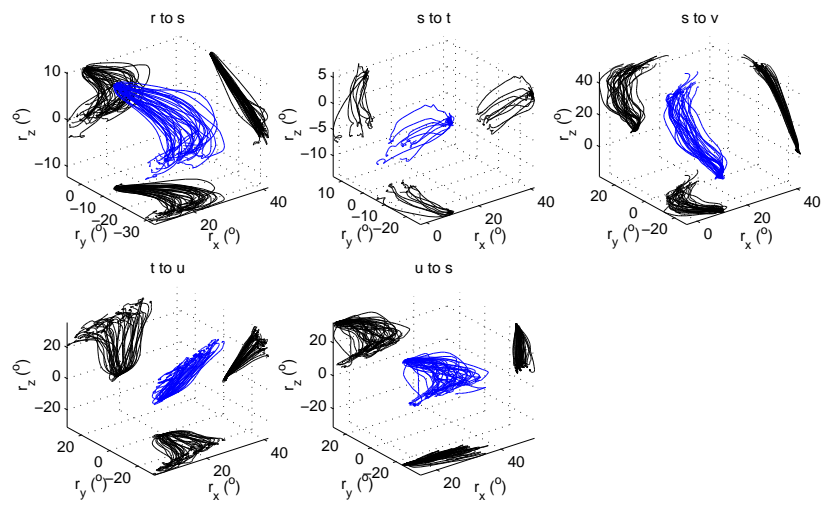


Figure E.4: Trajectories of the forearm control movements (orientation) for Subject 5.

# Appendix F

## Trajectory of upper arm control movements (orientation)

The orientations of the control movements for the upper arm are shown here for all subjects except subject 3 (this is shown in Figure 6.8).

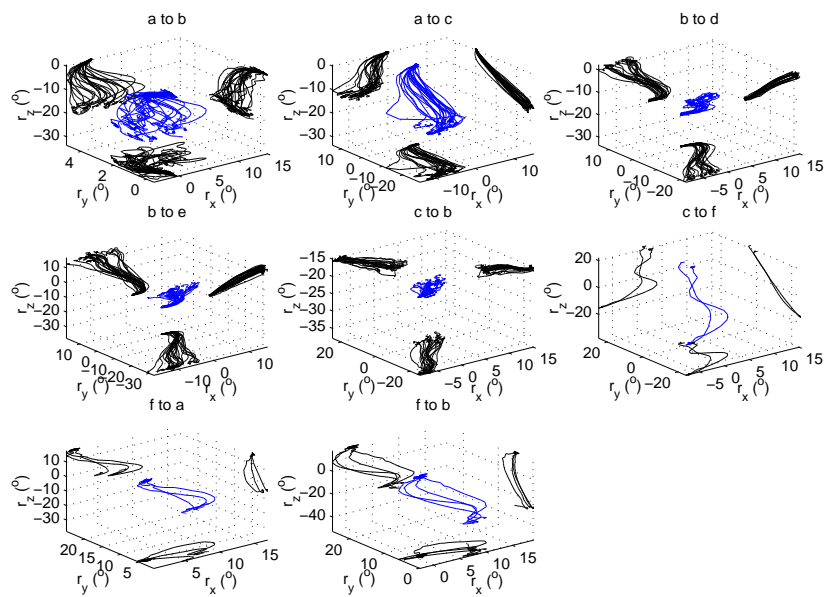


Figure F.1: Trajectories of the upper arm control movements (orientation) for Subject 1.

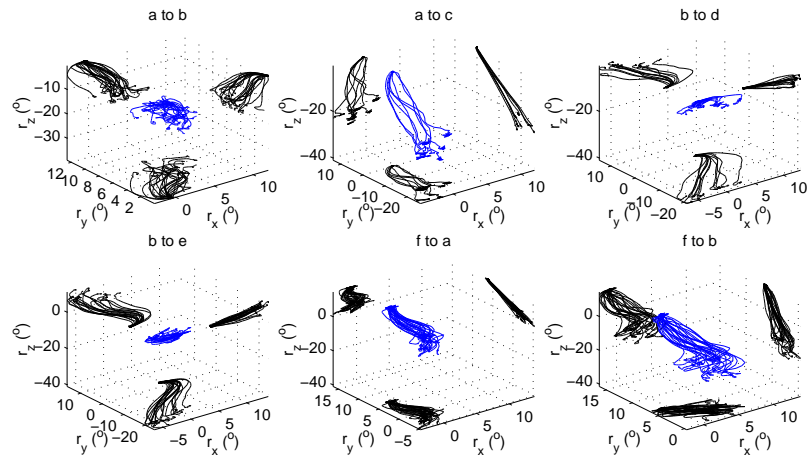


Figure F.2: Trajectories of the upper arm control movements (orientation) for Subject 2.

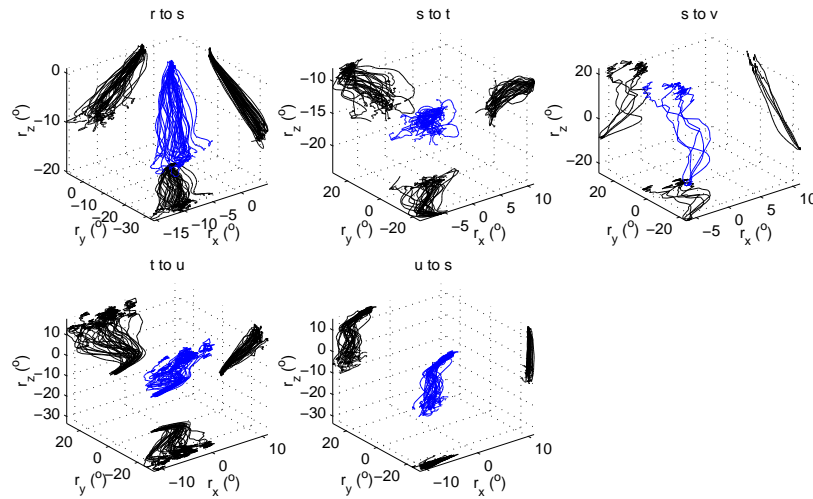


Figure F.3: Trajectories of the upper arm control movements (orientation) for Subject 4.

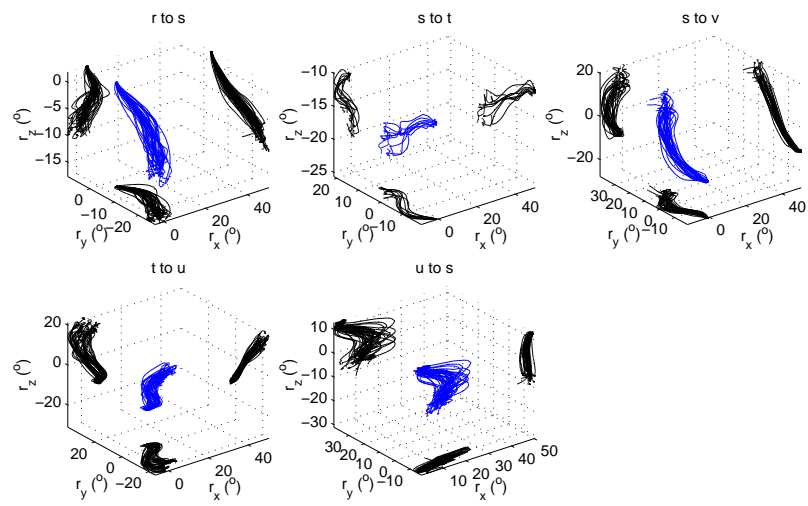


Figure F.4: Trajectories of the upper arm control movements (orientation) for Subject 5.

# Appendix G

## Velocity of control (single step) movements

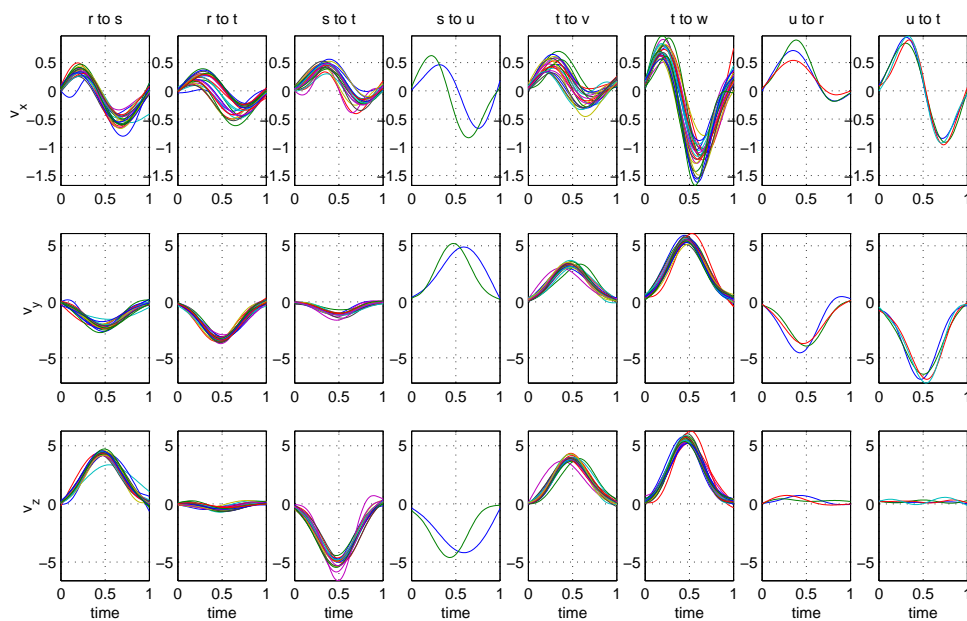


Figure G.1: Subject 1: Velocity during control movements.

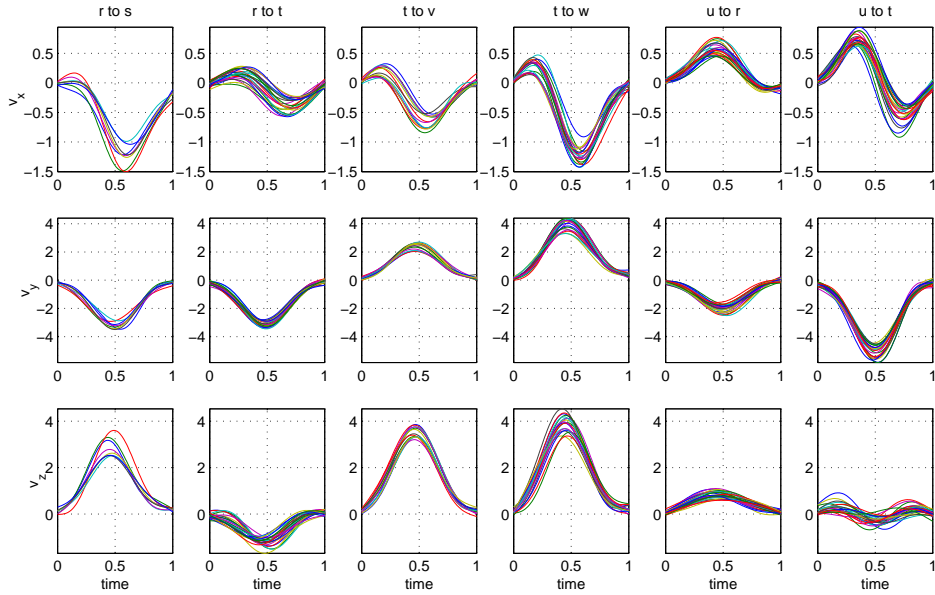


Figure G.2: Subject 2: Velocity during control movements.

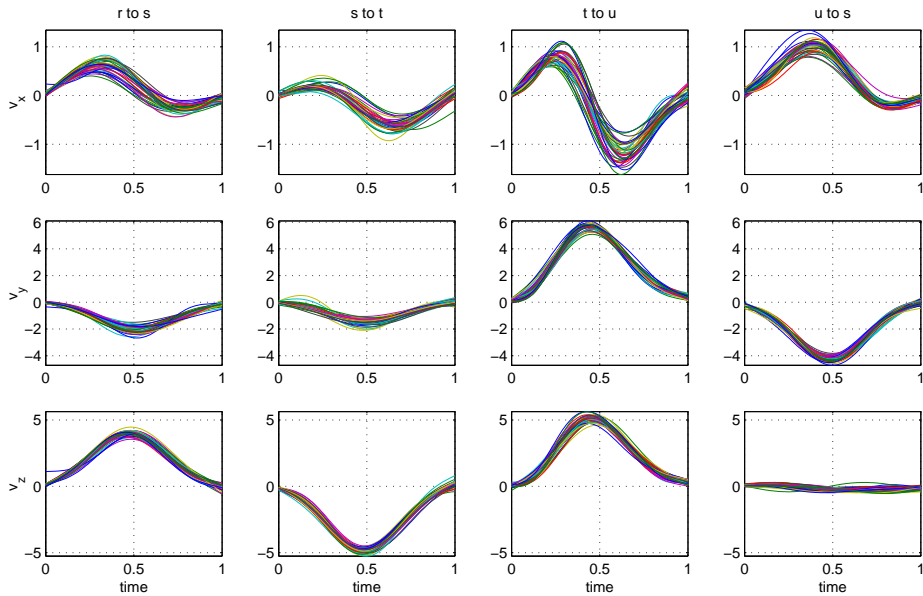


Figure G.3: Subject 3: Velocity during control movements.

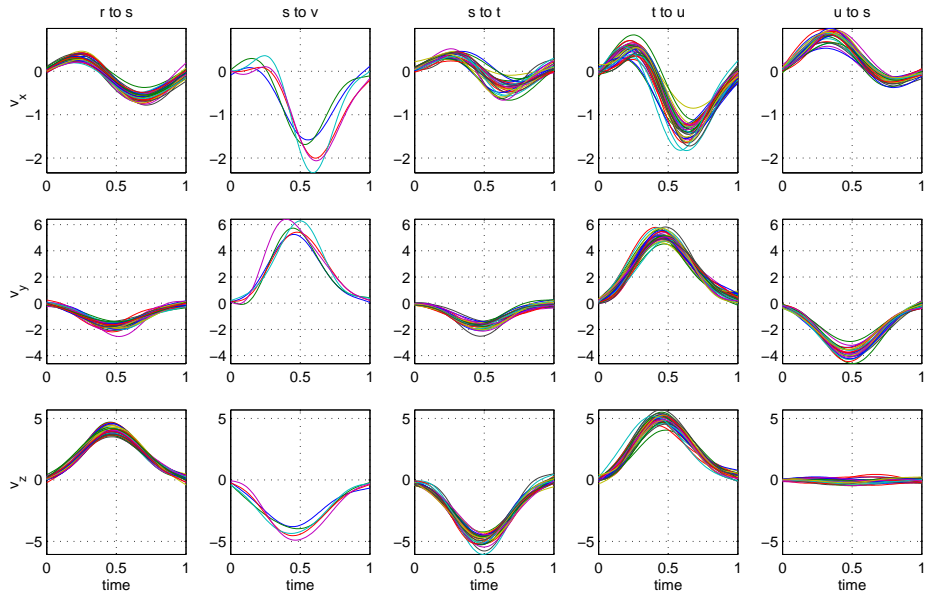


Figure G.4: Subject 4: Velocity during control movements.

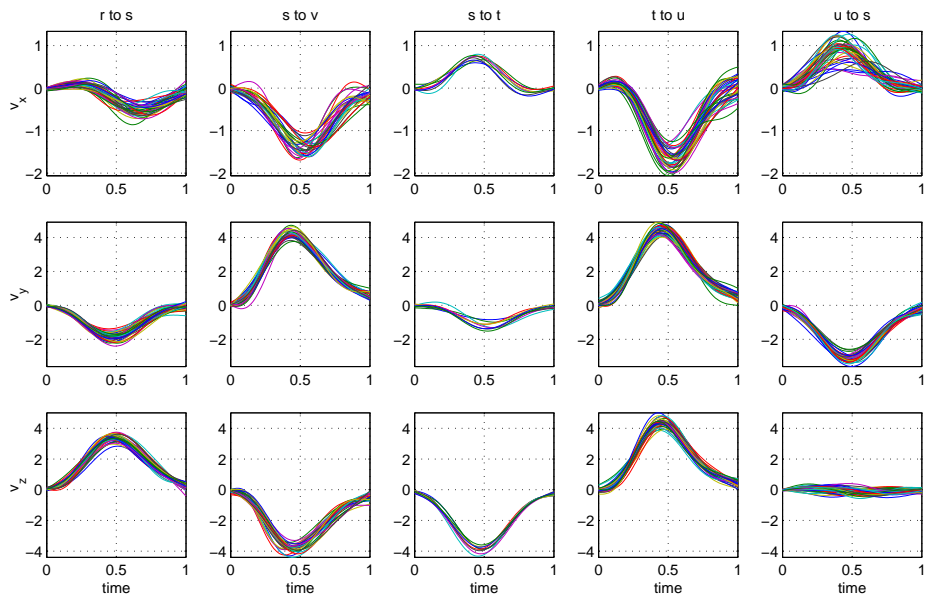


Figure G.5: Subject 5: Velocity during control movements.

# Appendix H

## Forearm angular velocity of control (single step) movements

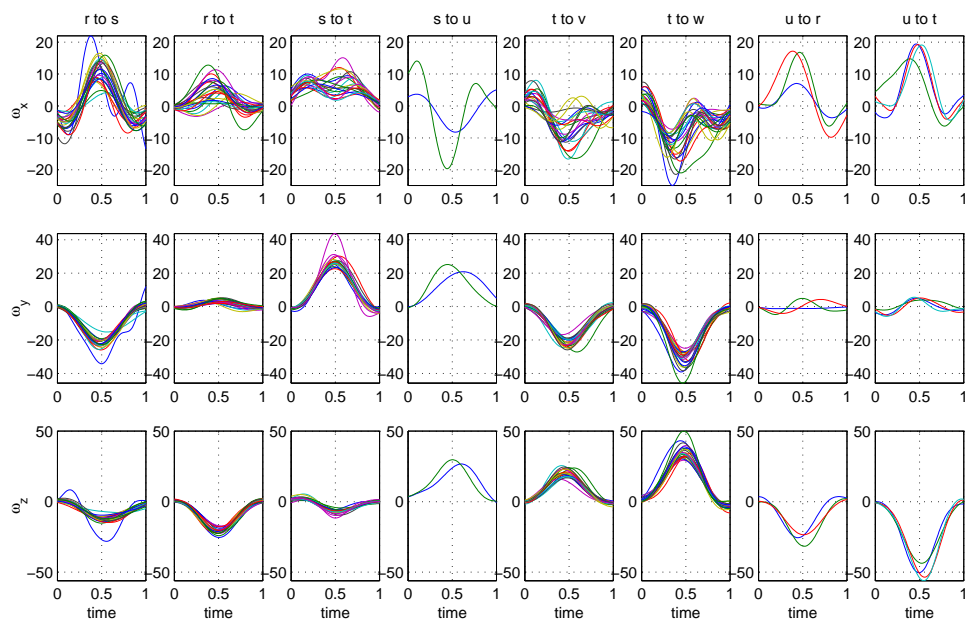


Figure H.1: Subject 1: Forearm angular velocity during control movements.

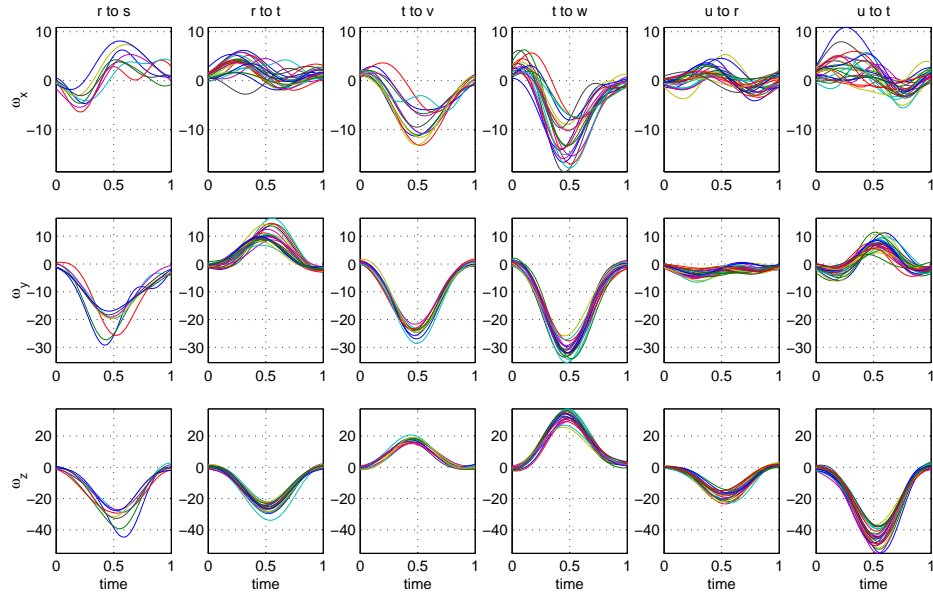


Figure H.2: Subject 2: Forearm angular velocity during control movements.

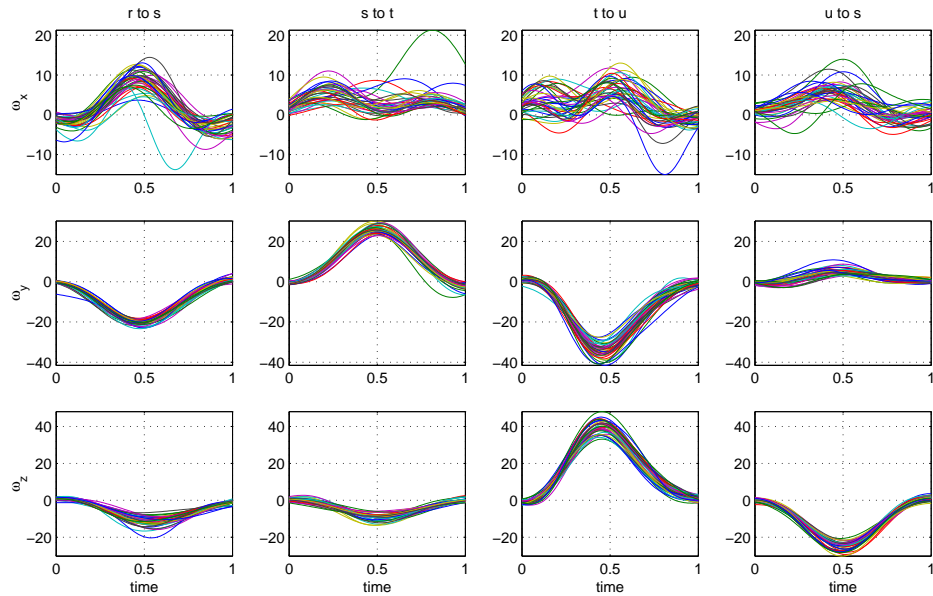


Figure H.3: Subject 3: Forearm angular velocity during control movements.

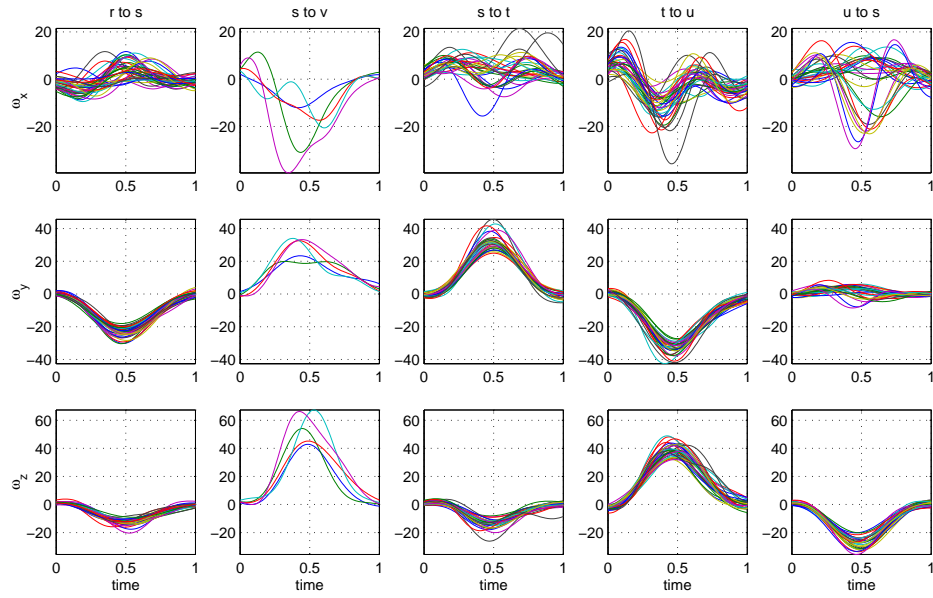


Figure H.4: Subject 4: Forearm angular velocity during control movements.

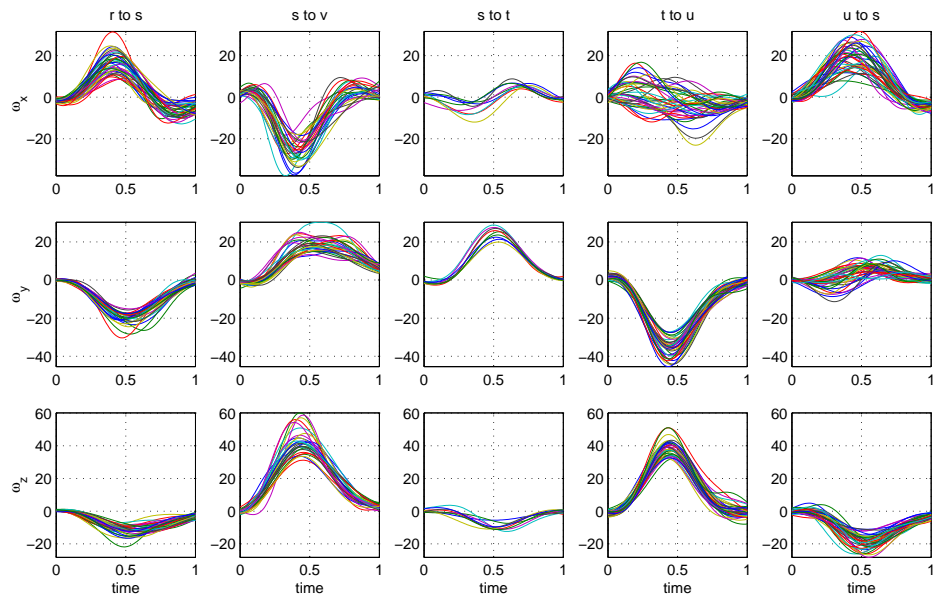


Figure H.5: Subject 5: Forearm angular velocity during control movements.

# Appendix I

## Upper arm angular velocity of control (single step) movements

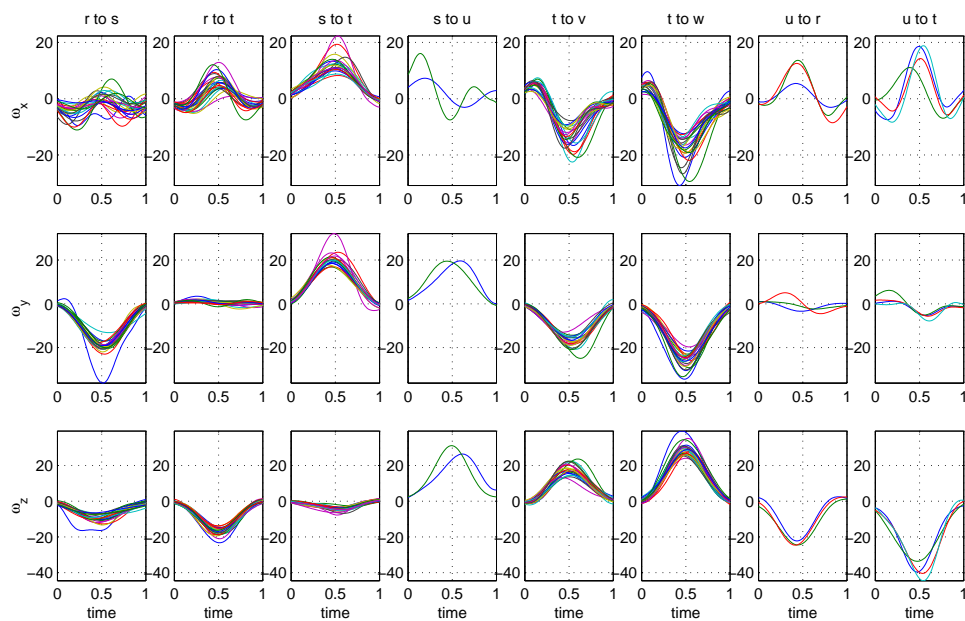


Figure I.1: Subject 1: Upper arm angular velocity of control movements.

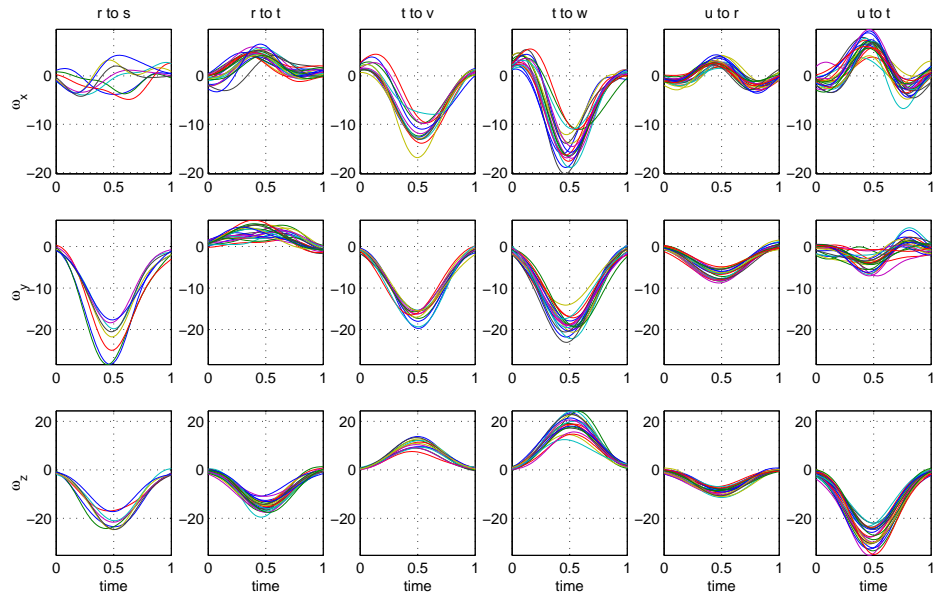


Figure I.2: Subject 2: Upper arm angular velocity of control movements.

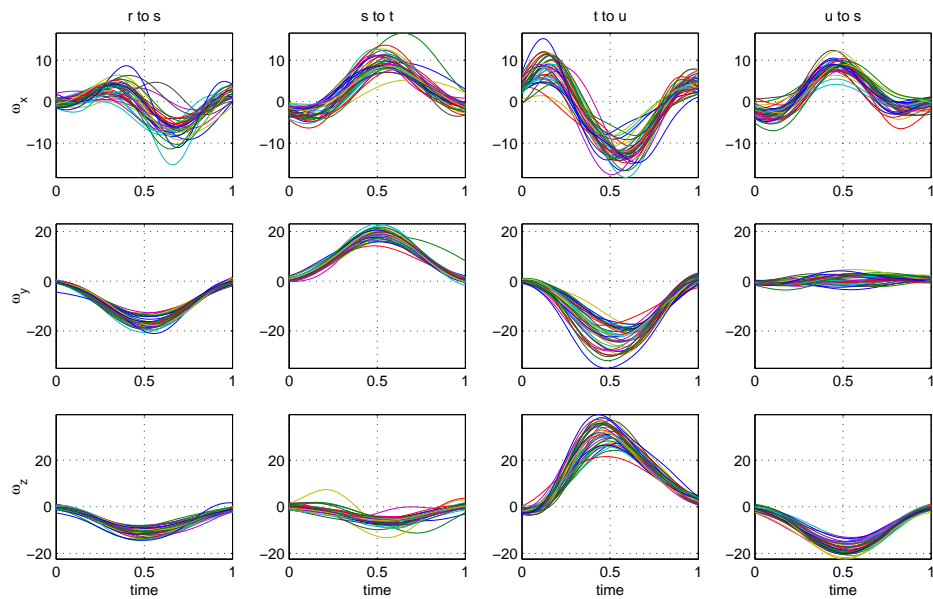


Figure I.3: Subject 3: Upper arm angular velocity of control movements.

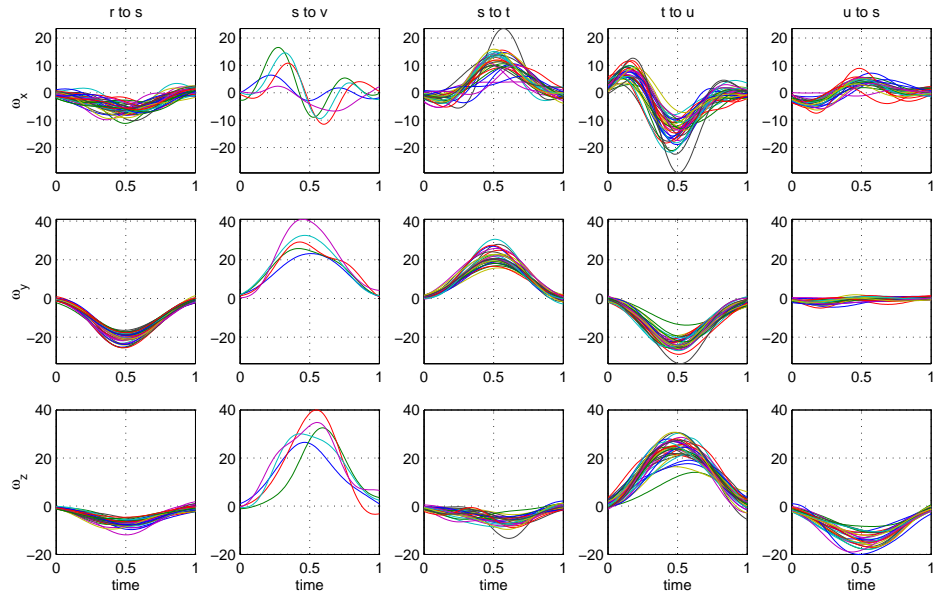


Figure I.4: Subject 4: Upper arm angular velocity of control movements.

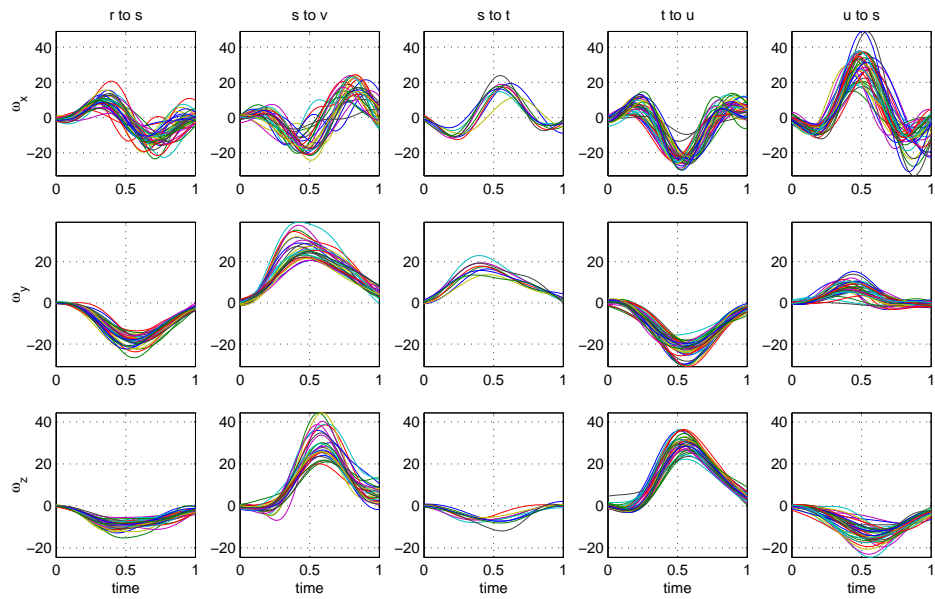


Figure I.5: Subject 5: Upper arm angular velocity of control movements.

## Appendix J

# Comparison of planning schemes for double step movements in two-dimensional Fick coordinates

The following graphs show the predictions of the two dimensional models (in terms of  $\theta_F$  and  $\phi_F$ ), for the superposition scheme and the abort-replan scheme, compared with the experimental data. In the following graphs, red represents the experimental data, the dashed blue line the first control movement, the blue solid line the prediction of the superposition scheme and the green line the prediction of the abort-replan scheme.

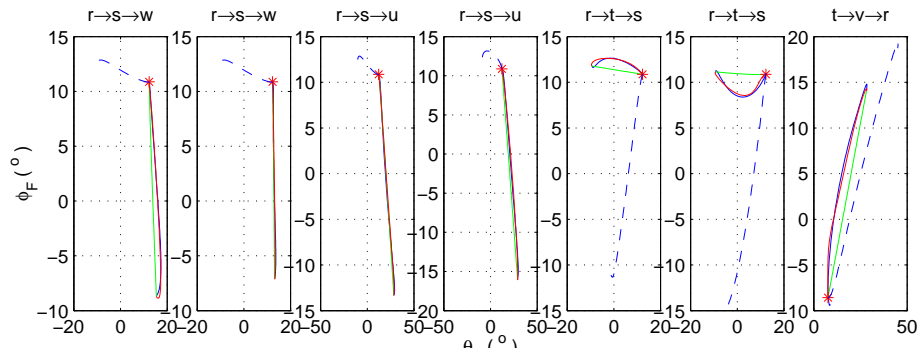


Figure J.1: Predicted and actual 2D Fick trajectories with large overlap (greater than 0.6) for the forearm for Subject 1

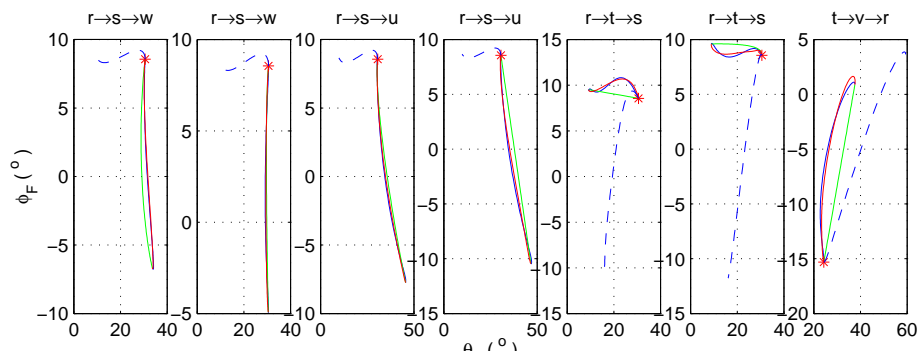


Figure J.2: Predicted and actual 2D Fick trajectories with large overlap (greater than 0.6) for the upper arm for Subject 1

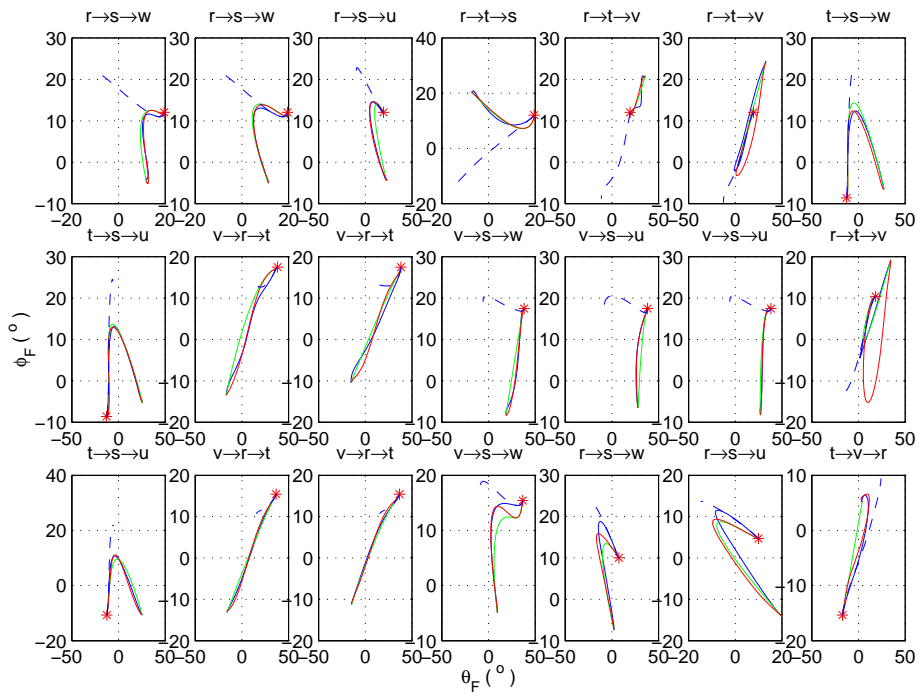


Figure J.3: Predicted and actual 2D Fick trajectories with large overlap (greater than 0.6) for the forearm for Subject 2



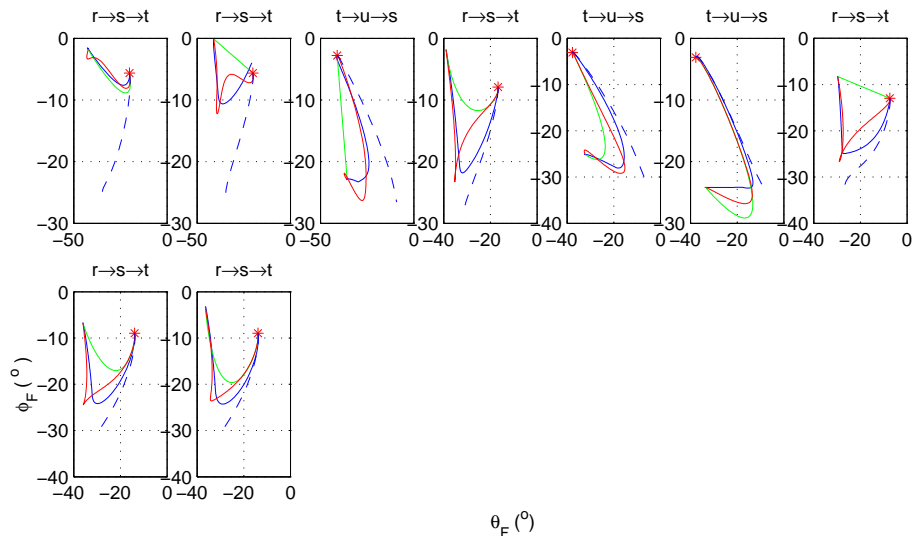


Figure J.5: Predicted and actual 2D Fick trajectories with large overlap (greater than 0.6) for the forearm for Subject 3

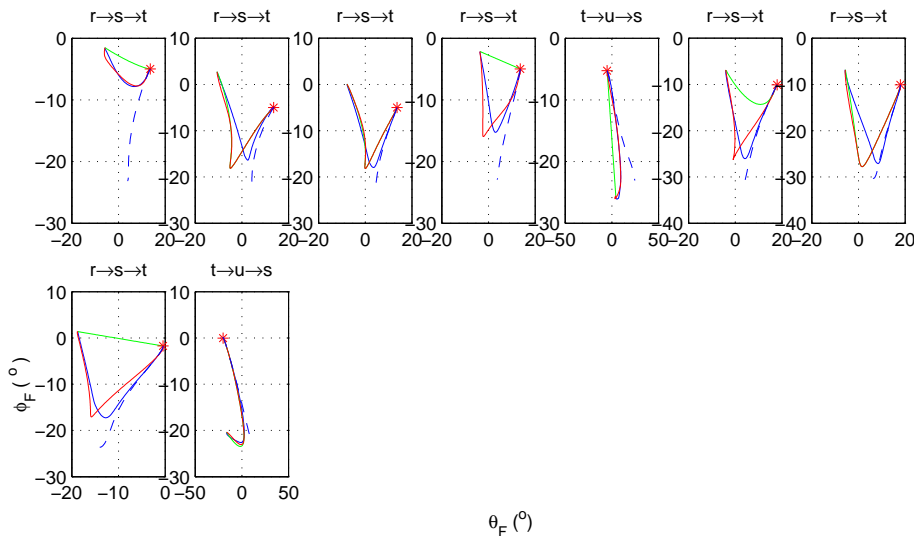


Figure J.6: Predicted and actual 2D Fick trajectories with large overlap (greater than 0.6) for the upper arm for Subject 3

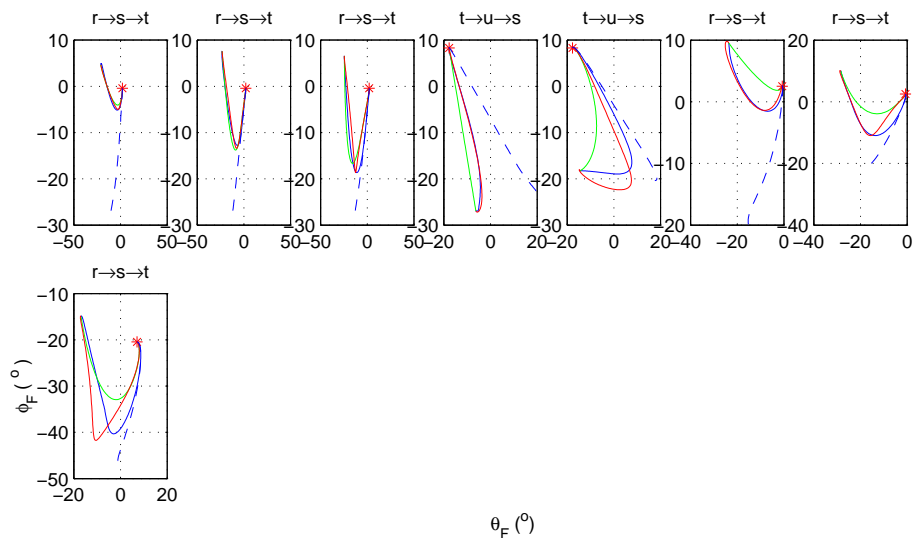


Figure J.7: Predicted and actual 2D Fick trajectories with large overlap (greater than 0.6) for the forearm for Subject 4

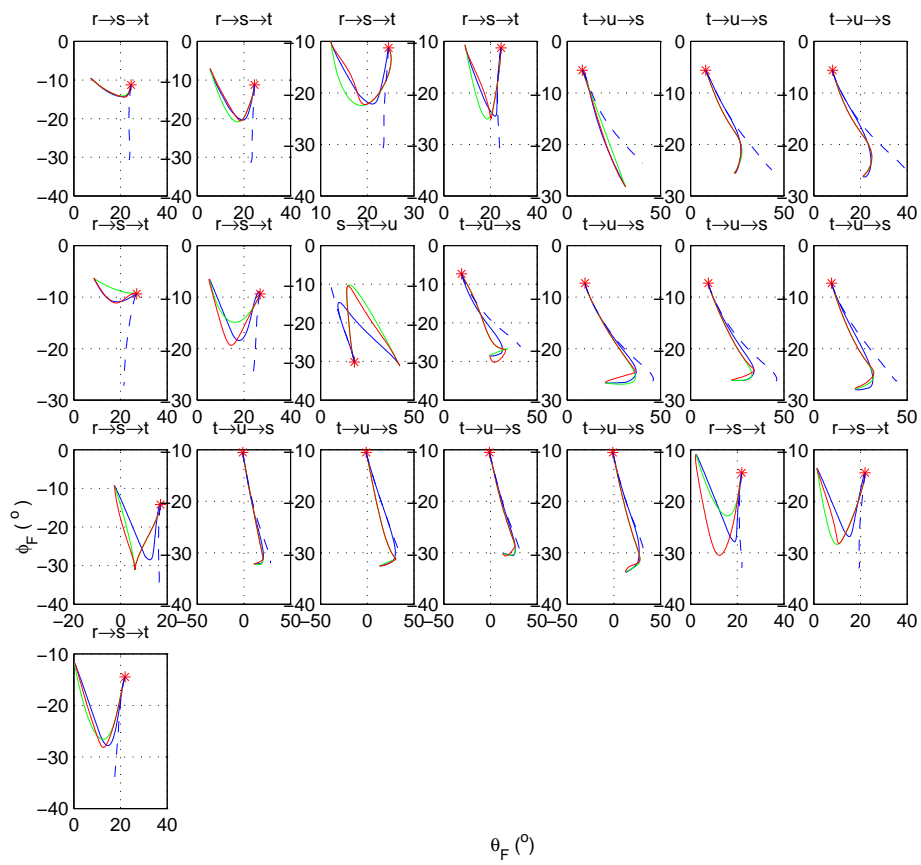


Figure J.8: Predicted and actual 2D Fick trajectories with large overlap (greater than 0.6) for the upper arm for Subject 4

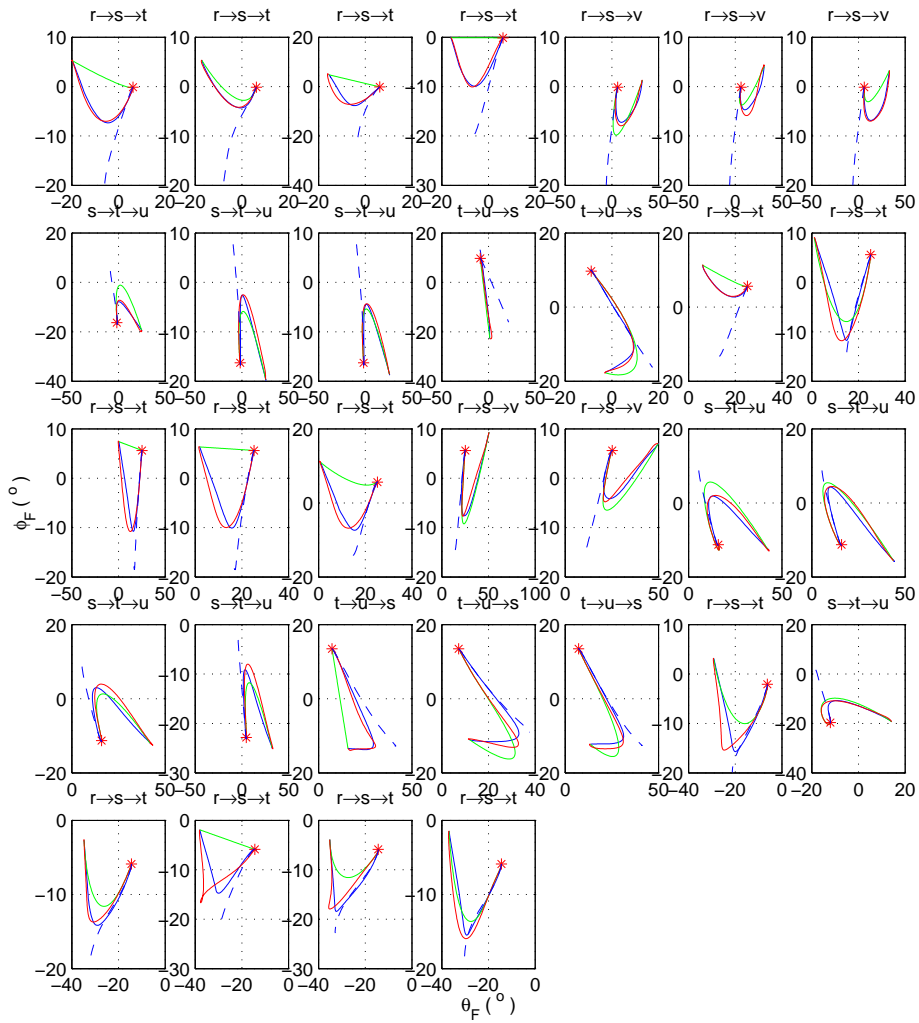


Figure J.9: Predicted and actual 2D Fick trajectories with large overlap (greater than 0.6) for the forearm for Subject 5

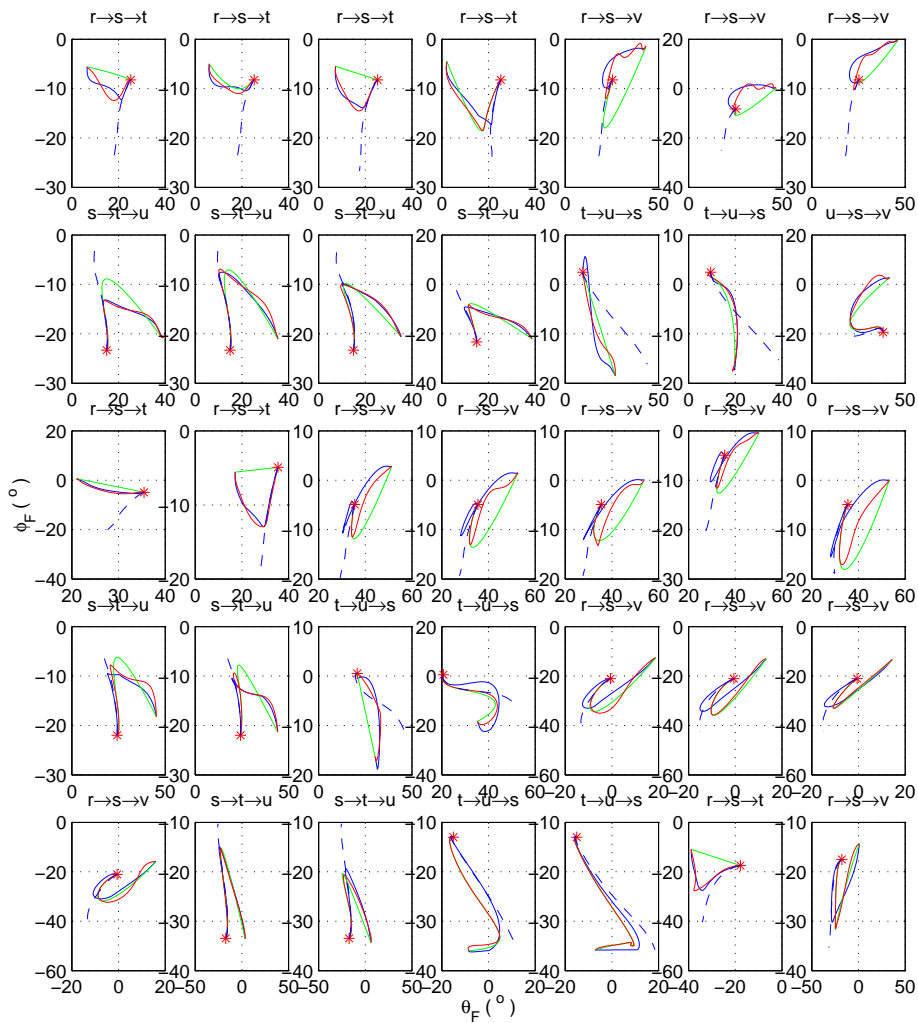


Figure J.10: Predicted and actual 2D Fick trajectories with large overlap (greater than 0.6) for the upper arm for Subject 5

# Appendix K

## Summary of errors during 2D superposition

These graphs show the mean (the height of bar graph) and the standard deviation (the length of the error bar) for the two dimensional Fick coordinate superposition scheme (in blue) compared to an abort replan scheme (in red), divided into no or small overlap (N/S) - less than 0.2, moderate overlap (M) - between 0.2 and 0.6, and large overlap(L) - greater than 0.6. Each row represents the ISI time shown next to it. The results are only shown for groups where 3 or more trials are found.

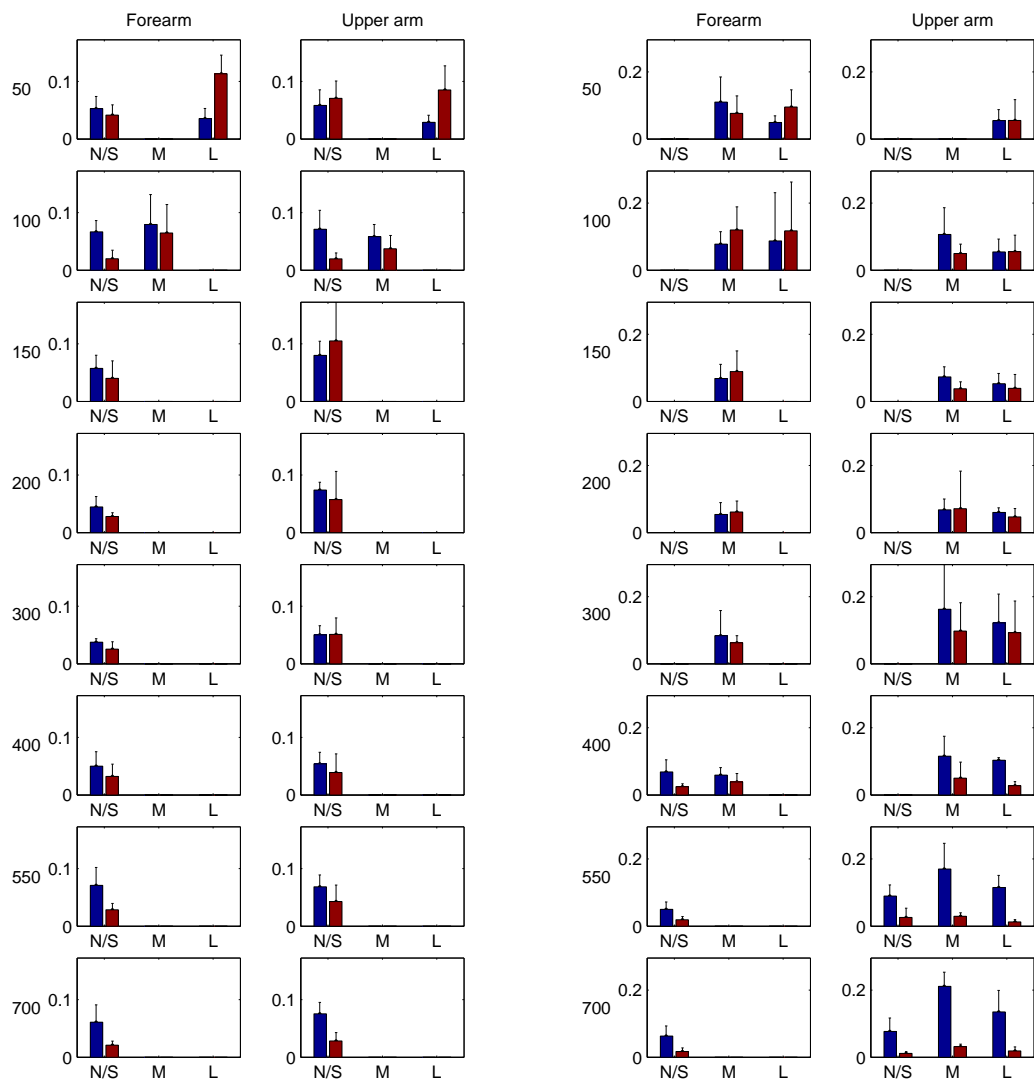


Figure K.1: Comparison of errors between the two-dimensional superposition and abort-replan scheme for Subject 1 (left) and Subject 2 (right).

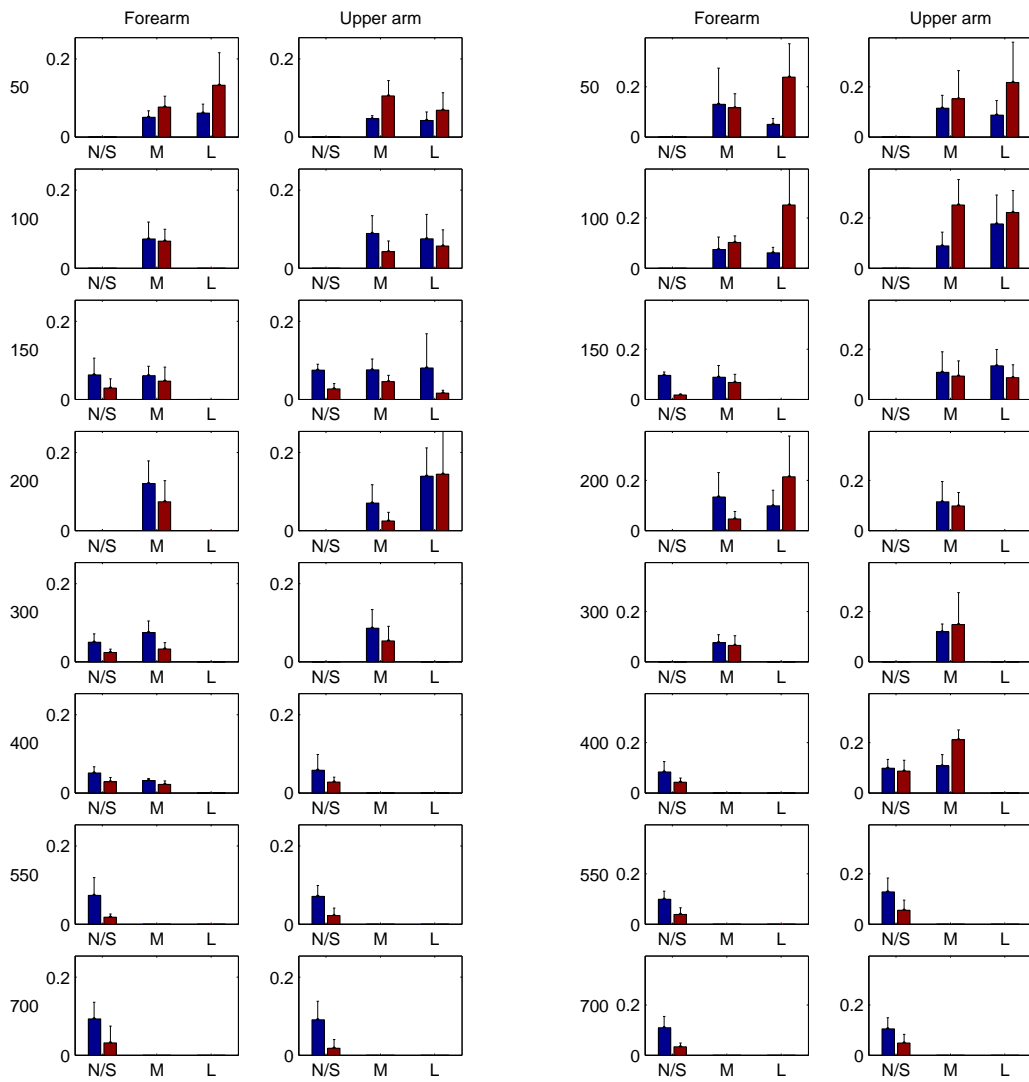


Figure K.2: Comparison of errors between the two-dimensional superposition and abort-replan scheme for Subject 4 (left) and Subject 5 (right).

## Appendix L

# Comparison of planning schemes for double step movements in rotation vector space

These graphs show rotation vectors during double step movements in components -  $r_x$  (blue),  $r_y$ (green) and  $r_z$ (red). The dashed lines shows the experimental data, the solid line the prediction with a second order surface Donders' constraint on orientation, the dotted line the prediction of a Listing's law constraint on orientation (only the  $r_x$  component shown) and the dotted-dash line the prediction for a second order surface constraint on coordinate velocity.

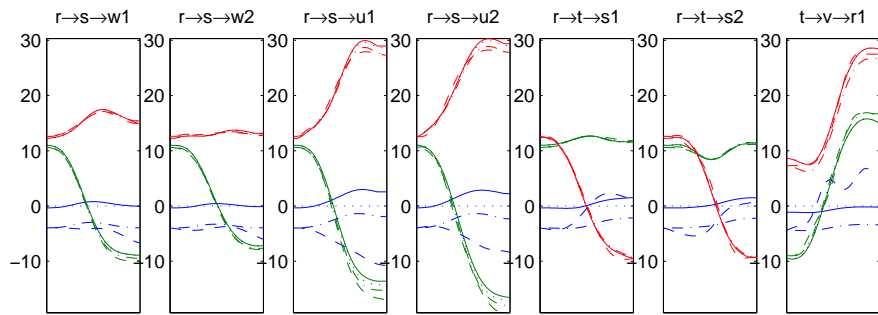


Figure L.1: Predicted and actual rotation vectors (in degrees) with large overlap (greater than 0.6) for the forearm for Subject 1.

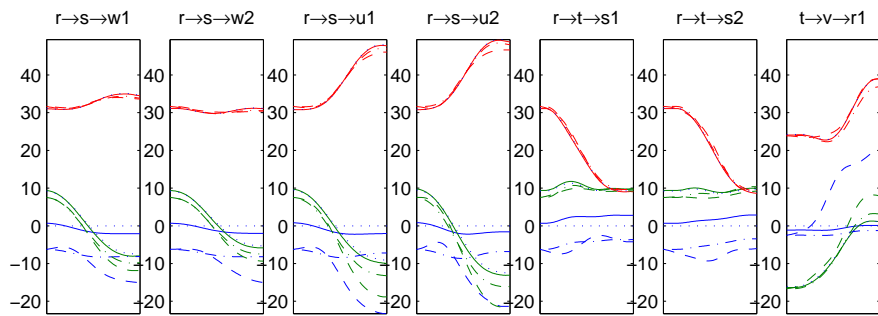


Figure L.2: Predicted and actual rotation vectors (in degrees) with large overlap (greater than 0.6) for the upper arm for Subject 1.

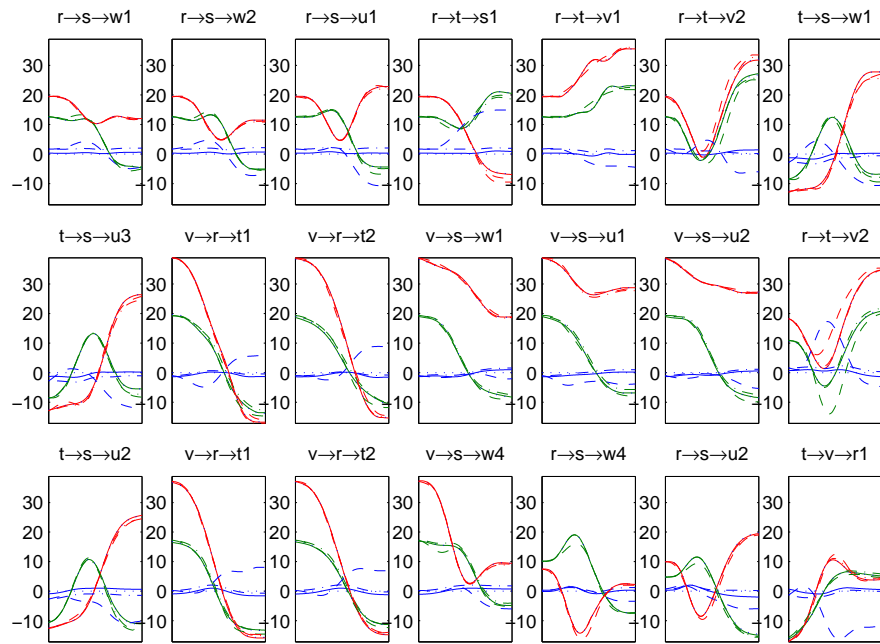


Figure L.3: Predicted and actual rotation vectors (in degrees) with large overlap (greater than 0.6) for the forearm for Subject 2.

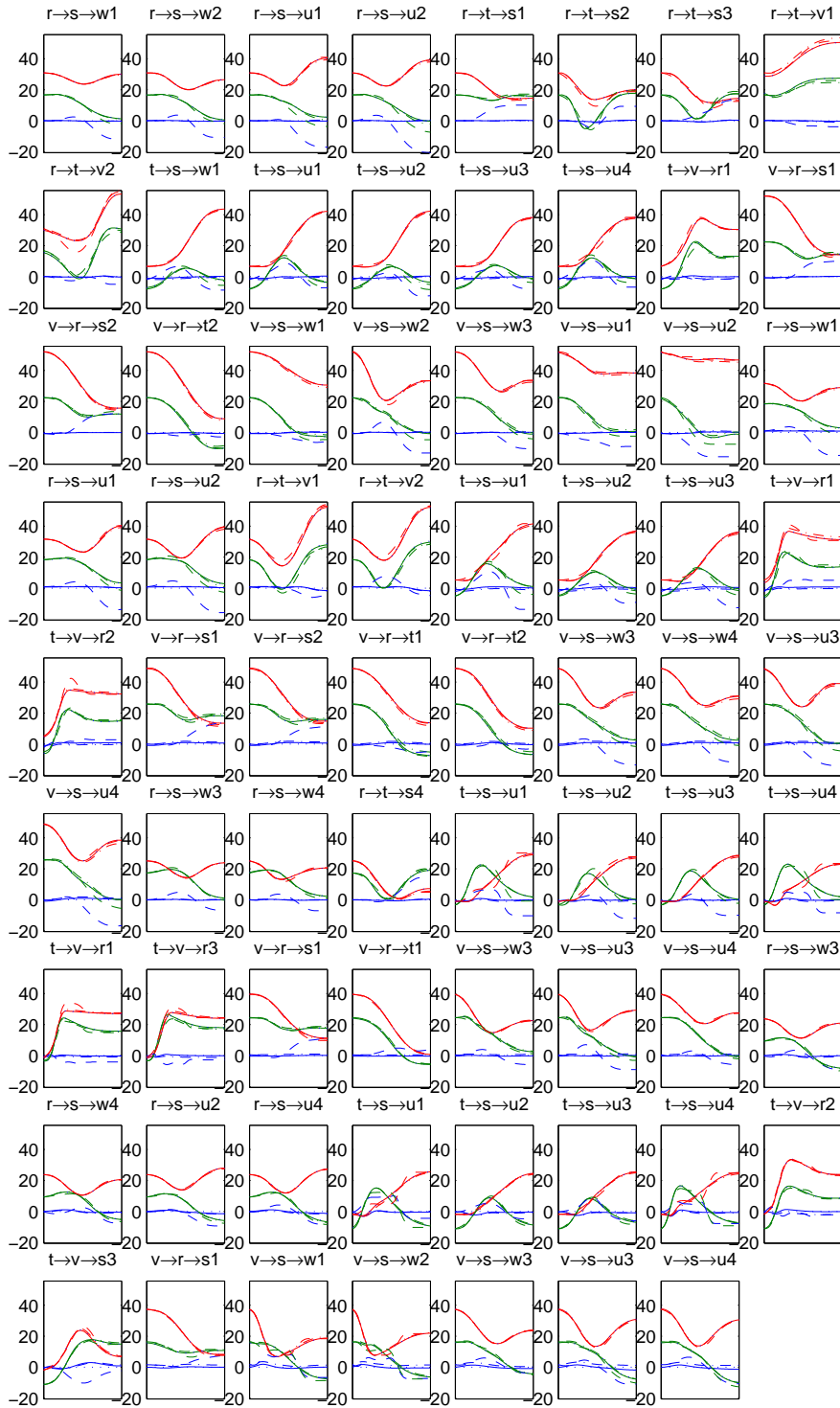


Figure L.4: Predicted and actual rotation vectors (in degrees) with large overlap (greater than 0.6) for the upper arm for Subject 2.

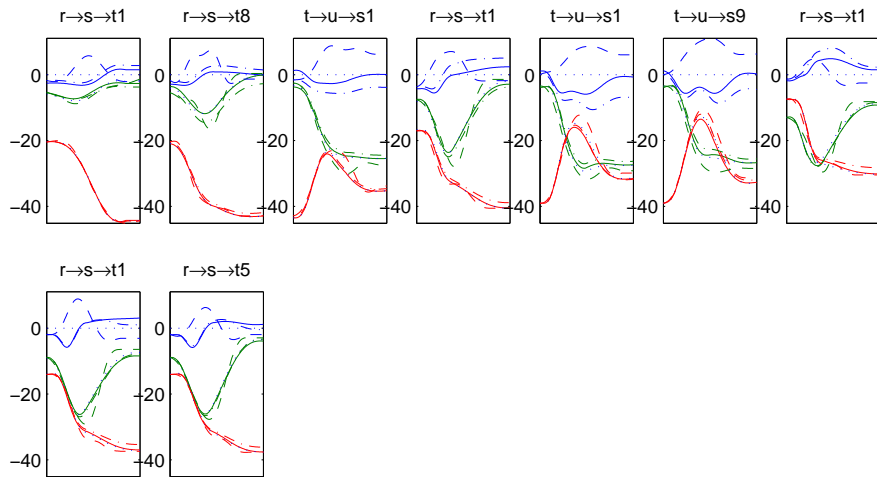


Figure L.5: Predicted and actual rotation vectors (in degrees) with large overlap (greater than 0.6) for the forearm for Subject 3.

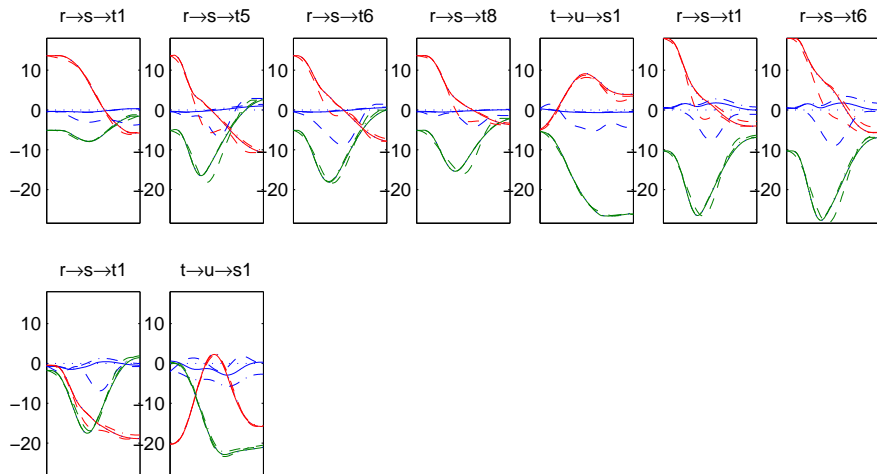


Figure L.6: Predicted and actual rotation vectors (in degrees) with large overlap (greater than 0.6) for the upper arm for Subject 3.

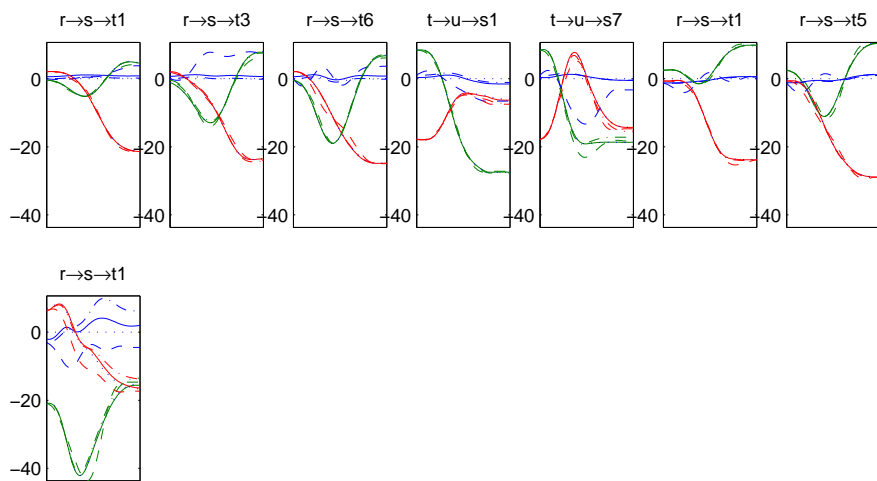


Figure L.7: Predicted and actual rotation vectors (in degrees) with large overlap (greater than 0.6) for the forearm for Subject 4.

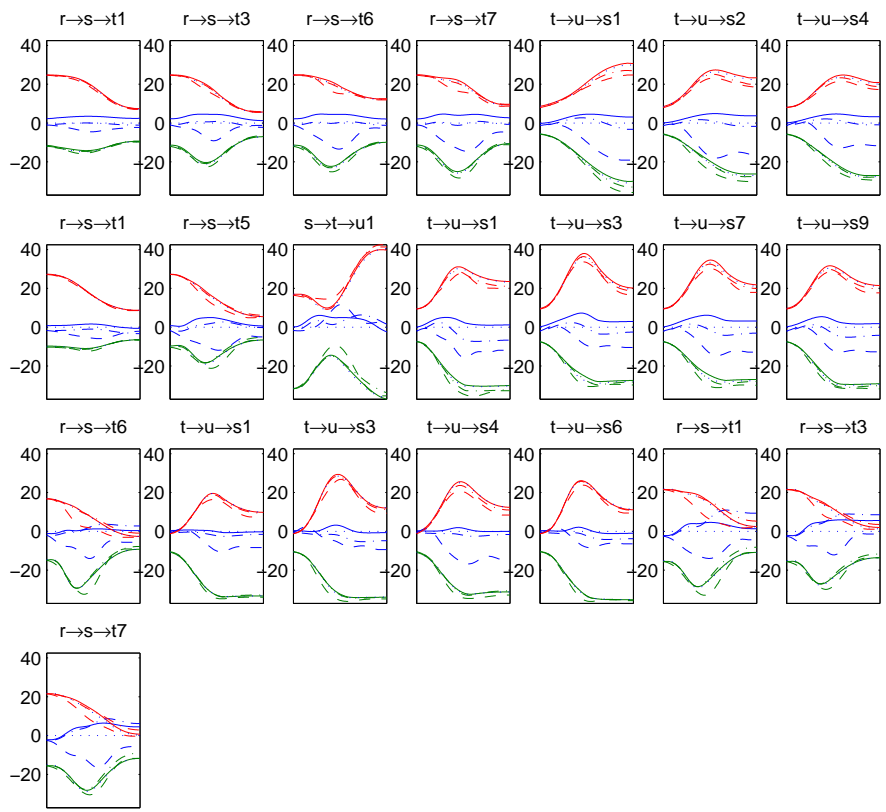


Figure L.8: Predicted and actual rotation vectors (in degrees) with large overlap (greater than 0.6) for the upper arm for Subject 4.

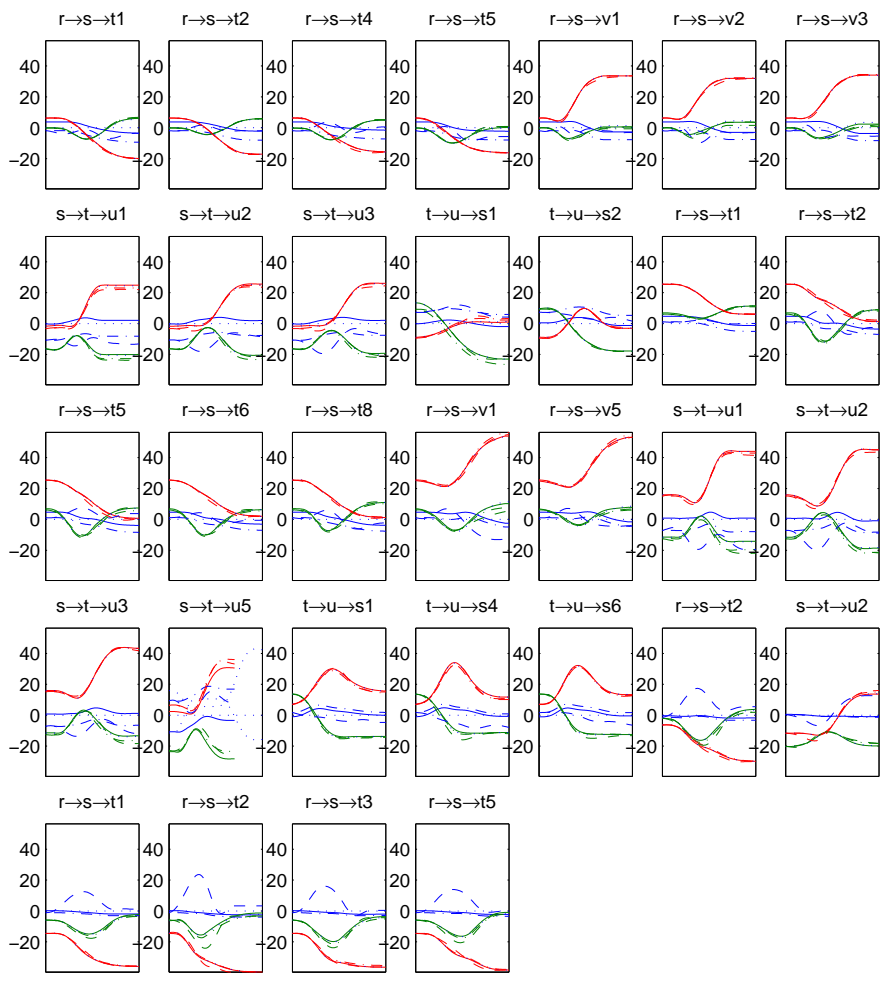


Figure L.9: Predicted and actual rotation vectors (in degrees) with large overlap (greater than 0.6) for the forearm for Subject 5.

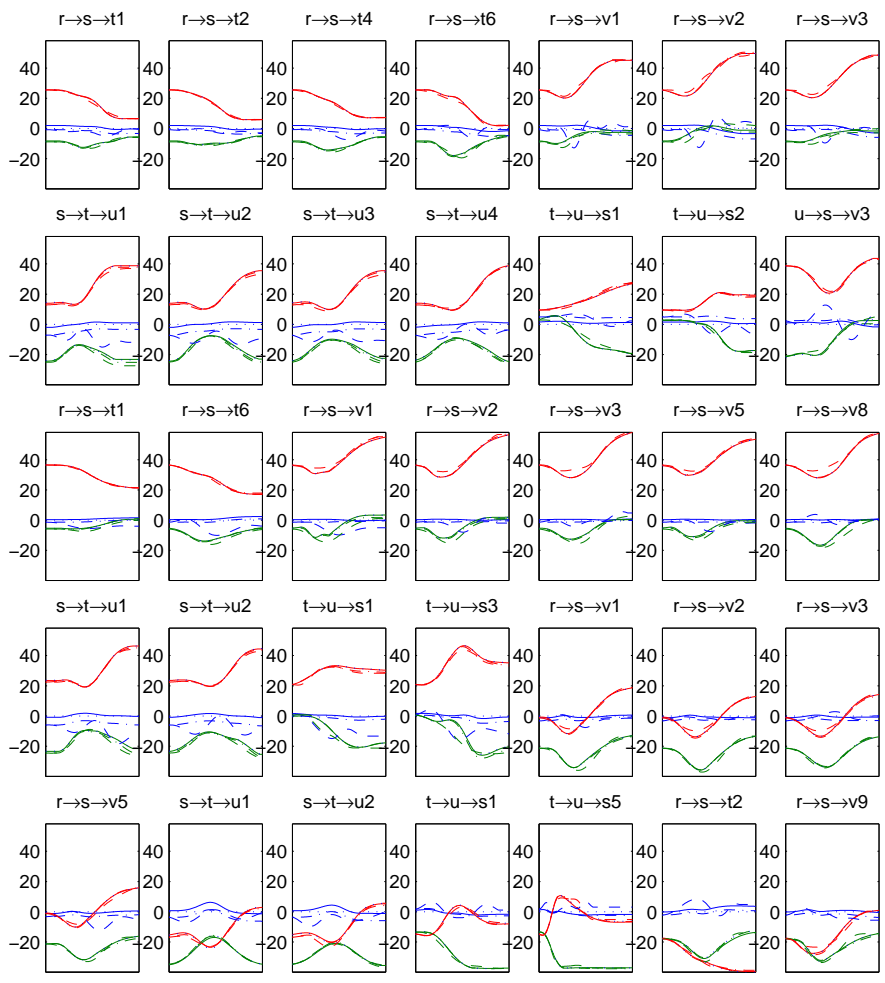


Figure L.10: Predicted and actual rotation vectors (in degrees) with large overlap (greater than 0.6) for the upper arm for Subject 5.

# Appendix M

## Summary of errors after superposition in rotation vector space

These graphs show the mean (the height of bar graph) and the standard deviation (the length of the error bar) for the three dimensional rotation vector models compared with the actual data. Blue shows the superposition scheme with a second order surface Donders' law constraint, green is with a flat Listing's plane constraint, and red is when a coordinate velocity constraint is used. The results are divided into no or small overlap (N/S) - less than 0.2, moderate overlap (M) - between 0.2 and 0.6, and large overlap(L) - greater than 0.6. Each row represents the ISI time shown next to it. The results are only shown for groups where 3 or more trials are found.

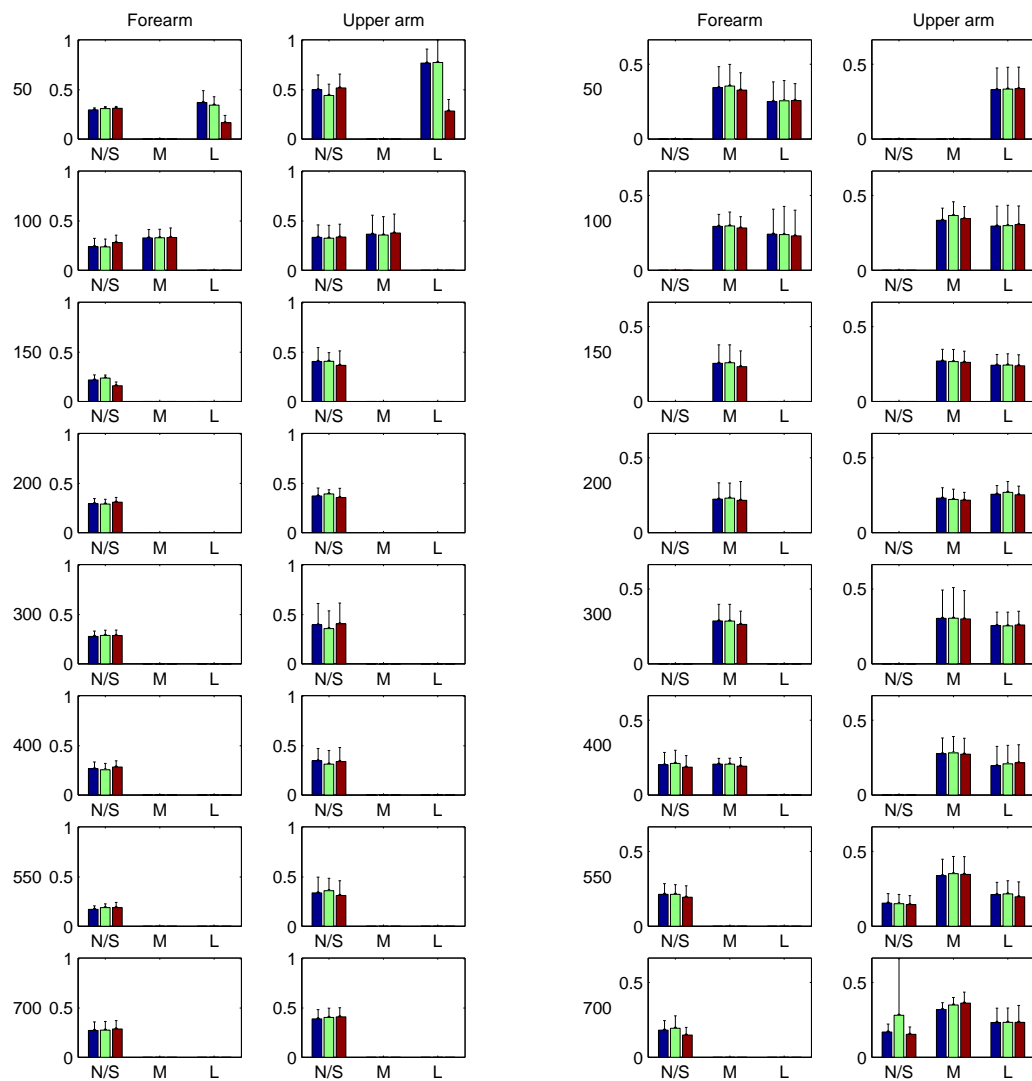


Figure M.1: Comparison of errors between the three dimensional models for Subject 1 (left) and Subject 2 (right).

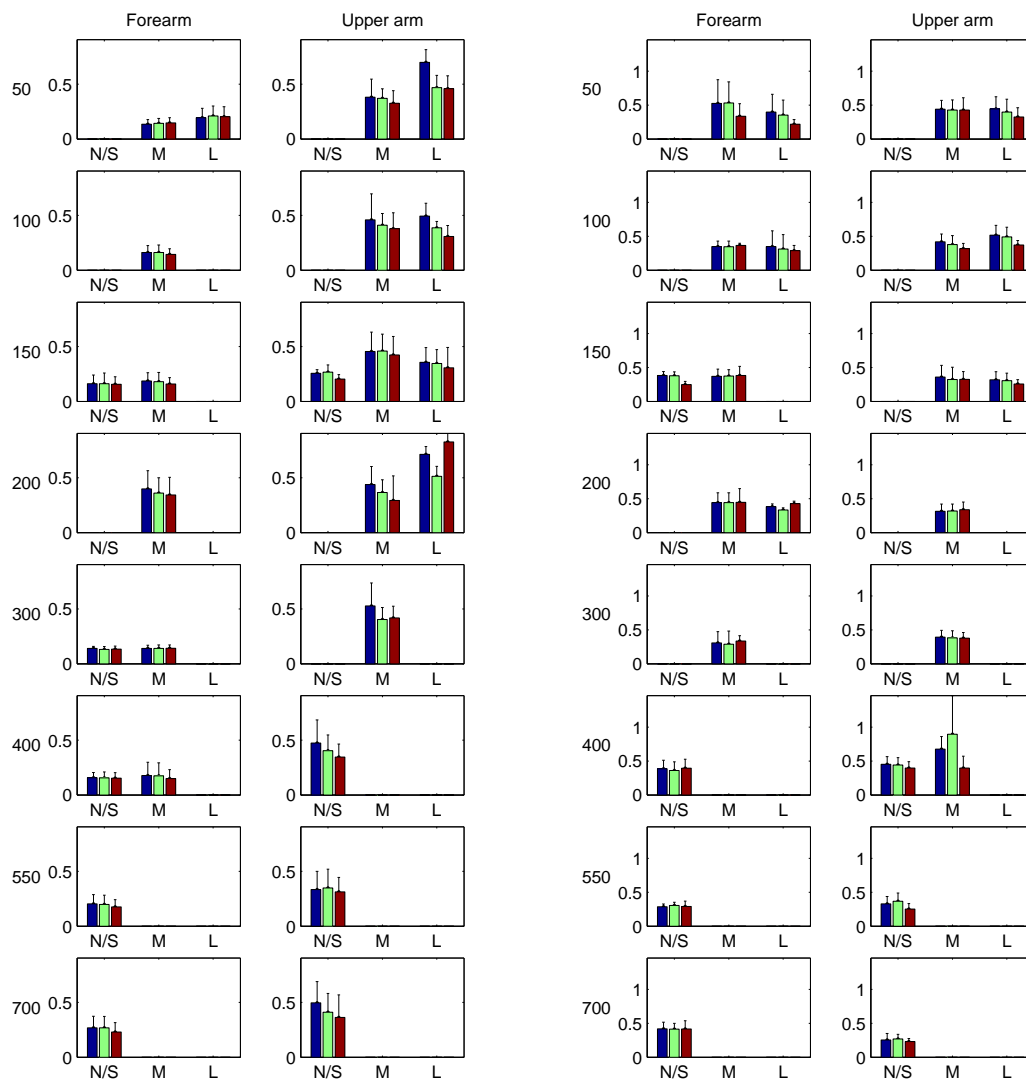


Figure M.2: Comparison of errors between the three dimensional models for Subject 4 (left) and Subject 5 (right).